

**MONTHLY VARIABILITY IN THE PHYSICAL
PROPERTIES OF THE WATER MASSES OFF
KYRENIA**

**A THESIS SUBMITTED TO THE GRADUATE
SCHOOL OF APPLIED SCIENCES
OF
UNIVERSITY OF KYRENIA**

**By
ÇAĞRI DELİCEİRMAK**

**In Partial Fulfilment of the Requirements for
the Degree of Master of Science
in
Maritime Transportation and Management Engineering**

KYRENIA, 2019

**Çağrı DELİCEİRMAK: MONTHLY VARIABILITY IN THE PHYSICAL
PROPERTIES OF THE WATER MASSES OFF KYRENIA**

**Approval of Director of Graduate School of
Applied Sciences**

Prof. Dr Levent KAYRIN

**We certify this thesis is satisfactory for the award of the degree of Master of Science
in
Maritime Transportation and Management Engineering**

Examining Committee in Charge:

Prof. Dr.	Committee Chairman
Prof. Dr. İlkey Salihoğlu	Supervisor
Prof. Dr.	
Prof. Dr.	
Prof. Dr.	

I hereby declare that all information in this document has been obtained and presented in accordance with academic rules and ethical conduct. I also declare that, as required by these rules and conduct, I have fully cited and referenced all material and results that are not original to this work.

Name, Last Name:

Signature:

Date:

ACKNOWLEDGEMENTS

This study was supported by the Scientific and Technological Research Council of Turkey (TUBITAK) grants: CAYDAG - 114Y139 “Determination of the influence of anthropogenic and natural processes on the Cilician Basin (between the Turkish Republic of Northern Cyprus and Turkey) Marine Ecosystem. The scientific cruises were supported both financially and in-kind by the University of Kyrenia, Near East University, and Middle East Technical University, Institute of Marine Sciences.

I would like to express my special appreciation and gratitude to my advisor, Prof. Dr. İlkyay Salihoğlu, for his support, patience, guidance and immense knowledge. I am grateful to have the opportunity to study and work with him. He is the one who inspired and encouraged me to learn and study about oceanography. It was not possible to deepen my knowledge and interest without him. He is a great mentor that each student and each scientist would like to have. He has been a great mentor to me not only in science but in every manner. Thanks for everything Hocam.

I would to thank Prof. Dr. Mohammed Abdul Latif for his help, support and kindness. His help is not limited to the interpretation of the physical oceanographic data, but he taught and inspired me a lot about physical oceanography. I will always remember not only the scientific contributions he made, but also his kindness, patience, guidance and knowledge.

I need to mention special thanks and appreciations to Assist. Prof. Dr Devrim Tezcan, Dr Hasan Örek and Dr Yeşim Ak Örek. They were there whenever I need them. They helped, supported and trusted me in every manner from the beginning. I learned how to conduct oceanographic cruises and oceanographic fieldwork. I learned a lot from them. They have been advisors, and they have been friends. Thanks for everything.

Many thanks to Myroshnychenko Volodymyr for his help with data processing.

I am also grateful to the crew of R/V Teal Jr, Zekeriya Dogan, Akin Hurdeniz, Lutfu Sirac and Ercan Bayar for their help and contribution.

Last but not least, I want to thank my beloved one, Selin. She is my motivation; she is my everything.

And of course, great thanks to my family, by all means.

ABSTRACT

The first oceanographic time-series study of the Northern Cyprus, the Kıbrıs Time Series study (KTS), was carried out between November 2015 and June 2018, with monthly intervals on a five nautical mile zonal section offshore Kyrenia. Highly systematic, comprehensive and sub-meso scale KTS studies were conducted with relatively high frequency in order to investigate physical oceanographic features, their temporal and spatial variabilities, and interactions between coastal and open water masses in the Kyrenia region, north coast of Cyprus in the southwestern Cilician Basin. The results revealed that the general circulation of the Cilician Basin is a, highly complex and dynamic system, with meandering and reversing currents and reappearing cyclonic / anti-cyclonic mesoscale eddies with temporal and spatial variabilities. The dominant driving mechanism of the general circulation temporally and spatially changes between current systems and quasi-permanent eddies. Mixing and stratification processes, multi-layered vertical structure of the water column, and water masses (i.e. LSW, MAW, LIW and EMDW) identical to the Cilician basin were observed throughout the study. Furthermore, for the first time in literature, the possibility of regional Levantine Intermediate Water (LIW) formation in the Cilician Basin, and particularly in the study area was observed. Significant salinity increases and changes in physical oceanographic characteristics on the upper thermocline were observed in the study area, especially in 2017 and 2018.

Keywords: Oceanographic time series; Kıbrıs Time Series (KTS); LIW formation; Physical Oceanography; Salinity shift; Cilician Basin; Northern Cyprus.

ÖZET

Kuzey Kıbrıs kıyılarındaki ilk oşinografik zaman serisi çalışmaları “Kıbrıs Zaman Serisi (KTS)”, Kasım 2015 ile Haziran 2018 tarihleri arasında, Girne açıklarında 5 Deniz Mili (nm) uzunluğundaki bir hat üzerinde aylık aralıklarla gerçekleştirilmiştir. Kilikya Baseni güney batısında ve Kıbrıs’ın kuzey kıyılarında yer alan Girne bölgesinin zaman ve mekâna bağımlı fiziksel oşinografik özellikleri ve kıyı-açık deniz su kütleleri etkileşimleri incelenmiştir. Göreceli yüksek frekanslı zaman serisi çalışmaları, sistematik, kapsamlı ve sub-meso ölçekli olarak gerçekleştirilmiştir. Veri analizleri, Kilikya Baseni genel dolaşım sisteminin, menderesli ve ters yönlü akıntı sistemleri ile zaman-mekân değişkenliklerine sahip, siklonik / anti-siklonik orta ölçekli döngülerin etkisi altında, karmaşık ve dinamik bir sistem olduğunu ortaya koymaktadır. Kilikya baseni su kütlesi genel dolaşımı, yön ve hız olarak zaman ve mekâna bağlı iyi tanımlanmış akıntı sistemleri etkisi altında olduğu görülmekte, bazen de yarı kararlı orta ölçekli döngülerin etkisi altında olduğu görülmektedir. Deniz suyu yoğunluğundan kaynaklanan katmanlaşma ve karışım süreçleri KTS çalışmalarında gözlemlenmiştir. Çalışma süresince, literatürde belirtilen, Kilikya basenine özgü su kütlelerinin (LSW, MAW, LIW ve EMDW) varlığı ortaya konmuştur. Ayrıca, Doğu Akdeniz’deki birkaç orta ölçekli alanda olduğu bilinen Levant Ara Suyunun (LIW) Kilikya Baseni genelinde ve özellikle de çalışma alanında bölgesel olduğu ilk kez bu çalışmada ortaya konmuştur. KTS çalışması verilerinde dikkat çeken önemli bir olgu, özellikle 2017 ve 2018 yılları yaz aylarında, konservatif yapıdaki deniz suyu tuzluluğunda belirgin artış olması ve üst termoklinde fiziksel oşinografik özelliklerdeki değişiklikler olduğudur.

Anahtar Kelimeler: Oşinografik zaman serisi; Kıbrıs Zaman Serisi (KTS); LIW oluşumu; Tuzluluk değişimi; Fiziksel Oşinografi; Kilikya Baseni; Kuzey Kıbrıs.

TABLE OF CONTENTS

ACKNOWLEDGEMENTS	iv
ABSTRACT	v
ÖZET	vi
TABLE OF CONTENTS	vii
LIST OF TABLES	ix
LIST OF FIGURES	x
LIST OF ABBREVIATIONS	xiv
Chapter 1: INTRODUCTION	1
1.1 General Circulation of the Mediterranean Sea	4
1.2 The Eastern Mediterranean Basin.....	6
1.2.1 Historical Background	7
1.2.2 General Circulation of the Eastern Mediterranean Sea	9
1.2.3 Sub-basin Scale and Meso-scale Circulations of the Eastern Mediterranean Sea	14
1.3 The Levantine Basin	16
1.3.1 The Meteorology of the Levantine Basin	17
1.4 Aim of this Work.....	18
Chapter 2: MATERIAL METHOD	19
2.1 Kıbrıs Time Series Studies	19
2.2 KTS Study Area and Sampling Stations.....	21
2.3 KTS Sampling Strategy	21
2.4 Research Vessel and Instruments	23
2.5 Data Sampling	24

2.6 Data Analyses	25
2.6.1 CTD Data Analyses	25
2.6.2 Meteorological Data	26
Chapter 3: RESULTS	27
3.1 Physical Oceanographic Characteristics of the KTS Region	27
3.2 Time Series Plots of KTS Studies	49
3.2.1 Station K07	49
3.2.2 Station K06	53
3.2.3 Station K05	54
3.2.4 Station K04	55
3.2.5 Station K03	58
3.2.6 Station K02	59
3.2.7 Station K01	61
Chapter 4: DISCUSSIONS	49
4.1 Physical Oceanographic Characteristics of the Study Area	65
4.2 Salinity Shift and Change of Upper Thermocline Characteristics in KTS Area	73
REFERENCES	81

LIST OF TABLES

Table 1.1: Water mass characteristics of the Levantine Intermediate Water (LIW).....	11
Table 2.1: KTS station details.	21
Table 2.2: KTS oceanographic cruise dates.	22
Table 2.3: KTS sampling parameters.	23
Table 2.4: Seabird 19plus V2 SeaCAT profiler technical specifications (from Seabird product manual, version 15, page12).....	24
Table 2.5: Parameters obtained by using “SBE Data Processing” software.	25
Table 2.6: List of meteorological parameters obtained from the T.R.N.C Meteorological Office.	26
Table 4.1: LIW characteristics at KTS station K07.....	69
Table 4.2: Monthly comparison of total annual evaporation between January 2015 to June 2018.....	79
Table 4.3: Total evaporation in oceanographic spring and summer seasons between 2015 and 2018.	80

LIST OF FIGURES

Figure 1.1: The geography and bathymetry of the entire Mediterranean Sea. Modified from (El-Geziry & Bryden, 2010).....	1
Figure 1.2: Schematic representation of general circulation and thermohaline cells of the Mediterranean Sea (Robinson et al., 2001).	3
Figure 1.3: Schematized representation of the mean surface geostrophic circulation in the Mediterranean Sea (Poulain et al., 2010).	3
Figure 1.4: Water masses of the Mediterranean Sea (adapted from http://www.grida.no/resources/5885).	5
Figure 1.5: Levantine Intermediate Water (LIW) circulation at 500m depth in the Mediterranean basin. Adopted from (El-Geziry & Bryden, 2010).....	12
Figure 1.6: The Mediterranean Sea thermohaline circulation scheme. (a) is the behaviour of the Eastern Mediterranean Sea before the EMT. (b) is the behaviour of the Eastern Mediterranean Sea during EMT (Bergamasco & Malanotte-Rizzoli, 2010).....	13
Figure 1.7: Sub-basin scale and mesoscale circulation features in the eastern Mediterranean (Robinson et al., 2001).	15
Figure 1.8: Bathymetry of the Levantine Basin (Özsoy et al., 1991).....	16
Figure 2.1: TUBITAK Project Code No: 114Y139 sampling stations.	20
Figure 2.2: “Kıbrıs Time Series” (KTS) sampling stations within the framework of 114Y139 numbered TUBITAK Project.	20
Figure 3.1: T-S diagram of station K07 throughout the KTS studies, form November 2015 to June 2018.....	27
Figure 3.2: November 2015 cruise results of the station K07. (a): T-S diagram. (b): Temperature vs depth profile. (c) Salinity vs depth profile. (d): Potential density vs depth profile. (e): Oxygen vs depth profile.	28
Figure 3.3: December 2015 cruise results of the station K07. (a): T-S diagram. (b): Temperature vs depth profile. (c) Salinity vs depth profile. (d): Potential density vs depth profile. (e): Oxygen vs depth profile.	30

Figure 3.4: January 2016 cruise results of the station K07. (a): T-S diagram. (b): Temperature vs depth profile. (c) Salinity vs depth profile. (d): Potential density vs depth profile. (e): Oxygen vs depth profile.	30
Figure 3.5: February 2016 cruise results of the station K07. (a): T-S diagram. (b): Temperature vs depth profile. (c) Salinity vs depth profile. (d): Potential density vs depth profile. (e): Oxygen vs depth profile.	31
Figure 3.6: March 2016 cruise results of the station K07. (a): T-S diagram. (b): Temperature vs depth profile. (c) Salinity vs depth profile. (d): Potential density vs depth profile. (e): Oxygen vs depth profile.	32
Figure 3.7: May 2016 cruise results of the station K07. (a): T-S diagram. (b): Temperature vs depth profile. (c) Salinity vs depth profile. (d): Potential density vs depth profile. (e): Oxygen vs depth profile.	33
Figure 3.8: June 2016 cruise results of the station K07. (a): T-S diagram. (b): Temperature vs depth profile. (c) Salinity vs depth profile. (d): Potential density vs depth profile. (e): Oxygen vs depth profile.	34
Figure 3.9: August 2016 cruise results of the station K07. (a): T-S diagram. (b): Temperature vs depth profile. (c) Salinity vs depth profile. (d): Potential density vs depth profile. (e): Oxygen vs depth profile.	35
Figure 3.10: September 2016 cruise results of the station K07. (a): T-S diagram. (b): Temperature vs depth profile. (c) Salinity vs depth profile. (d): Potential density vs depth profile. (e): Oxygen vs depth profile.	36
Figure 3.11: October 2016 cruise results of the station K07. (a): T-S diagram. (b): Temperature vs depth profile. (c) Salinity vs depth profile. (d): Potential density vs depth profile. (e): Oxygen vs depth profile.	37
Figure 3.12: November 2016 cruise results of the station K07. (a): T-S diagram. (b): Temperature vs depth profile. (c) Salinity vs depth profile. (d): Potential density vs depth profile. (e): Oxygen vs depth profile.	38
Figure 3.13: February 2017 cruise results of the station K07. (a): T-S diagram. (b): Temperature vs depth profile. (c) Salinity vs depth profile. (d): Potential density vs depth profile. (e): Oxygen vs depth profile.	39

Figure 3.14: March 2017 cruise results of the station K07. (a): T-S diagram. (b): Temperature vs depth profile. (c) Salinity vs depth profile. (d): Potential density vs depth profile. (e): Oxygen vs depth profile.	40
Figure 3.15: April 2017 cruise results of the station K07. (a): T-S diagram. (b): Temperature vs depth profile. (c) Salinity vs depth profile. (d): Potential density vs depth profile. (e): Oxygen vs depth profile.	42
Figure 3.16: July 2017 cruise results of the station K07. (a): T-S diagram. (b): Temperature vs depth profile. (c) Salinity vs depth profile. (d): Potential density vs depth profile. (e): Oxygen vs depth profile.	42
Figure 3.17: September 2017 cruise results of the station K07. (a): T-S diagram. (b): Temperature vs depth profile. (c) Salinity vs depth profile. (d): Potential density vs depth profile. (e): Oxygen vs depth profile.	43
Figure 3.18: October 2017 cruise results of the station K07. (a): T-S diagram. (b): Temperature vs depth profile. (c) Salinity vs depth profile. (d): Potential density vs depth profile. (e): Oxygen vs depth profile.	43
Figure 3.19: November 2017 cruise results of the station K07. (a): T-S diagram. (b): Temperature vs depth profile. (c) Salinity vs depth profile. (d): Potential density vs depth profile. (e): Oxygen vs depth profile.	44
Figure 3.20: February 2018 cruise results of the station K07. (a): T-S diagram. (b): Temperature vs depth profile. (c) Salinity vs depth profile. (d): Potential density vs depth profile. (e): Oxygen vs depth profile.	45
Figure 3.21: March 2018 cruise results of the station K07. (a): T-S diagram. (b): Temperature vs depth profile. (c) Salinity vs depth profile. (d): Potential density vs depth profile. (e): Oxygen vs depth profile.	46
Figure 3.22: April 2018 cruise results of the station K07. (a): T-S diagram. (b): Temperature vs depth profile. (c) Salinity vs depth profile. (d): Potential density vs depth profile. (e): Oxygen vs depth profile.	47
Figure 3.23: June 2018 cruise results of the station K07. (a): T-S diagram. (b): Temperature vs depth profile. (c) Salinity vs depth profile. (d): Potential density vs depth profile. (e): Oxygen vs depth profile.	48
Figure 3.24: Time series plots of station K07. (a): temperature versus depth, (b): salinity versus depth, (c): potential density versus depth at K07.	50

Figure 3.25: Time series plots of station K06. (a): temperature versus depth, (b): salinity versus depth, (c): potential density versus depth at K06.	52
Figure 3.26: Time series plots of station K05. (a): temperature versus depth, (b): salinity versus depth, (c): potential density versus depth at K05.	56
Figure 3.27: Time series plots of station K04. (a): temperature versus depth, (b): salinity versus depth, (c): potential density versus depth at K04.	57
Figure 3.28: Time series plots of station K03. (a): temperature versus depth, (b): salinity versus depth, (c): potential density versus depth at K03.	60
Figure 3.29: Time series plots of station K02. (a): temperature versus depth, (b): salinity versus depth, (c): potential density versus depth at K02.	62
Figure 3.30: Time series plots of station K01. (a): temperature versus depth, (b): salinity versus depth, (c): potential density versus depth at K01.	64
Figure 4.1: Evaporation and wind speed data from October 2016 to April 2017 (upper figure) and October 2017 to April 2018 (lower figure).	66
Figure 4.2: Water masses defined in the T-S diagram of the KTS studies.	68
Figure 4.3: Salinity profiles of 114Y139 Code numbered TUBITAK Project stations in November 2015.	71
Figure 4.4: Salinity profiles of 114Y139 Code numbered TUBITAK Project stations in October 2016.	71
Figure 4.5: Salinity profiles of 114Y139 Code numbered TUBITAK Project stations in July 2017.	72
Figure 4.6: Salinity profiles of 114Y139 Code numbered TUBITAK Project stations in November 2017.	72
Figure 4.7: Shifts of water mass characteristics between years observed on the T-S diagram of KTS studies.	75
Figure 4.8: Salinity profiles of KTS station K07 during stratified seasons between 2015 and 2018.	76
Figure 4.9: Time series plots of salinity measurements vs depth. (a): Station K01. (b): Station K03. (c): Station K07.	77
Figure 4.10: Total annual evaporation data between January 2015 and January 2018.	79

LIST OF ABBREVIATIONS

AC:	Algerian Current
ADW:	Adriatic Deep Water
AIS:	Atlantic Ionian Stream
AMC:	Asia Minor Current
ASW:	Adriatic Surface Water
AW:	Atlantic Water
CC:	Cilician Current
CC:	Cretan Cyclone
CDW:	Cretan Deep Water
CE:	Cyprus Eddy
Chl-a:	Chlorophyll-a
CIW:	Cretan Intermediate Water
CLBC:	Central Levantine Basin Current
CTD:	Conductivity, Temperature, Depth
dBar:	Decibar
DNA:	Deoxyribonucleic acid
EAG:	Eastern Alboran Gyre
EMDW:	East Mediterranean Deep Water
EMT:	Eastern Mediterranean Transient
EOS-80:	Equation of State 1980
hPa:	Hectopascal
HPLC:	High-Performance Liquid Chromatography
Hz:	Hertz
IA:	Ionian Anticyclones
IG:	Ierapetra Gyre
IOC:	Intergovernmental Oceanographic Commission
ISW:	Ionian Surface Water
ITS-90:	International Temperature Scale 1990
kHz:	kilohertz
KTS:	Kıbrıs Time Series
kW:	Kilowatt
LIW:	Levantine Intermediate Water
LIWEX Group:	Levantine Intermediate Water Experiment Group
LIWEX:	Levantine Intermediate Water Experiment
LSW:	Levantine Surface Water
MAW:	Modified Atlantic Water
MC Series:	Marine Climate Series
METU IMS:	Middle East Technical University, Institute of Marine Sciences
MIJ:	Mid-Ionian Jet
MME:	Mersa-Matruh Eddy
MMJ:	Mid-Mediterranean Jet
NC:	Northern Current
nm:	Nautical Mile

NTG:	North Tyrrhenian Gyre
ODV:	Ocean Data Viewer
ORP:	Oxidation-Reduction Potential
P:	Profile Sampling
PA:	Pelops Anticyclone
PAR:	Photosynthetically Active Radiation
PG:	Pelops Gyre
Phyto:	Phytoplankton
POC:	Particulate Organic Carbon
POEM BC:	Physical Oceanography of the Eastern Mediterranean Biology - Chemistry
POEM:	Physical Oceanography of the Eastern Mediterranean
ppm:	Parts Per Million
PSS78:	Practical Salinity Scale 1978
R/V:	Research Vessel
Redox:	Reduction/Oxidation
RG:	Rhodes Gyre
S/m:	Siemens/meters
S:	Surface Sampling
SAG:	Southern Adriatic Gyre
ShE:	Shikmona Eddy
SST:	Sea Surface Temperature
Sv:	Sverdrup
TLW:	Transition Layer Water
TP:	Total Phosphorus
TRNC:	Turkish Republic of Northern Cyprus
T-S Diagram:	Temperature - Salinity Diagram
TUBITAK:	The Scientific and Technological Research Council of Turkey
UK:	United Kingdom
UNESCO:	The United Nations Educational, Scientific and Cultural Organization
USA:	United States of America
WAC:	Western Adriatic Current
WAG:	Western Alboran Gyre
WCG:	West Cyprus Gyre
WMDW:	West Mediterranean Deep Water
WP2:	Working Party 2
Zoo:	Zooplankton

CHAPTER 1

INTRODUCTION

The Mediterranean Sea is a partially enclosed, practically isolated nonlinear oceanic system which interacts with and exchanges heat, mass and other properties with the North Atlantic Ocean. It is connected to the world ocean through the narrow (~13 km) and shallow (~300 m) Strait of Gibraltar (El-Geziry & Bryden, 2010; Robinson, Leslie, Theocharis, & Lascaratos, 2001). The Mediterranean Sea covers a surface area of about $2.5 \times 10^6 \text{ km}^2$. It is divided into two sub-basins: The Western Mediterranean Basin ($0.85 \times 10^6 \text{ km}^2$) and the Eastern Mediterranean Basin ($1.65 \times 10^6 \text{ km}^2$), linked with the shallow Strait of Sicily where maximum depths are about 500 meters at the western sill (El-Geziry & Bryden, 2010; Hainbucher et al., 2015). The average depth of the Mediterranean Sea is 1500 meters, and the maximum depth is about 5000 meters at the Ionian Sea, in the Eastern Mediterranean Basin (El-Geziry & Bryden, 2010). The geography and bathymetry of the Mediterranean Sea are presented in Figure 1.1.

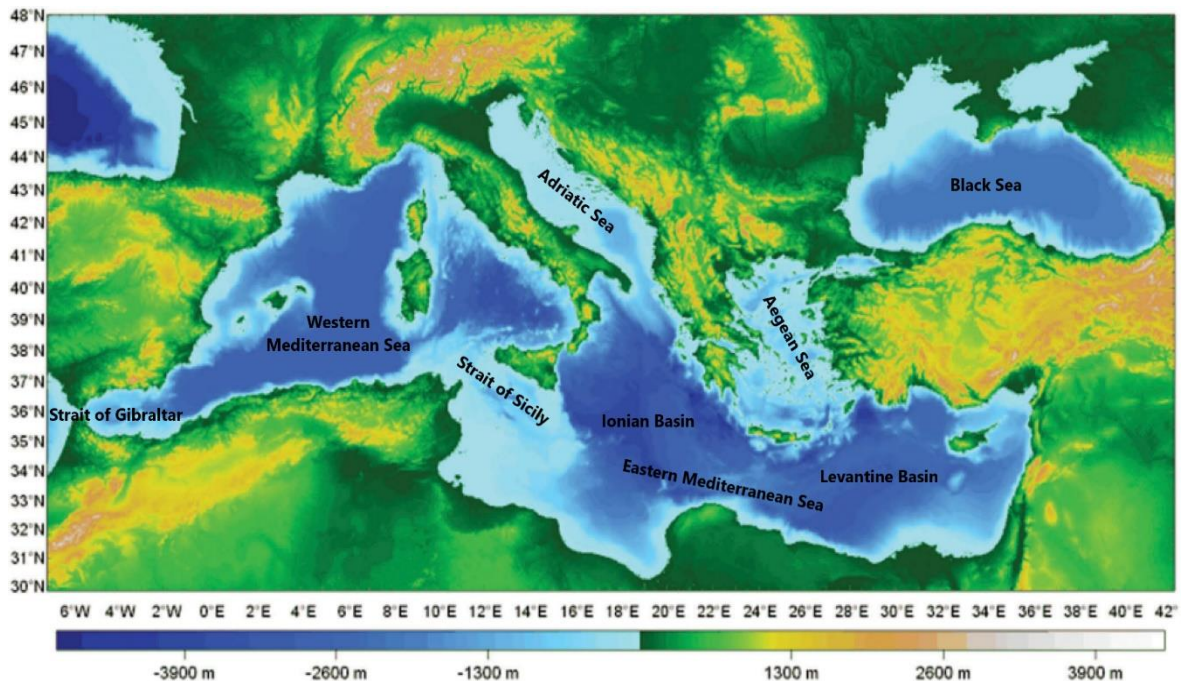


Figure 1.1: The geography and bathymetry of the entire Mediterranean Sea. Modified from (El-Geziry & Bryden, 2010)

The Mediterranean Sea is one of the most important and curious semi-enclosed oceanic systems. It can be considered as a mini oceanic laboratory. Most of the physical processes fundamental to the world ocean also occurs in the Mediterranean Sea either analogously or identically but on smaller spatial and time scales (Marullo, Santoleri, Malanotte-Rizzoli, & Bergamasco, 1999; Robinson et al., 2001; Velaoras, Krokos, Nittis, & Theocharis, 2014). Water mass formations, their transportations, air-sea interactions and multiscale circulations are the most important physical oceanographic components of the Mediterranean Sea (Robinson & Golnaraghi, 1993). Wind stress, buoyancy fluxes and water exchange through the various straits in the Mediterranean Sea are the major forces that affect the general circulation due to heat and freshwater fluxes (Robinson et al., 2001).

The approximate evaporation rate is 1.27 m/year. Precipitation is 0.59 m/year, and river run-off is 0.010 Sverdrup (Sv). Inflow of the Atlantic Water is 0.72-0.92 Sv and outflow of the Mediterranean water is 0.68-0.88 Sv (Robinson et al., 2001; Tanhua et al., 2013). As the evaporation exceeds precipitation and river run-off, the entire Mediterranean Sea is an evaporation (concentration) basin (Malanotte-Rizzoli & Hecht, 1988; Robinson et al., 2001; Tanhua et al., 2013). Heat and freshwater deficits (Pinardi et al., 2015) are balanced by the two-layered fluxes through the Strait of Gibraltar (Hainbucher et al., 2015; Hecht, Pinardi, & Robinson, 1988; Malanotte-Rizzoli & Hecht, 1988; Pinardi et al., 2015; Salihoğlu et al., 1990). The upper layer is the less saline and relatively warm influx of Atlantic Water at surface and subsurface depths. The lower layer is the saltier and relatively colder efflux of Mediterranean Water at intermediate depths which are separated with salinity and temperature gradients at depths of about 150 meters (Malanotte-Rizzoli & Hecht, 1988; Robinson et al., 2001). Particularly the efflux of Mediterranean Water plays an important role. It is balancing the mass deficit of the Mediterranean Sea, and also transports saltier waters to the North Atlantic Ocean, thus contributes to the North Atlantic Deep Water (NADW) formation process and even possibly to the global thermohaline circulation (Bergamasco & Malanotte-Rizzoli, 2010; Malanotte-Rizzoli & Robinson, 1988; Robinson & Golnaraghi, 1993; Velaoras et al., 2014). The Mediterranean Sea is also connected to the Black Sea through the relatively narrow and shallow Turkish Strait System (The Dardanelles/The Marmara Sea/The Bosphorus) and to the Red Sea through the Suez Canal. According to a review by Unluata et al., (1990), in comparison to the Strait of Gibraltar,

water exchanges between the Mediterranean Sea and the Black Sea are relatively small (inflow: 0.039 Sv, outflow: 0.030 Sv) but still significant (Tanhua et al., 2013). Water exchanges through the Suez Canal are not significant due to its small size (Malanotte-Rizzoli & Hecht, 1988).

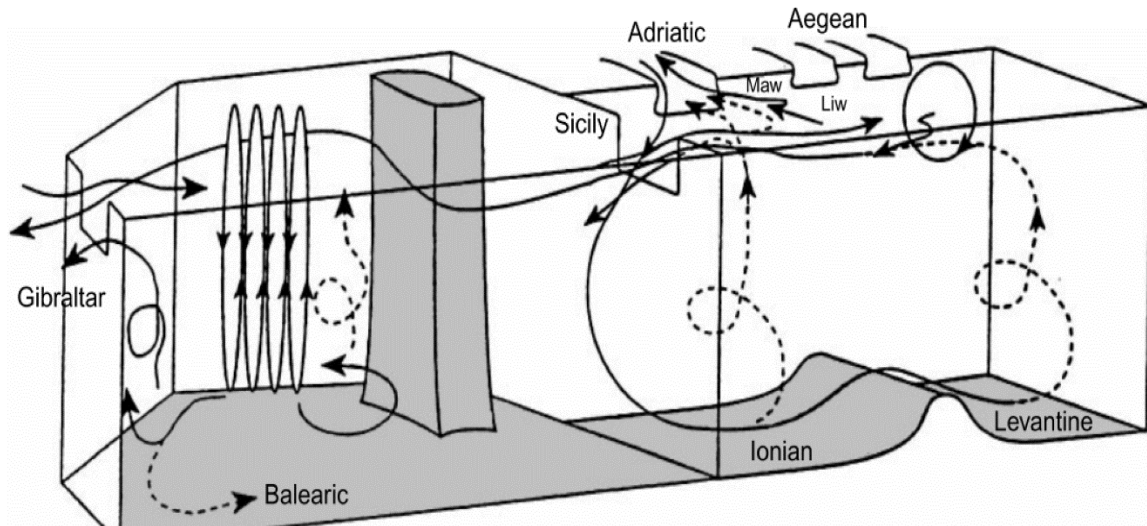


Figure 1.2: Schematic representation of general circulation and thermohaline cells of the Mediterranean Sea (Robinson et al., 2001).

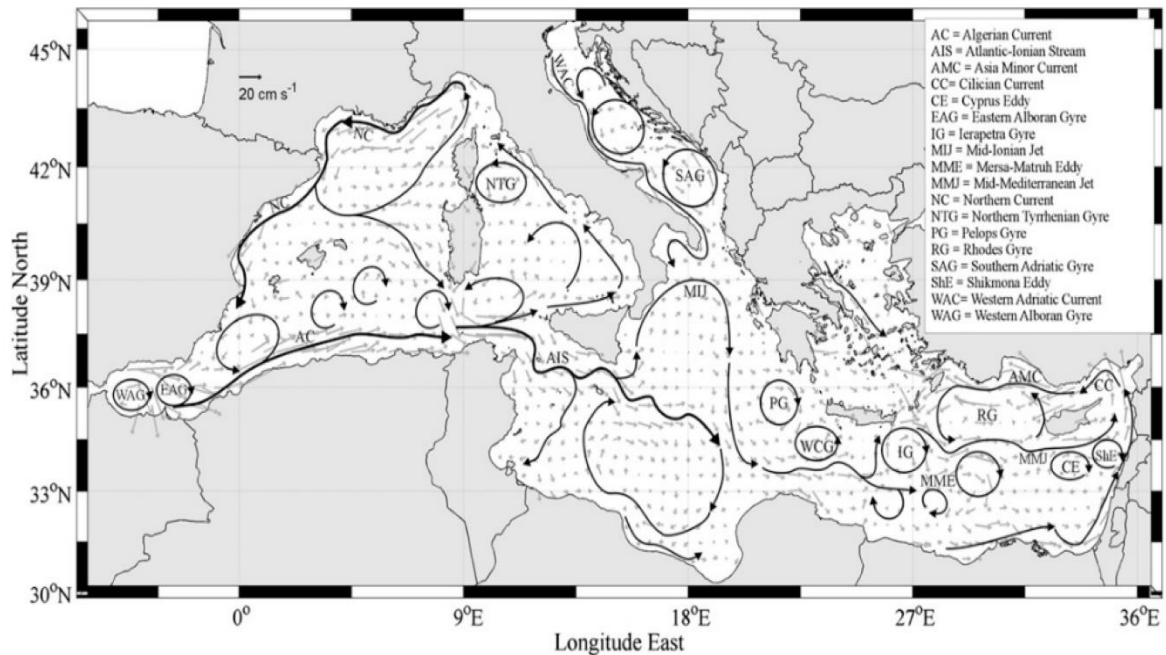


Figure 1.3: Schematized representation of the mean surface geostrophic circulation in the Mediterranean Sea (Poulain et al., 2010).

1.1 General Circulation of the Mediterranean Sea

General circulation of the Mediterranean Sea, including the thermohaline circulation (vertical circulation) (Figure 1.2) is a complex and dynamic system. It composed and interacts on different spatial (i.e. basin scale, sub-basin scale and mesoscale) and temporal scales (Cardin, Civitarese, Hainbucher, Bensi, & Rubino, 2015; Malanotte-Rizzoli & Robinson, 1988; Robinson et al., 1991, 2001; The POEM Group, 1992). The Mediterranean Sea circulation is generally characterised by cyclonic gyres in northern regions and anti-cyclonic gyres in southern regions (Pinardi et al., 2015). General circulation effected by multiple driving forces (i.e. internal dynamics, atmospheric conditions and topography), which forms meandering and bifurcating currents and jets, permanent and quasi-permanent gyres and energetic eddies (Figure 1.3) (Robinson et al., 2001).

As shown in Figure 1.4, the general circulation pattern of the Mediterranean Sea is determined by three distinguished water masses (surface, intermediate and deep waters) which flow separately and independently both in the Eastern and Western Mediterranean basins (El-Geziry & Bryden, 2010; Hecht et al., 1988). In the surface layer, relatively warm and fresh Atlantic Water (AW) inflows to the Mediterranean Sea through the Strait of Gibraltar. It circulates to the easternmost part of the Mediterranean Sea, to the Levantine Basin, between the sea surface and ~150 meters, with an anti-clockwise pattern (El-Geziry & Bryden, 2010; Hecht et al., 1988; Malanotte-Rizzoli & Hecht, 1988; Salihoğlu et al., 1990). Relatively colder and saltier Levantine Intermediate Water (LIW), which forms locally in the Levantine Basin, flows westward from Levantine Basin at intermediate depths, between 150 and 600 meters, and outflows to the Atlantic Ocean through the Strait of Gibraltar (El-Geziry & Bryden, 2010; Hecht et al., 1988; Malanotte-Rizzoli & Hecht, 1988). Due to the shallow sill at the Strait of Sicily, only AW and LIW exchange between Western and Eastern Mediterranean basins (Hecht et al., 1988; Alex Lascaratos, Roether, Nittis, & Klein, 1999; Pinardi et al., 2015). These two water masses, the AW and the LIW at the surface and intermediate depths, characterise the open cell of the upper thermohaline circulation (thermocline circulation) in the Mediterranean Sea. The AW spreading from the Strait of Gibraltar to the Levantine Basin, transforming to LIW by convecting in Levantine Basin and returning to the Atlantic Ocean through the Strait of Gibraltar (Bergamasco & Malanotte-Rizzoli, 2010; Alex Lascaratos et al., 1999).

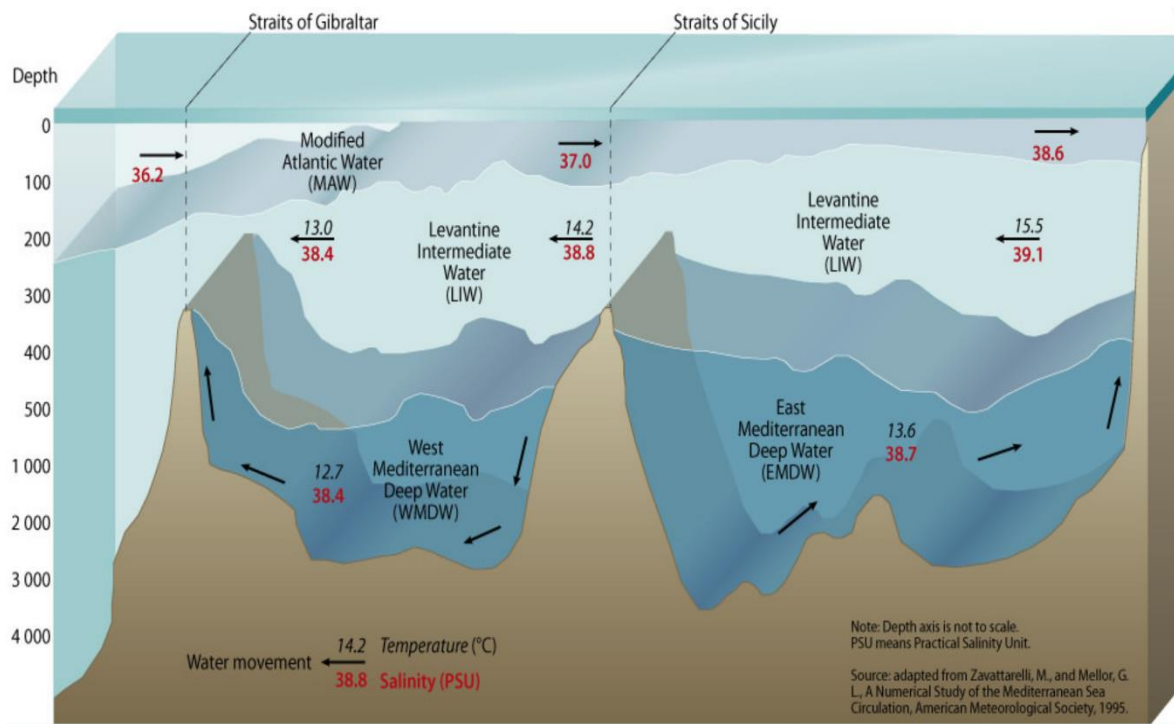


Figure 1.4: Water masses of the Mediterranean Sea (adapted from <http://www.grida.no/resources/5885>).

Since the shallow sill of the Strait of Sicily acts as a natural barrier between the Eastern and the Western Mediterranean Basins, deep waters forms separately and independently both in the Western and the Eastern Mediterranean Basins (Hainbucher et al., 2015; Alex Lascaratos et al., 1999). Closed-cell internal thermohaline circulations and deep-water formations both in Eastern and Western Basins show distinct differences but also some analogies to each other (Hainbucher et al., 2015; Alex Lascaratos et al., 1999; Pinardi et al., 2015; Robinson et al., 2001). Transformation of surface and intermediate waters to the deep waters characterise closed cells of thermohaline circulations both in the Western and the Eastern Basins (Bergamasco & Malanotte-Rizzoli, 2010; Alex Lascaratos et al., 1999). In the Western Basin, deep waters, referred to as the West Mediterranean Deep Water (WMDW), forms in the Gulf of Lions during winter seasons by excessive cooling and evaporation due to local meteorological events, cold and dry northerly winds, the “Mistrals” (Alex Lascaratos et al., 1999). Presence of cyclonic circulation and the LIW at intermediate depths are crucial in the formation of deep waters in the area (Alex Lascaratos et al., 1999). The properties of the East Mediterranean Deep Water (EMDW) and closed cell of thermohaline circulation are discussed in the next sections.

1.2 The Eastern Mediterranean Basin

The Eastern Mediterranean Basin is the largest body of water ($1.65 \times 10^6 \text{ km}^2$) in the Mediterranean Sea which is located at the east of the Sicily Strait (El-Geziry & Bryden, 2010; Malanotte-Rizzoli & Hecht, 1988). The Eastern Mediterranean basin is divided into four sub-basins, namely the Ionian, the Levantine, the Adriatic and the Aegean. The Ionian is the largest and the deepest basin of the Eastern Mediterranean. The Adriatic lies between Italy and the Balkans. It is connected to the Ionian Sea through the Strait of Otranto. The Aegean is connected to the Levantine Basin through straits between Greece, Turkey, Rhodes and Crete. The Levantine Basin, which is the subject of this study, is located at the easternmost part of the Mediterranean Sea. Average depths of the Levantine Basin are 2500 – 3000 meters, with a maximum depth of 4500 meters located southeast of Rhodes (El-Geziry & Bryden, 2010; Malanotte-Rizzoli & Hecht, 1988). Two major sub-basins of the Eastern Mediterranean Sea are the Ionian and Levantine Basins, divided by the wide (300 km) and deep (1800 m) Cretan Passage. However, the flow between these two sub-basins is not significantly affected due to the large size of the Cretan Passage (Malanotte-Rizzoli & Hecht, 1988).

The Eastern Mediterranean Sea is partially enclosed, and exchanges heat, mass and other properties with adjacent seas (i.e. the Black Sea, the Sea of Marmara, the Aegean Sea, the Adriatic Sea, the Levantine and Ionian Seas, the West Mediterranean) (Alhammoud, Béranger, Mortier, Crépon, & Dekeyser, 2005; Malanotte-Rizzoli & Hecht, 1988; Robinson et al., 1991). Hydrography and water masses of the Eastern Mediterranean Sea are characterised by local meteorological events, topographic features and water exchanges between the adjacent seas through the various straits (i.e. the Bosphorus and the Dardanelles, the Rhodes, the Karpathos, the Kassos, the Cretan Passage, the Otranto, the Sicily). These passages and straits control and determine the flow between basins (Cardin et al., 2015; Malanotte-Rizzoli & Hecht, 1988; Robinson et al., 1991). Although it is not adjacent to the Eastern Mediterranean Sea, the Strait of Gibraltar is very important for the Eastern Mediterranean hydrography and water masses. It feeds the Eastern Mediterranean with AW inflow and also connecting and controlling the fluxes between the Mediterranean Sea and the Atlantic Ocean (Malanotte-Rizzoli & Hecht, 1988).

1.2.1 Historical Background

The first oceanographic investigation in the Eastern Mediterranean Sea was carried out by the Austro-Hungarian ship *Pola* back in 1890. In 1912, Nielsen published the first Mediterranean Current Map based on the data collected by the Danish ship *Thor* in 1910 (Özsoy et al., 1991). Nielsen's picture, which for almost 50 years remained the most accepted and approved pattern, was defined the Mediterranean Sea as linear and stationary ocean with broad currents evolving smoothly and forming continuous circulation pattern from the Western to the Eastern Mediterranean Sea (Bergamasco & Malanotte-Rizzoli, 2010). From 1948 to 1968, several oceanographic cruises conducted in the region by different USA ships, French *Calypso* and Japanese *Shoyo-Maru*, but the results of these cruises did not significantly change the Nielsen's pattern (Özsoy et al., 1991).

In 1961, the German oceanographer Georg Wüst discovered the water masses in the Mediterranean Sea as well as their formations, evolutions and properties (salinity, temperature, oxygen). He also discovered the open thermohaline circulation cell of the Mediterranean Sea (Bergamasco & Malanotte-Rizzoli, 2010; Tanhua et al., 2013; Wüst, 1961). In his publication (Wüst, 1961), he presented the inflow of AW, intermediate convection in the Levantine Basin and outflow of the tongue-like LIW to the Atlantic Ocean. In the same publication, he also presented the thermohaline circulation and deep-water formation locations in the Gulf of Lions and Southern Adriatic Sea (Bergamasco & Malanotte-Rizzoli, 2010).

During the mid-sixties, Russian oceanographers, led by Ovchinnikov, analysed the data collected from extensive Vavilov cruises in the Mediterranean Sea and described the driving mechanisms of the Mediterranean Sea circulation, particularly AW and LIW circulation. They presented advanced geopotential maps and more importantly, they revealed the differences between summer and winter circulations (Özsoy et al., 1991).

Since the beginning of the sixties, Israeli oceanographers collected and analysed the data collected in south-eastern Levantine Basin. Contrary to Nielsen's circulation map, they found anti-cyclonic circulation in the region (Özsoy et al., 1991). Beginning from the mid-seventies, Israeli oceanographers started to use modern Conductivity – Temperature – Depth (CTD) methodology. They conducted extensive research, the “Marine Climate (MC

Series)”, over a period for more than five years in the south-eastern Levantine Basin. The results of MC Series revealed an anti-cyclonic pattern in the region with mesoscale eddies, jets and filaments (Özsoy et al., 1991).

Until the beginning of the eighties, Wust’s description remained the undisputed circulation pattern of the Mediterranean Sea (Bergamasco & Malanotte-Rizzoli, 2010). In 1982, an international cooperative research program, the POEM (Physical Oceanography of the Eastern Mediterranean), supported by the IOC of UNESCO was initiated. The program aimed to investigate and determine the circulations patterns, fundamental processes of the Eastern Mediterranean Sea, and also to construct realistic models for physical, chemical and biological studies. Scientists from Turkey, Croatia, Cyprus, Egypt, England, France, Germany, Greece, Israel, Italy, UK and USA participated in the program (The POEM Group, 1992). The first field studies were conducted under the POEM-V program. Five general scientific cruises conducted with oceanographic vessels from Turkey, Israel, Greece, Italy and Germany between 1985 and 1987. Three more general scientific cruises were carried out between 1991 and 1995 under the POEM-BC program, with biological and chemical components. The last fieldwork of the POEM program, the “LIWEX Group (The Levantine Intermediate Water Experiment Group)” was carried out in the winter of 1995 (Bergamasco & Malanotte-Rizzoli, 2010). Basin scale, sub-basin scale and mesoscale upper thermocline circulation of the Eastern Mediterranean Sea, as well as its features, driving dynamics, structure and patterns were revealed by the results of fully reanalysed data of the POEM program. Additionally, results identified the densities of 29.05 – 29.10 kg/m³ is the primary pathway of the LIW. The results also revealed that the Levantine Basin is a region where multiple and different water mass formations occurs (Bergamasco & Malanotte-Rizzoli, 2010; Hecht et al., 1988; Malanotte-Rizzoli & Hecht, 1988; Malanotte-Rizzoli & Robinson, 1988; Özsoy, Hecht, & Ünlüata, 1989; Özsoy et al., 1993; Robinson et al., 1991; The LIWEX Group, 2003; The POEM Group, 1992).

In late nineties and the 2000s, mostly national but also some international oceanographic researches were conducted in the north-eastern Levantine Basin and the Cilician Basin by the oceanographic institutes in Turkey. “Winter circulation and convection in Antalya Basin” (Onken & Yuce, 2000) and “Circulation, hydrographic and nutrient characteristics of the Cilician Basin” (Kucuksezgin & Pazi, 2006) are some of the relevant studies

conducted in the region. In last twenty years, several national and multi-national studies are being continuously carried out by METU IMS in the region. The “Erdemli Time Series” (ETS) study, which is conducting by METU IMS in Mersin Bay over thirty years, is very important for the oceanographic studies in the region.

Most recently, the 114Y139 Code numbered TUBITAK Project (Salihoglu et al., 2019) was carried out in the Cilician Basin to investigate the physical, chemical and biological dynamics of the region.

1.2.2 General Circulation of the Eastern Mediterranean Sea

General circulation of the Eastern Mediterranean Sea is a highly complex and dynamic system. It consists of three different spatial scales (i.e. basin scale, sub-basin scale and mesoscale) in continuous interaction, which determines the general circulation patterns of the Eastern Mediterranean Sea (The POEM Group, 1992). As previously shown in Figure 1.2, the thermohaline circulation consists of an external (open) and an internal (closed) cell. The external thermohaline cell of the Eastern Mediterranean exchange waters with the West Mediterranean, thus with the Atlantic Ocean through the Strait of Sicily and Strait of Gibraltar respectively. The internal thermohaline cell circulates in the Eastern Mediterranean, which comprises the Ionian and the Levantine Basins (The POEM Group, 1992).

Atlantic Water (AW) enters to the Mediterranean Sea through the Strait of Gibraltar with 36.15 - 36.20 per mille of salinity and ~15.0 °C of temperature. It flows eastward with anti-clockwise pattern through the north coast of Africa, penetrates to the Eastern Mediterranean through the Strait of Sicily and spreads to the easternmost part of the Mediterranean Sea, to the Levantine Basin (Figure 1.3) (Bergamasco & Malanotte-Rizzoli, 2010; Hecht et al., 1988). Along its path to the Levantine Basin, AW bifurcates and penetrates to the Balearic Sea, the Tyrrhenian Sea and the Ionian Sea respectively, forms mostly anti-cyclonic gyres and meandering currents (Bergamasco & Malanotte-Rizzoli, 2010; El-Geziry & Bryden, 2010; Hecht et al., 1988; Malanotte-Rizzoli & Hecht, 1988). As it flows eastward, the AW is continuously modifying. Its depth and salinity increase (~37.50 per mille at the Strait of Sicily ~38.60 per mille at the Cretan Passage and >38.60 per mille in the Levantine Basin)

due to atmospheric interactions and mixing with the surface waters and waters underneath, and eventually transform to become Modified Atlantic Water (MAW) (Bergamasco & Malanotte-Rizzoli, 2010; El-Geziry & Bryden, 2010; Hecht et al., 1988; A Lascaratos, Williams, & Tragou, 1993; Malanotte-Rizzoli & Hecht, 1988; Özsoy et al., 1989). Although its salinity increases, MAW still maintains its low salinity characteristic, between 36.15 – 38.70 per mille and can be identified throughout the Mediterranean Sea. It is located just below the warm and saline surface mixed layer, Levantine Surface Water (LSW) in the eastern basin with a salinity of >39.10 per mille and temperature of ~25.0 °C (A Lascaratos et al., 1993), that forms due to excessive heat, evaporation and relatively weak winds during summer season. The LSW thus allows the MAW to maintain its relatively low salinity properties by limiting its atmospheric interaction (Akpınar, Yılmaz, Fach, & Salihoglu, 2016; Malanotte-Rizzoli & Hecht, 1988; Özsoy et al., 1989). During winter intense mixing processes and lower evaporation rates suppress the hot and saline surface water formation (LSW formation), and consequently, MAW depletes faster than in summer (Malanotte-Rizzoli & Hecht, 1988; Özsoy et al., 1989).

Excessive surface heat loss and evaporation due to local meteorological events, cold and dry north-northeasterly winds, the “Poyraz”, cause the LSW to become denser during winter, mix with the MAW and subsequently sink to intermediate depths, forming the Levantine Intermediate Water (LIW) (Akpınar et al., 2016; Bergamasco & Malanotte-Rizzoli, 2010; El-Geziry & Bryden, 2010; Özsoy et al., 1989; Robinson & Golnaraghi, 1993; The LIWEX Group, 2003). Water mass characteristics of the LIW are displayed in Table 1.1. LIW, can be identified throughout the Mediterranean Sea with its subsurface salinity maximum between 38.40 – 39.10 per mille, decreasing towards west (Hecht et al., 1988; Malanotte-Rizzoli & Hecht, 1988). LIW formation is not localised at Rhodes Gyre but occurs at several locations in the northern and southern Levantine basins. (The LIWEX Group, 2003; The POEM Group, 1992). Figure 1.2 The LIW, which is the predominant source of the salty Mediterranean efflux (Alex Lascaratos et al., 1999; Marullo et al., 1999; Robinson & Golnaraghi, 1993; The POEM Group, 1992) flows westward from Levantine Basin to the Strait of Gibraltar, at intermediate depths, between 200 and 600 meters. The LIW circulates below inflowing AW, mixing with the adjacent waters above and underneath, as shown in Figure 1.2. The LIW also mixes with the East Mediterranean Deep Water (EMDW) and the

West Mediterranean Deep Water (WMDW) before outflow to the Atlantic Ocean with 38.40 per mille salinity and ~13.5 °C temperature (Bergamasco & Malanotte-Rizzoli, 2010; El-Geziry & Bryden, 2010; Malanotte-Rizzoli & Hecht, 1988; Robinson & Golnaraghi, 1993; Robinson et al., 2001; The POEM Group, 1992). As shown in Figure 1.5, one branch of the LIW recirculates into the Eastern Mediterranean Sea, one branch enters the Adriatic Sea where it contributes to the deep-water formation, and another branch of the LIW exits through the Strait of Sicily just below inflowing MAW (The POEM Group, 1992). The net influx and efflux through the Strait of Sicily are estimated to be 1 – 1.5 Sv (Robinson & Golnaraghi, 1993; The POEM Group, 1992).

Table 1.1: Water mass characteristics of the Levantine Intermediate Water (LIW).
* adopted from (A Lascaratos et al., 1993).

	Temperature °C	Salinity per mille	Potential Density kg/m ³
*Wust [1961]	15.5	39.10	29.05
*Lacombe and Tchernia [1972]	15.7	39.10	28.98
*Özturgut [1976]	16.2 – 16.4	39.12 - 39.15	28.85 - 28.87
*Ovchinnikov [1984]	14.7 – 14.9	39.03 - 39.06	29.12 - 29.15
*Plakhin and Smirnov [1984]	14.5	38.85	29.06
*Hecht [1986]	15.5 ± 0.4	39.02 ± 0.05	28.91 - 29.01
*Hecht et al. [1988]	15.5 ± 0.5	38.98 ± 0.06	28.86 - 28.99
Küçüksezgin and Pazi [2006]	16.0 – 17.0	39.10 – 39.20	28.90 – 29.20
Salihoğlu et al. [2019]	16.0 – 17.0	39.10	28.87
This study [2015 – 2016]	~16.50	~39.10	~28.87
This study [2017]	~17.50	~39.21	~28.65
This study [2018]	~18.50	~39.39	~28.50

With the preconditioning of density increase due to saltiness, the internal thermohaline cell of the Eastern Mediterranean Basin is similar to the global “conveyor belt” in the North Atlantic but smaller in scale, with ~125 years of renewal time (Bergamasco & Malanotte-Rizzoli, 2010; Robinson & Golnaraghi, 1993; The POEM Group, 1992). Traditionally, the

driving source of the internal thermohaline cell of the Eastern Mediterranean is the Adriatic Deep Water (ADW). It formed in the South Adriatic Sea during winter time when waters become denser and sink as a result of cooling and evaporation due to local meteorological events, cold and dry northerly winds, the "Bora" (Bergamasco & Malanotte-Rizzoli, 2010; Alex Lascaratos et al., 1999; Pinardi et al., 2015; Robinson et al., 2001; The POEM Group, 1992). Similar to the Western Basin, open ocean formation processes occur in this area with preconditioning of cyclonic gyre and with contributions of MAW and LIW (Alex Lascaratos et al., 1999; Robinson et al., 2001). ADW spreads out through the Otranto Straits, fills the deepest parts of the Ionian Sea and the Levantine Sea respectively and forms the East Mediterranean Deep Water (EMDW) (Bergamasco & Malanotte-Rizzoli, 2010; Alex Lascaratos et al., 1999; Robinson et al., 2001).

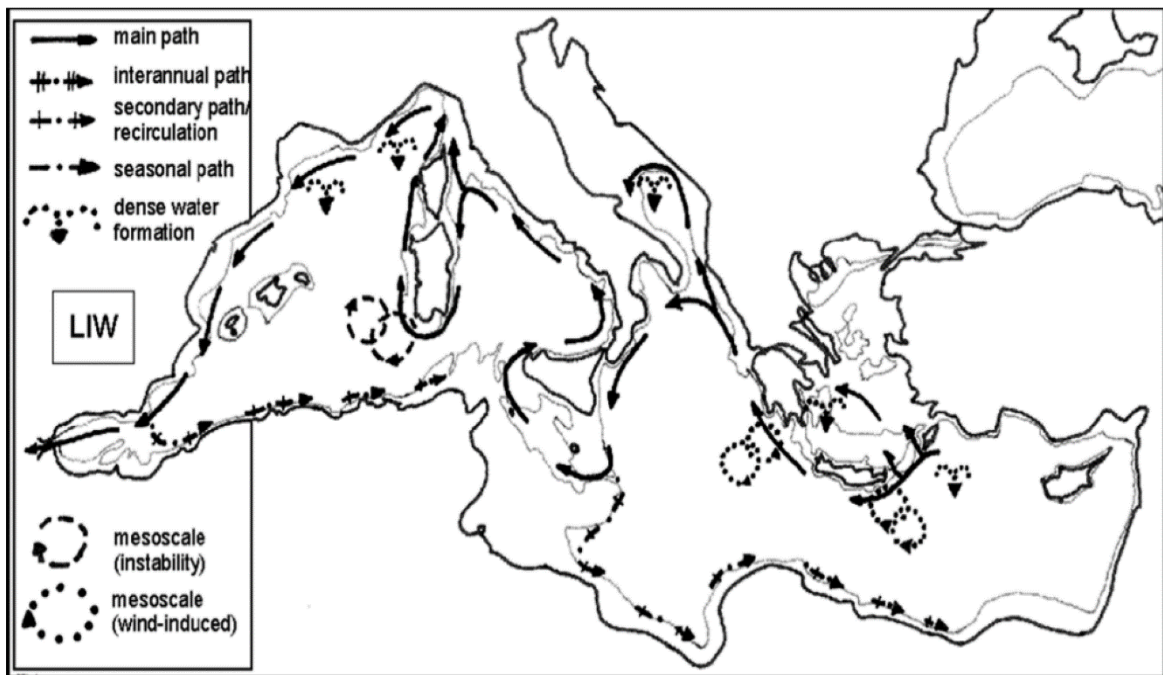


Figure 1.5: Levantine Intermediate Water (LIW) circulation at 500m depth in the Mediterranean basin. Adopted from (El-Geziry & Bryden, 2010).

In late 1980's and early 1990s, the POEM group identified warmer, high saline and denser water mass formations in the Southern Aegean Sea or the Cretan Sea. They also identified a transition, later named as Eastern Mediterranean Transient (EMT) that shifts the driving source of deep waters from the South Adriatic Sea to the South Aegean Sea or Cretan Sea

(Figure 1.6) (Bergamasco & Malanotte-Rizzoli, 2010; Robinson et al., 2001). These denser waters, namely Cretan Intermediate Water (CIW) and Cretan Deep Water (CDW), formed in the Cretan Sea due to continuous salinity increases and excessive cooling in the area, spread out through the Cretan Arc Straits to the Ionian and Levantine Basins below the EMDW of Adriatic origin (Bergamasco & Malanotte-Rizzoli, 2010; Alex Lascaratos et al., 1999; Robinson et al., 2001). This transition replaced the old EMDW of Adriatic origin by lifting it several hundred meters in the water column and consequently changing the characteristics of intermediate and deep waters of the Eastern Mediterranean, even possibly the characteristics of the entire Mediterranean Sea (Bergamasco & Malanotte-Rizzoli, 2010; Alex Lascaratos et al., 1999; Robinson et al., 2001).

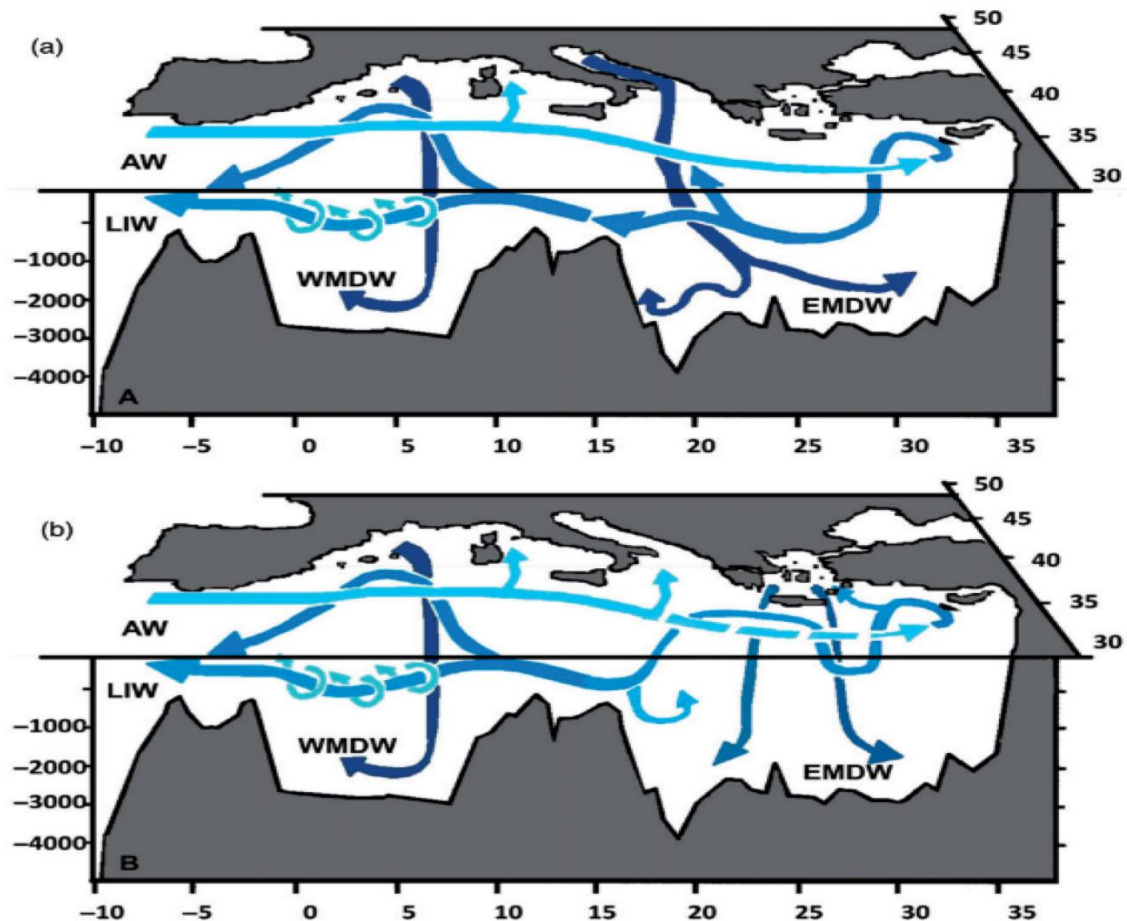


Figure 1.6: The Mediterranean Sea thermohaline circulation scheme. (a) is the behaviour of the Eastern Mediterranean Sea before the EMT. (b) is the behaviour of the Eastern Mediterranean Sea during EMT (Bergamasco & Malanotte-Rizzoli, 2010).

1.2.3 Sub-basin Scale and Meso-scale Circulations of the Eastern Mediterranean Sea

Circulation patterns of the Eastern Mediterranean Basin are characterised by energetic sub-basin scale cyclonic and anti-cyclonic gyres which are linked by interconnecting jets and currents with variable structures (i.e. spatial and temporal variabilities, shape, strength, meander pattern and bifurcation structure) (Robinson et al., 2001; The POEM Group, 1992). The major gyres and streams which determine the main thermocline circulation pattern are shown in Figure 1.7. The anti-cyclonic Ionian and Pelops gyres and cyclonic Cretan gyre are located in the Ionian Basin. The cyclonic Rhodes gyre, anti-cyclonic Mersa-Matruh gyre and anti-cyclonic Shikmona eddy are located in the Levantine Basin, Atlantic-Ionian Stream (AIS), Mid-Ionian Jet (MIJ), Mid-Mediterranean Jet (MMJ), Asia-Minor Current (AMC) and the Cilician Current (CC) are the major streams flows in the Eastern Mediterranean Basin (Robinson et al., 2001; The POEM Group, 1992).

Atlantic originated MAW penetrates to the Eastern Mediterranean Sea by AIS through the Strait of Sicily. It meanders first to the north into the northern Ionian Sea then to the southeast to feed the MMJ. It continues to flow eastward through the Cretan Passage between Rhodes and Mersa-Matruh gyres to the easternmost part of the Levantine Basin (Bergamasco & Malanotte-Rizzoli, 2010; Robinson et al., 2001; The POEM Group, 1992). According to Bergamasco & Malanotte-Rizzoli (2010), the stream which forms sharp meanders in the Ionian Sea is named as MIJ and then it becomes MMJ, referred as Central Levantine Basin Current (CLBC) in (Özsoy et al., 1993; The LIWEX Group, 2003), before entering the Cretan Passage. Along its path, some part of MMJ encircles the Rhodes Gyre and eventually connects with westward flowing AMC, and some part encircles the Mersa-Matruh Gyre (Özsoy et al., 1993). MMJ bifurcates once more at the southwest of Cyprus where one branch flows northward through the west of Cyprus to feed the AMC (Özsoy et al., 1993; Robinson et al., 2001; The POEM Group, 1992). The second branch continues to flow east through south of Cyprus to the coasts of Israel where it bifurcates again to the north to feed the CC which feeds the AMC, and to the south to the Shikmona eddies (Robinson et al., 2001; The POEM Group, 1992).

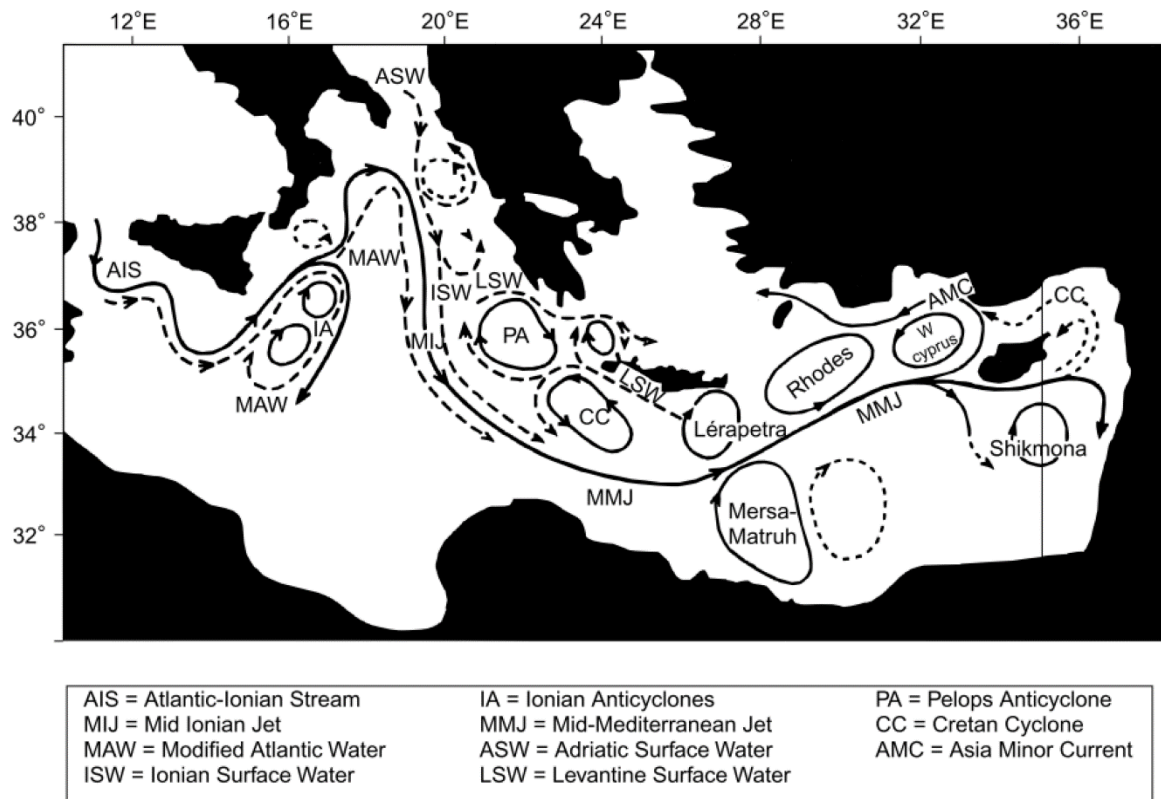


Figure 1.7: Sub-basin scale and mesoscale circulation features in the eastern Mediterranean (Robinson et al., 2001).

In the Ionian Basin, a broad and multi-centred Ionian anti-cyclonic system is located at the northwest Ionian Sea. Quasi-permanent anti-cyclonic Pelops and cyclonic Cretan gyres are located at the south of Peloponnesus Peninsula and Crete respectively (Bergamasco & Malanotte-Rizzoli, 2010). In the Levantine Basin, the region between Rhodes and Cyprus is a broad cyclonic region, consist of few cyclonic centres including the Rhodes Gyre which the AMC is the northern border and the West Cyprus Gyre (WCG). Meso-scale and quasi-permanent anti-cyclonic eddies of Ierapetra, Antalya and Anaximander located in the southeast of Crete, in Antalya Basin and between the Anaximander Seamount and Turkish coast, respectively (Onken & Yuce, 2000). Mersa-Matruh is a strong anti-cyclonic gyre located off the Egyptian coast. Quasi-permanent Shikmona eddies are part of south-eastern Levantine anti-cyclonic system at south of Cyprus (Robinson et al., 2001; The POEM Group, 1992). Generally, the diameter of the sub-basin scale gyres varies between 200 and 350 km (Robinson et al., 2001). The average speed of the sub-basin scale gyres and jets in upper thermohaline is ~20 cm/s (Robinson et al., 2001; The POEM Group, 1992).

1.3 The Levantine Basin

As mentioned above, the Levantine Basin is the easternmost part of the Mediterranean Sea, encircled by northeast Africa, Asia Minor and Cretan Archipelago. It is the second-largest sub-basin of the Eastern Mediterranean Sea with a total volume of $7.5 \times 10^5 \text{ km}^3$. Levantine Basin communicates with the Ionian Basin through the Cretan Passage and with the Aegean Sea through the straits of Rhodes, Karpathos and Kassos. The continental shelf of the Levantine Basin is generally narrow except for the Gulf of Iskenderun and the Nile Fan. Major bathymetric features are shown in Figure 1.8; the Hellenic Trench (3000 – 3500 m) and the Herodotus Abyssal Plain (~3000 m) which are separated by the Mediterranean Ridge (~2500 m). Distinct sub-basins are the Rhodes (~4000 m), the Antalya (~2500 m), the Lattakia (~1500 m) and the Cilician (~1000 m), which is the particular subject of this study. The Anaximander Seamount (~1500 m), located between Rhodes and Antalya and the Eratosthenes Seamount (1000 m), located at the south of Cyprus are the other bathymetric features of the Levantine Basin (Özsoy et al., 1989).

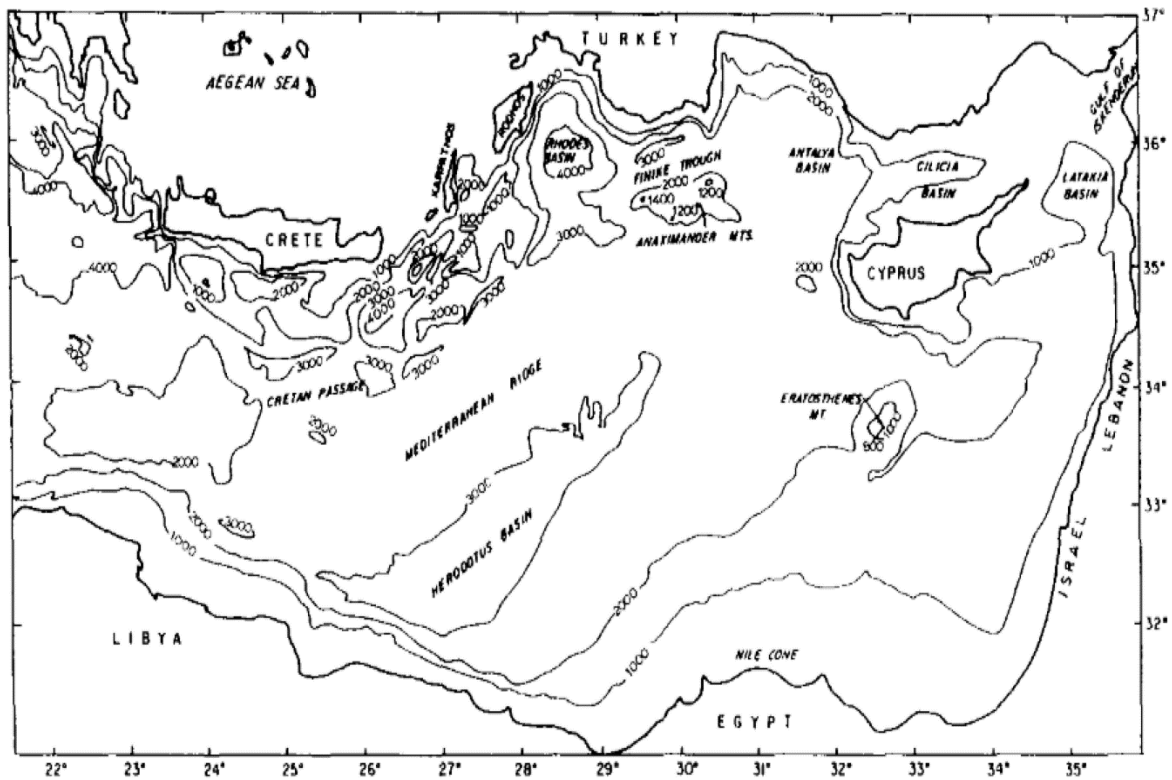


Figure 1.8: Bathymetry of the Levantine Basin (Özsoy et al., 1991).

The Cilician Basin is the north-eastern part of the Levantine Basin, located between the north of Cyprus and south of Turkey, from Antalya Basin to the Iskenderun Bay. The circulation of the Cilician Basin is a highly complex and dynamic system, with meandering and reversing currents and reappearing cyclonic/anti-cyclonic energetic mesoscale eddies with temporal variabilities (Kucuksezgin & Pazi, 2006; Özsoy et al., 1989, 1991). It is connected with the Lattakia Basin by a narrow sill with depths of ~ 700 meters extending from Cyprus (Cape Andreas) to Iskenderun at the east. At the west, it is connected with Antalya Basin through sharp depth gradients from 1000 meters to 2000 meters (Özsoy et al., 1989).

1.3.1 The Meteorology of the Levantine Basin

Meteorological events in the Levantine Basin shows extreme variabilities due to different atmospheric systems and the topography of the region (Akpınar et al., 2016; Özsoy et al., 1989). Summer and autumn seasons are dominated by Westerlies, Etesian and coastal sea breeze system. Northerly Etesian winds in the southern Aegean Sea reinforce dominant Westerlies which result in a west-northwest wind regime blowing over the Levantine Basin. On the other hand, extratropical cyclones and dry local wind systems, such as Poyraz and Sirocco winds, dominates the region during winter and spring seasons. (Özsoy et al., 1989). Extratropical cyclones arrive to the northern Levantine Basin mostly from the Ionian Basin but also North Africa. Following the cyclones, cold and dry north-northeasterly Poyraz winds blow from the Taurus Mountains at the southeast coast of Turkey. The "Poyraz" wind causes excessive heat and buoyancy losses, which affect the oceanographic variability of the entire region (Özsoy et al., 1989). These significant buoyancy losses due to strong cold and dry winds are considered as the primary source of the LIW formation in the area (Onken & Yuce, 2000; Özsoy et al., 1989; Wüst, 1961). Warm and dry southerly winds, the Sirocco winds, blow from north African and Arabian Deserts, advecting warm and dry air masses to the region, and become humid at the northern Levantine Basin (Özsoy et al., 1989).

1.4 Aim of this Work

This study aims to investigate the formation and dissipation of sub-mesoscale and mesoscale physical oceanographic features, their temporal and spatial variabilities, and the interactions between coastal and open water masses off the coast of Kyrenia, Cyprus. Also, to understand physical oceanographic characteristics of the region and to determine any significant changes occurred since previous regional studies.

CHAPTER 2

MATERIALS AND METHODS

The oceanographic data presented in this study were collected within the framework of TUBITAK Project Code No:114Y139, entitled “Determination of the influence of anthropogenic and natural processes on the Cilician Basin (Between Turkish Republic of Northern Cyprus and Turkey) Marine Ecosystem”.

The project has been carried out from June 2015 to May 2018 in the Cilician Basin, to investigate physical and biogeochemical properties of the region. During the study, a total of eleven seasonal cruises conducted at a total of twenty-six stations (denoted as “T” and “A” stations in Figure 2.1). A further achievement of the project worth mentioning here is the first oceanographic time-series study of the Turkish Republic of Northern Cyprus (T.R.N.C), namely the “Kıbrıs Time Series (KTS)”, was established in November 2015, offshore of Kyrenia (denoted as “K” stations in Figure 2.2).

2.1 Kıbrıs Time Series Studies

Historically the first oceanographic time-series study, “Kıbrıs Time Series” (KTS) of the Turkish Republic of Northern Cyprus (T.R.N.C.), was established under the framework of TUBITAK Project 114Y139. KTS studies were the first oceanographic studies conducted by a local university in the Turkish Republic of Northern Cyprus. KTS studies have been conducted monthly to investigate physical and biogeochemical properties and variabilities of the study area, and to investigate spatial and temporal interactions between coastal and open sea waters in the area. In this scope, highly systematic and comprehensive researches were conducted under the KTS studies. The first KTS cruise was conducted on 12th of November 2015, and a total of twenty-six cruises were conducted during the project. Although the TUBITAK Project Code No: 114Y139 had been terminated, KTS studies continue to be carried out by the own sources of the University of Kyrenia (UoK).

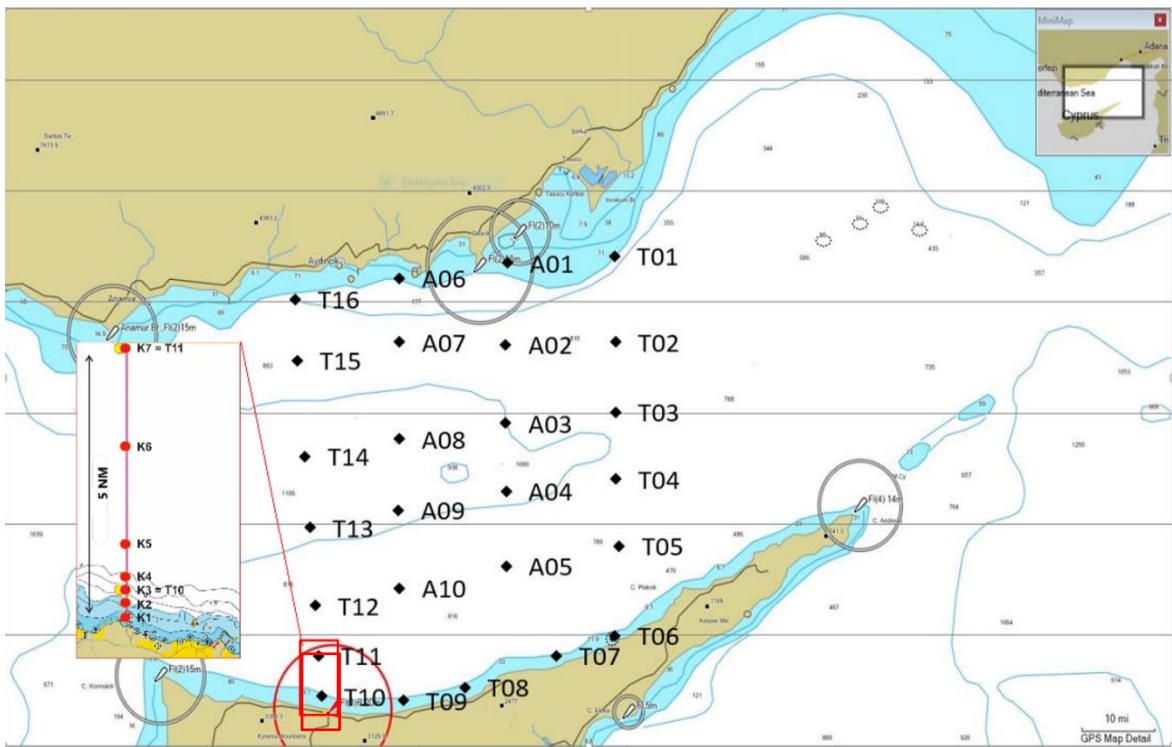


Figure 2.1: TUBITAK Project Code No: 114Y139 sampling stations.

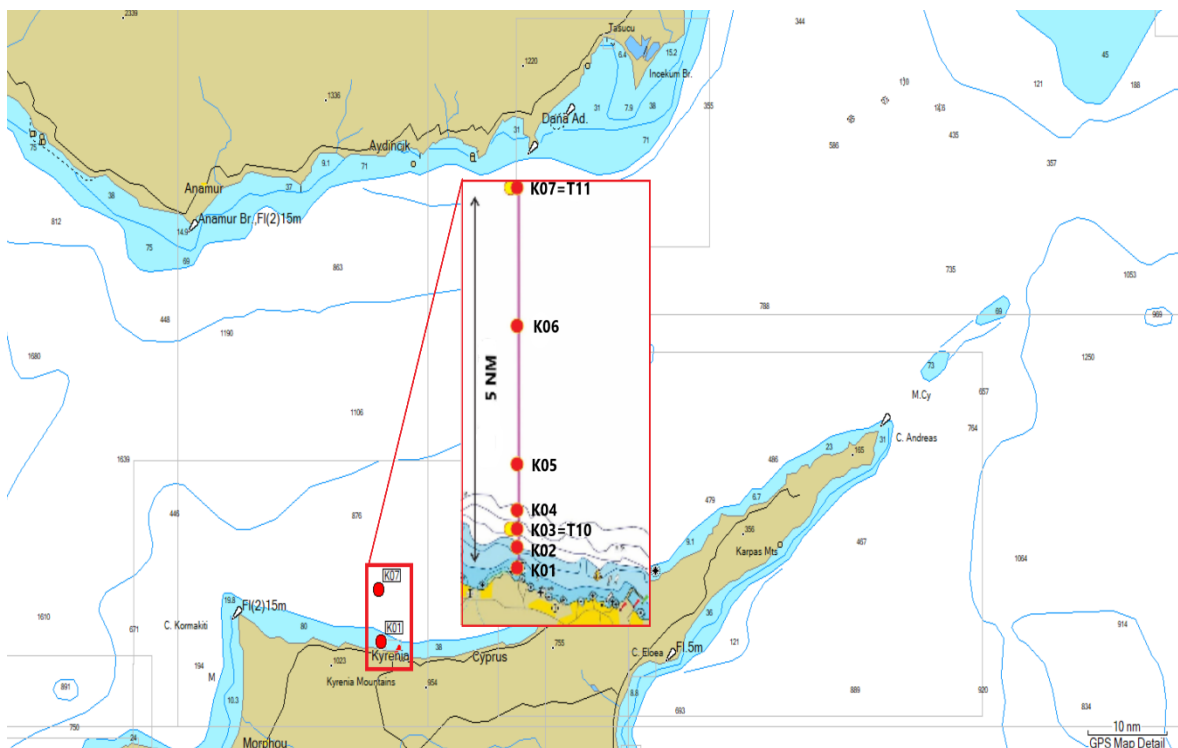


Figure 2.2: “Kıbrıs Time Series” (KTS) sampling stations within the framework of 114Y139 numbered TUBITAK Project.

2.2 KTS Study Area and Sampling Stations

KTS study area is geographically located 2.5 nautical miles (nm) west of Kyrenia Port, offshore of Yılan Adası (Figure 2.1). KTS studies were conducted at seven stations (K01 to K07) on a 5 nm zonal transect, offshore of Kyrenia. Station details are given in Table 2.1.

Since the continental shelf of the region is narrow and deepening rapidly towards offshore, the coastal stations K01, K02, K03 and K04 are distributed within about 0.5 nm to cover the shallow zone as well, so they are very close to each other. While stations K05, K06 and K07 are located respectively at 1.5, 3.5 and 5 nm from the coastline.

Table 2.1: KTS station details.

Station Name	Total Depth	Latitude / Longitude
K01	25 meters	35 21.171 N / 033 17.732 E
K02	50 meters	35 21.339 N / 033 17.710 E
K03	100 meters	35 21.572 N / 033 17.703 E
K04	150 meters	35 21.679 N / 033 17.726 E
K05	425 meters	35 22.525 N / 033 17.671 E
K06	610 meters	35 24.491 N / 033 17.439 E
K07	670 meters	35 26.218 N / 033 17.283 E

2.3 KTS Sampling Strategy

The first KTS cruise was carried out in November 2015. Since then, a total of twenty-seven monthly cruises were conducted until June 2018 (Table 2.2). The K01, K03 and K07 stations were sampled in a way to get a depth profile data, so they were assigned as profile (P) stations. At the stations K02, K04, K05 and K06 only sub-surface samples were collected so they were assigned as surface (S) stations. Detailed description of physical and biogeochemical studies conducted in KTS studies are given in Table 2.3.

Due to its aim, only the physical variables and parameters of the KTS studies were discussed in this study. Biochemical data were used to support the findings, whenever necessary.

Table 2.2: KTS oceanographic cruise dates.

Cruise No	Cruise Code	Cruise Date
1	KTS201511	12-13 November 2015
2	KTS201512	09 December 2015
3	KTS201601	29-30 January 2016
4	KTS201602	17 February 2016
5	KTS201603	9 March 2016
6	KTS201605	31 May 2016
7	KTS201606	13 June 2016
8	KTS201608	08-09 August 2016
9	KTS201609	10-11 September 2016
10	KTS201610	11 October 2016
11	KTS201611	25-26 November 2016
12	KTS201612	20 December 2016
13	KTS201701	23 January 2017
14	KTS201702	25-27 February 2017
15	KTS201703	28 March 2017
16	KTS201704	27 April 2017
17	KTS201705	25 May 2017
18	KTS201706	30 June 2017
19	KTS201707	24 July 2017
20	KTS201709	18 September 2017
21	KTS201710	19 October 2017
22	KTS201711	15 November 2017
23	KTS201801	16 January 2018
24	KTS201802	24 February 2018
25	KTS201803	27 March 2018
26	KTS201804	25-26 April 2018
27	KTS201806	27 June 2018

Table 2.3: KTS sampling parameters.

Station	CTD	pH	Dissolved Oxygen	Nutrients	TP	Chl-a	POC	Pigment HPLC	Phyto*	Zoo	Genetic DNA
K01	P	P	P	P	p ¹	P	p ¹	P	P	P	p ²
K02	P	S	P	S	-	S	-	S	S	-	-
K03	P	P	P	P	p ¹	P	p ¹	P	P	P	p ²
K04	P	S	P	S	-	S	-	S	S	-	-
K05	P	S	P	S	-	S	-	S	S	-	-
K06	P	S	P	S	-	S	-	S	S	-	-
K07	P	P	P	P	p ¹	P	p ¹	P	P	P	p ²

P: Profile Sampling

P: Profile

Discrete Sampling Depths

K01: 0, 10, 25m

K03: 0, 10, 25, 50, 75, 100m

K07: 0, 10, 25, 50, 75, 100, 125, 150, 200m

K02, K04, K05, K06: 0m

S: Surface Sampling

P¹: POC / TP profile

Discrete Sampling Depths

K01¹: 0, 10, 25m

K03¹: 0, 10, 50, 100m

K07: 0, 10, 50, 100, 200m

P²: DNA Profile

Discrete Sampling Depths

K01²: 15m

K03²: 10, 65m

K07²: 10, 50, 150m

Phyto*: *heterotrophic bacteria, flagellates, Synechococcus, diğerleri

2.4 Research Vessel and Instruments

R/V Teal Jr is the first registered research vessel of Turkish Republic of Northern Cyprus, owned and operated by University of Kyrenia. She is a 13.5 meters ex-trawler, modified and equipped with oceanographic research purposes. She has 8 knots cruising speed and about 250 litres per day diesel oil consumption with 1000 litres diesel oil capacity.

She is equipped with two Raymarine 50 – 250 kHz echo sounders. Raymarine E7 Model is the main echo sounder with 1 kilowatt (kW) transducer and the second one, Raymarine Dragon Fly Model, is installed with down vision Chirp Sonar. A hydraulic driven winch system with 1000 meters of 6 millimetres chrome cable, installed to deploy oceanographic instruments such as CTD (Conductivity, Temperature, Depth profiler without rosette sampler), 5 Litre capacity Niskin bottles, WP2 zooplankton net and sediment grab sampler. Main oceanographic instruments on R/V Teal Jr are; Seabird 19 plusV2 SeaCAT profiler, five litres Niskin bottles, WP2 zooplankton net and Hydrobios sediment grab sampler.

CTD was used to obtain a depth profile of the water column from the surface to the bottom. Niskin bottles used to collect water samples from designated depths (discrete seawater

sampling) and in each station and WP2 zooplankton net used for vertical sampling of the water column from designated depth to surface. A small wet lab with is equipped with a vacuum filtering apparatus, having the capacity of 12 filtering unit. A deep freezer, cooling to -22 °C, allows storage of the water samples, filtered samples and processed or non-processed other samples. With these specifications and instruments, R/V Teal Jr is capable of conducting about four days of continuous research cruises in territorial waters.

Table 2.4: Seabird 19plus V2 SeaCAT profiler technical specifications (from Seabird product manual, version 15, page12).

	Temperature (°C)	Conductivity (S/m)	Pressure
Measurement Range	-5 to +35	0 to 9	0 to full scale range: • <i>Strain-gauge sensor</i> : 20 / 100 / 350 / 600 / 1000 / 2000 / 3500 / 7000/10.500 meters
Initial Accuracy	± 0.005	± 0.0005	• <i>Strain-gauge sensor</i> : ± 0.1% of full scale range
Typical Stability	0.0002/month	0.0003/month	• <i>Strain-gauge sensor</i> : 0.1% of full scale range/year
Resolution	0.0001	<ul style="list-style-type: none"> • 0.00005 (most oceanic water; resolves 0.4 ppm in salinity). • 0.00007 (high salinity water; resolves 0.4 ppm in salinity). • 0.00001 (fresh water; resolves 0.1 ppm in salinity). 	• <i>Strain-gauge sensor</i> : 0.002% of full scale range
Sensor Calibration (measurement outside these ranges may be at slightly reduced accuracy due to extrapolation errors)	+1 to +32	0 to 9; physical calibration over range 2.6 to 6 S/m, plus zero conductivity (air)	Ambient pressure to full scale range in 5 steps
Real-Time Clock	32,768 Hz TCXO accurate to ±1 minute/year		
Sampling Speed	4 Hz (4 samples/sec)		
Memory	64 Mbyte non-volatile FLASH memory; maximum of 1000 cast headers		

2.5 Data Sampling

In every cruise and at every station of KTS studies, the CTD, Seabird 19plus V2 SeaCAT Model profiler, equipped with seawater conductivity, temperature, pressure, dissolved oxygen, turbidity, PAR and fluorescence sensors was used to measure and obtain the water column vertical profile from sea surface to the sea bottom. In addition to those sensors, pH and Oxidation Reduction Potential (ORP) sensor installed and used since January 2018. Sampling speed of the CTD was four samples per second, and the downcast and upcast winch speed was between 0.6 and 1.0 meter per second (m/s). Both downcast and upcast data were measured and stored into the CTD memory. Technical specification of CTD are given in Table 2.4. At the end of each cruise, all downcast and upcast data stored in CTD memory had been uploaded to a computer with the aid of Seaterm V2 (Version 2.6.3.104) software.

2.6 Data Analyses

2.6.1 CTD Data Analyses

The recorded CTD data were processed by using SBE Data Processing software (Version 7.26.7). Seven different processing steps had been used to obtain the best average data from the raw data. Total of sixteen different parameters were obtained by using SBE Data Processing software (Table 2.5). Sensors directly measured nine of these parameters and seven were calculated from CTD measurements by using SBE Data Processing software. Salinity and density values had been calculated from CTD measurements during data processing, by using Practical Salinity Scale 1978 (PSS78) (Fofonoff, 1985; Millero, 2011) and Equation of State 1980 (EOS-80) formula (Fofonoff, 1985; Millero, 2011), respectively.

Excel databases had been created by combination of processed CTD data and relevant cruise data (cruise name, date, time, station position and station bottom depth) for each KTS cruise. Furthermore, these databases were imported to Ocean Data Viewer (ODV) software (Version 5.1.0) and Sigma Plot software (Version 14.0) to create appropriate graphics and plots of each parameter.

Table 2.5: Parameters obtained by using “SBE Data Processing” software.

No	Parameter Name	Method	No	Parameter Name	Method
1	Pressure	Sensor	9	Redox	Sensor
2	Temperature	Sensor	10	Salinity	Calculated
3	Conductivity	Sensor	11	Potential Temperature	Calculated
4	Turbidity	Sensor	12	Potential Density	Calculated
5	Fluorescence	Sensor	13	Oxygen	Calculated
6	PAR (Photosynthetically Active Radiation)	Sensor	14	Oxygen Saturation	Calculated
7	Oxygen raw	Sensor	15	Depth	Calculated
8	pH	Sensor	16	Decent rate	Calculated

2.6.2 Meteorological Data

The meteorological data used in this study was obtained from the Meteorological Office of Turkish Republic of Northern Cyprus (KKTC Meteoroloji Dairesi). The meteorological station is located in Port of Kyrenia, about 2.5 nm east of the KTS site. Detailed list of meteorological parameters obtained from meteorological office is given in Table 2.6.

Table 2.6: List of meteorological parameters obtained from the T.R.N.C Meteorological Office.

Parameter	Unit	Date From	Date To
Wind Direction	degrees	01/08/2016	31/06/2018
Wind Speed	m/s	01/08/2016	31/06/2018
Wave Hight	m	01/08/2016	31/06/2018
Evaporation	mm	01/01/2015	31/06/2018
Mean Pressure	hPa	01/01/2015	31/06/2018
Sea Surface Temperature	°C	01/01/2015	31/06/2018
Air Temperature	°C	01/01/2015	31/06/2018
Humidity	per cent	01/01/2015	31/06/2018

CHAPTER 3

RESULTS

3.1 Physical Oceanographic Characteristics of the KTS Region

Station K07 is located at such a depth (about 670 m) that it contains all water masses of interest in the present study. The results of station K07 are presented in this section. Temperature - Salinity (T-S) diagrams, temperature [°C], salinity [per mille], potential density [kg/m^3], and dissolved oxygen [mg/l] versus depth profiles are presented to describe seasonal and annual mixing processes, stratification processes, presence of the LIW and all other water masses (i.e. LSW, MAW and EMDW) at station K07.

Figure 3.1 shows that LIW and all other water masses of the Levantine Basin (i.e. LSW, MAW and EMDW) were present in the area throughout the study, but were most pronounced and had identical properties in 2015 and 2016.

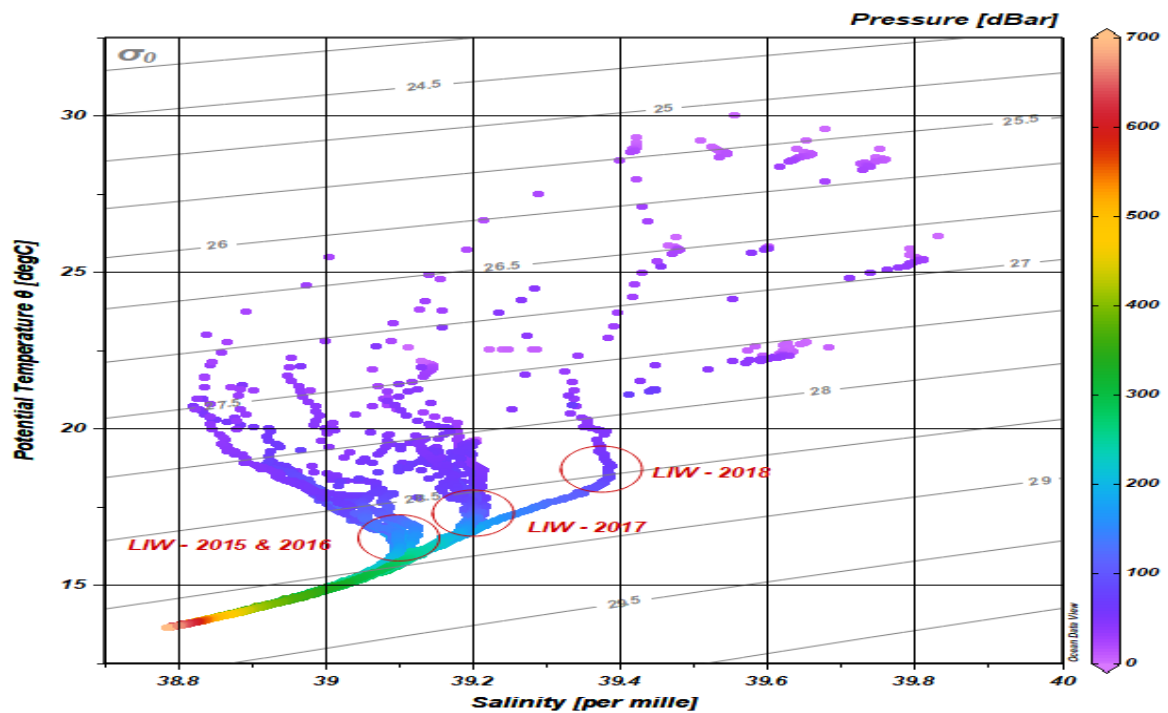


Figure 3.1: T-S diagram of station K07 throughout the KTS studies, from November 2015 to June 2018.

LIW, LSW, MAW and EMDW are clearly observed in all years, with different characteristics. In 2015 and 2016, the LIW in the TS diagram was identical “Scorpion tail” form, temperature (~ 16.50 °C), salinity (~ 39.10 per mille) and potential density (~ 28.87 kg/m³). However, in 2017 and 2018, significant salinity increases and shifts on temperature and potential density of LIW, LSW and MAW were observed in the upper thermocline.

During the first cruise of KTS studies in November 2015, the water column was well mixed and uniform from the sea surface to the depths of 50 meters, where thermocline, halocline, pycnocline and oxycline were located, as shown in Figure 3.2. Above thermocline, warm and saline Levantine Surface Water (LSW) with ~ 22.50 °C of temperature, ~ 39.30 per mille of salinity and ~ 27.35 kg/m³ of potential density was present, as shown in Figure 3.2.

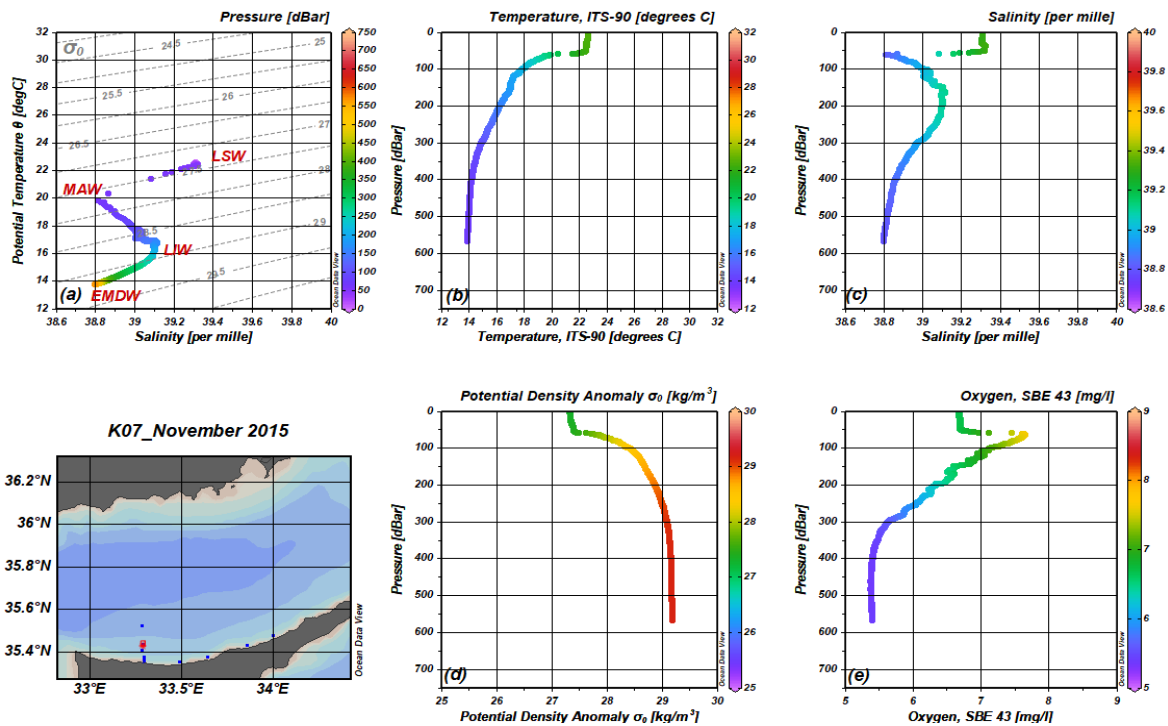


Figure 3.2: November 2015 cruise results of the station K07. (a): T-S diagram. (b): Temperature vs depth profile. (c) Salinity vs depth profile. (d): Potential density vs depth profile. (e): Oxygen vs depth profile.

Below the halocline, Modified Atlantic Water (MAW) was marked at 38.81 per mille of salinity, and 19.90 °C of temperature, located at a depth of 60 meters, as shown in Figure 3.2 (a) and (c). It is also observed that MAW was well oxygenated, as shown in Figure 3.2 (e).

Further below, as shown in Figure 3.2 (c), the deep salinity maximum Levantine Intermediate Water (LIW) was located at the depths of about 160 meters. LIW was clearly observed at 39.11 per mille of salinity, ~ 16.85 °C of temperature and ~ 28.75 kg/m³ of potential density in the T-S diagram, Figure 3.2 (a). At the bottom of the sea, dense and cold East Mediterranean Deep Water (EMDW) was observed with ~ 13.87 °C of temperature, ~ 38.80 per mille of salinity and ~ 29.17 kg/m³ of potential density as shown with orange colour in the T-S diagram, in Figure 3.2 (a).

In the December 2015 cruise, although Sea Surface Temperature (SST) was cooled down to ~ 19.50 °C (Figure 3.3 (b)), the water column was still stratified, though thermocline, halocline, pycnocline and oxycline were located at a depth of 60 meters, Figure 3.3. The upper 60 meters of the water column was well mixed and uniform. Above the thermocline, LSW with ~ 19.50 °C of temperature, ~ 39.20 per mille of salinity and ~ 28.10 kg/m³ of potential density was present (Figure 3.3). Below the halocline, MAW was marked at 38.98 per mille of salinity and 18.13 °C of temperature, at a depth of 70 meters, as shown in Figure 3.3 (a) and (c). It is also observed that MAW was well oxygenated, as shown in Figure 3.3 (e). Further below, (Figure.3.3(c)) LIW was located at depths of between 140 and 160 meters. LIW was marked at 39.12 per mille of salinity, ~ 16.50 °C of temperature and ~ 28.76 kg/m³ of potential density in the T-S diagram, Figure 3.3 (a). At the bottom of the sea, dense and cold EMDW was present in the area with ~ 13.83 °C of temperature, ~ 38.80 per mille of salinity and ~ 29.18 kg/m³ potential density, as shown with orange colour in the T-S diagram, Figure 3.3 (a).

During the January 2016 cruise, the study area was dominated with intense vertical mixing processes. The water column was well mixed and uniform from the sea surface to depths of about 150 meters, as clearly shown in Figure 3.4. LIW, MAW and LSW were disappeared in the study area, as shown in Figure 3.4 (a). Mixed layer temperature was marked at ~ 17.05 °C of temperature, ~ 39.14 per mille of salinity and ~ 28.73 kg/m³ of potential density. The mixed layer was oxygenated to the depths of about 100 meters, as shown in the oxygen profile, Figure 3.4 (e). At the bottom of the sea, dense and cold EMDW was present in the area with ~ 13.90 °C of temperature, ~ 38.82 per mille of salinity and ~ 29.18 kg/m³ of potential density, as shown with orange colour in the T-S diagram, Figure 3.4 (a).

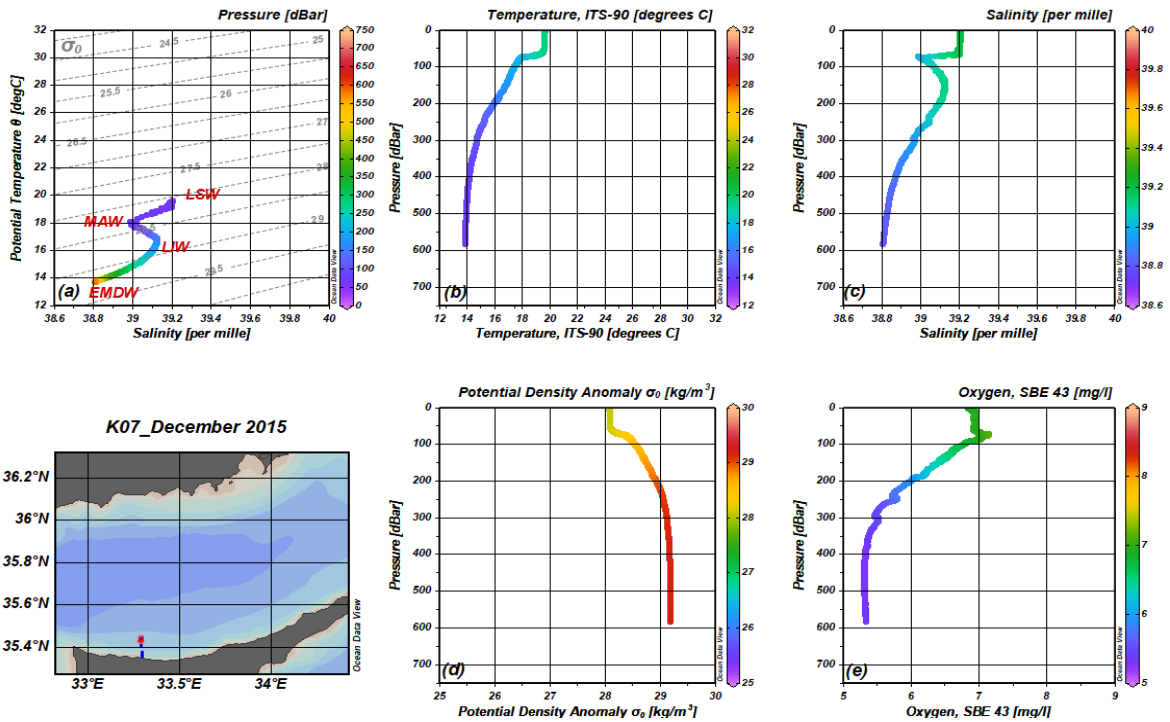


Figure 3.3: December 2015 cruise results of the station K07. (a): T-S diagram. (b): Temperature vs depth profile. (c) Salinity vs depth profile. (d): Potential density vs depth profile. (e): Oxygen vs depth profile.

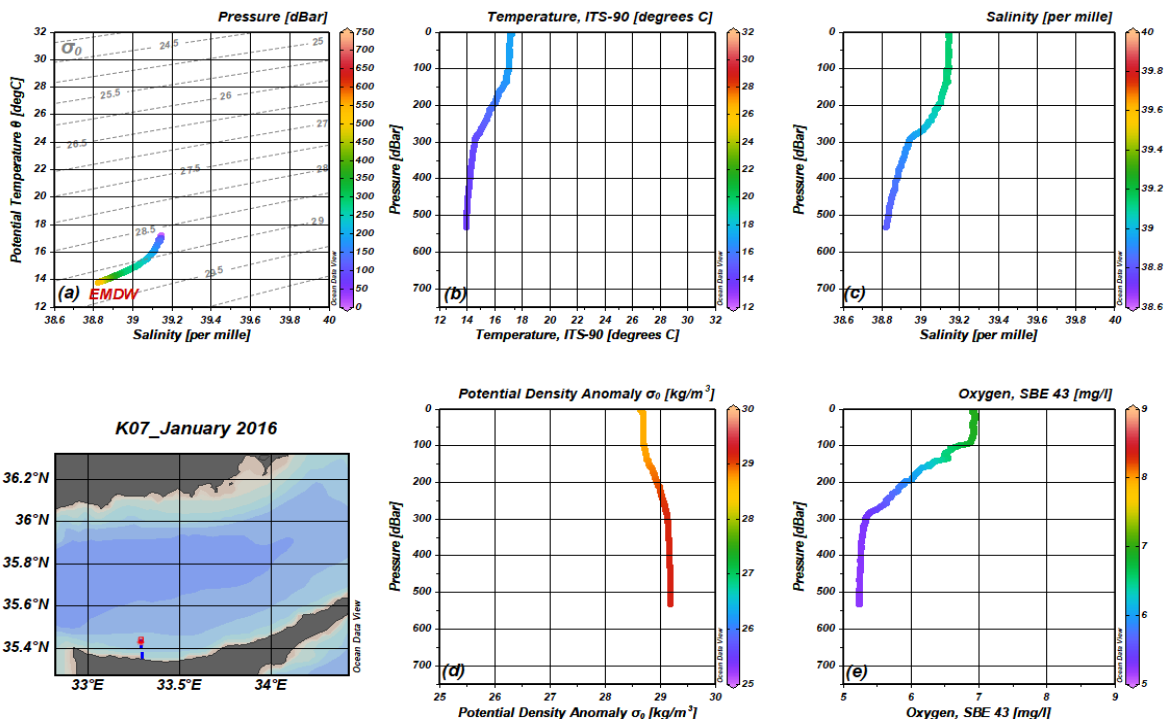


Figure 3.4: January 2016 cruise results of the station K07. (a): T-S diagram. (b): Temperature vs depth profile. (c) Salinity vs depth profile. (d): Potential density vs depth profile. (e): Oxygen vs depth profile.

In February 2016, the study area, as expected, was still dominated with intense vertical mixing processes. The water column was well mixed and uniform from the sea surface to the depths of about 150 meters, as shown in Figure 3.5. LIW, MAW and LSW were not present in the study area, as shown in Figure 3.5 (a). Mixed layer temperature was marked at ~ 17.10 °C of temperature, ~ 39.15 per mille of salinity and ~ 28.73 kg/m³ of potential density. Mix layer was oxygenated to the depths of about 150 meters, as shown in the oxygen profile, Figure 3.5 (e). At the bottom of the sea, dense and cold EMDW was present in the area with ~ 13.90 °C of temperature, ~ 38.82 per mille of salinity and ~ 29.18 kg/m³ potential density, as shown with orange colour in the T-S diagram, Figure 3.5 (a).

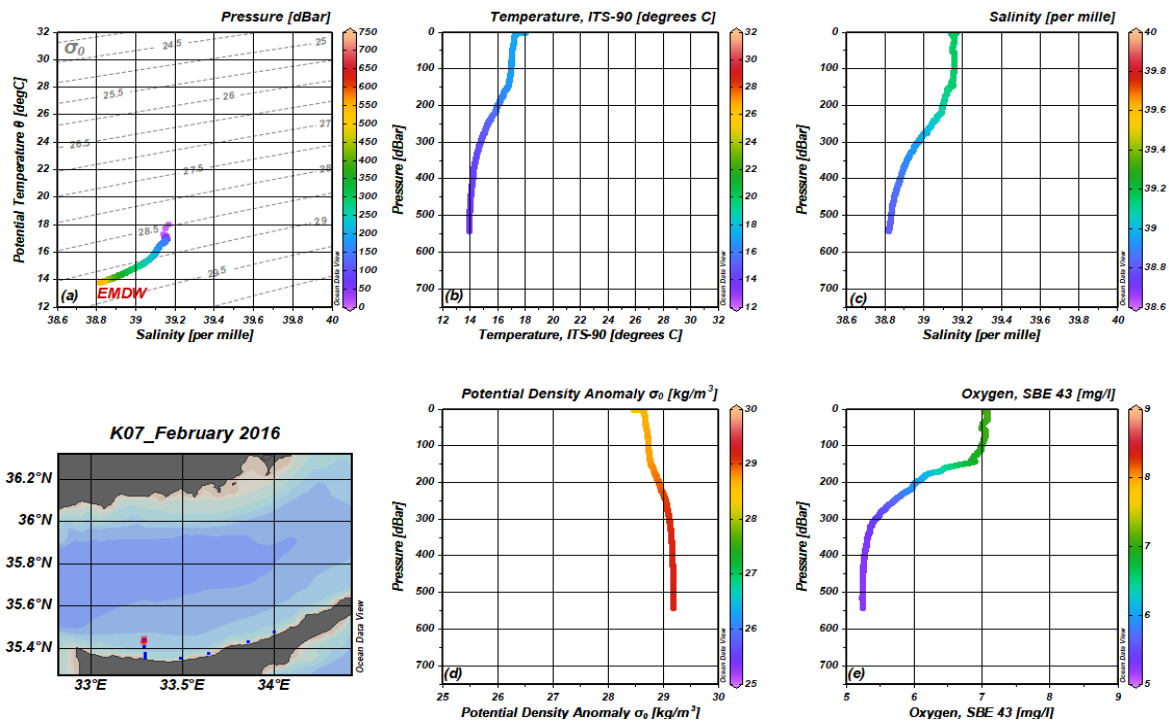


Figure 3.5: February 2016 cruise results of the station K07. (a): T-S diagram. (b): Temperature vs depth profile. (c) Salinity vs depth profile. (d): Potential density vs depth profile. (e): Oxygen vs depth profile.

During the March 2016 cruise, seasonal stratification of the water column was observed to be reformed at a depth of about 25 meters, as shown in Figure 3.6. Upper 25 meters of the water column were warmer and less dense with the temperature marked at ~ 17.80 °C and potential density at ~ 28.48 kg/m³ (Figure 3.6 (b) and (d)). Deep salinity maximum LIW was observed to reappear at the depths of between 70 and 120 meters in the study area. LIW was

marked at 39.14 per mille of salinity, ~ 16.95 °C of temperature and ~ 28.72 kg/m³ of potential density in the T-S diagram, Figure 3.6 (a). The water column was oxygenated to the depths of about 150 meters, as shown in the oxygen profile, Figure 3.6 (e). At the bottom of the sea, dense and cold EMDW was present with ~ 13.91 °C of temperature, ~ 38.82 per mille of salinity and ~ 29.18 kg/m³ potential density, as shown with orange colour in the T-S diagram, Figure 3.6 (a).

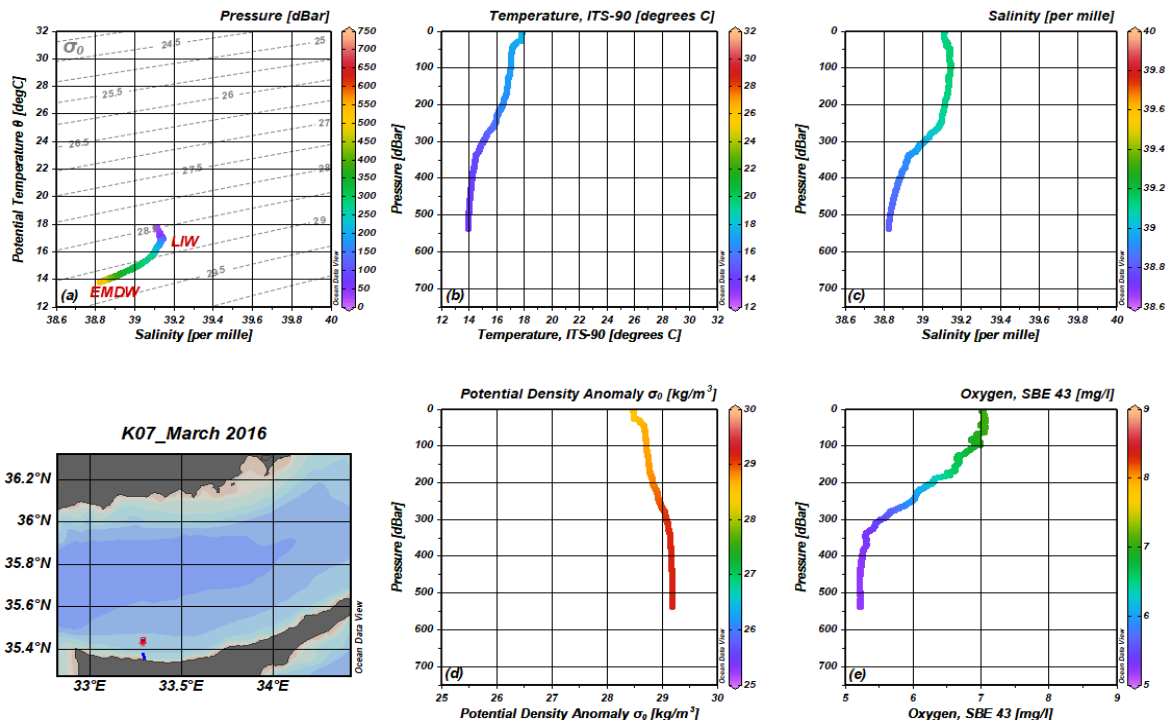


Figure 3.6: March 2016 cruise results of the station K07. (a): T-S diagram. (b): Temperature vs depth profile. (c) Salinity vs depth profile. (d): Potential density vs depth profile. (e): Oxygen vs depth profile.

At the May 2016 cruise, with the increasing temperatures over the course of spring, SST was observed to be warmed up to ~ 22.40 °C, and as shown in Figure 3.7 (a) and (b), seasonal stratification is observed to be established in the study area. The water column was well mixed and uniform from the sea surface to the depths of ~ 25 meters, where thermocline, halocline, pycnocline and oxycline were located, as shown in Figure 3.7. Above thermocline, warm and saline LSW with ~ 22.00 °C of temperature, ~ 39.15 per mille of salinity and ~ 27.37 kg/m³ of potential density was present in the area, as shown in Figure 3.7. Below the halocline, MAW was marked at 38.96 per mille of salinity and 18.66 °C of temperature, at a

depth of 43 meters, as shown in Figure 3.7 (a) and (c). It is also observed that MAW was well oxygenated, as shown in Figure 3.7 (e). Further below, as shown in Figure 3.7 (c), deep salinity maximum LIW was located at depths of between 140 and 190 meters. LIW was clearly observed at 39.10 per mille of salinity, ~ 16.60 °C of temperature and ~ 28.78 kg/m³ of potential density in the T-S diagram, Figure 3.7 (a). At the bottom of the sea, dense and cold East Mediterranean Deep Water (EMDW) was present in the area with ~ 13.79 °C of temperature, ~ 38.79 per mille of salinity and ~ 29.19 kg/m³ potential density, as shown with orange colour in the T-S diagram, Figure 3.7 (a).

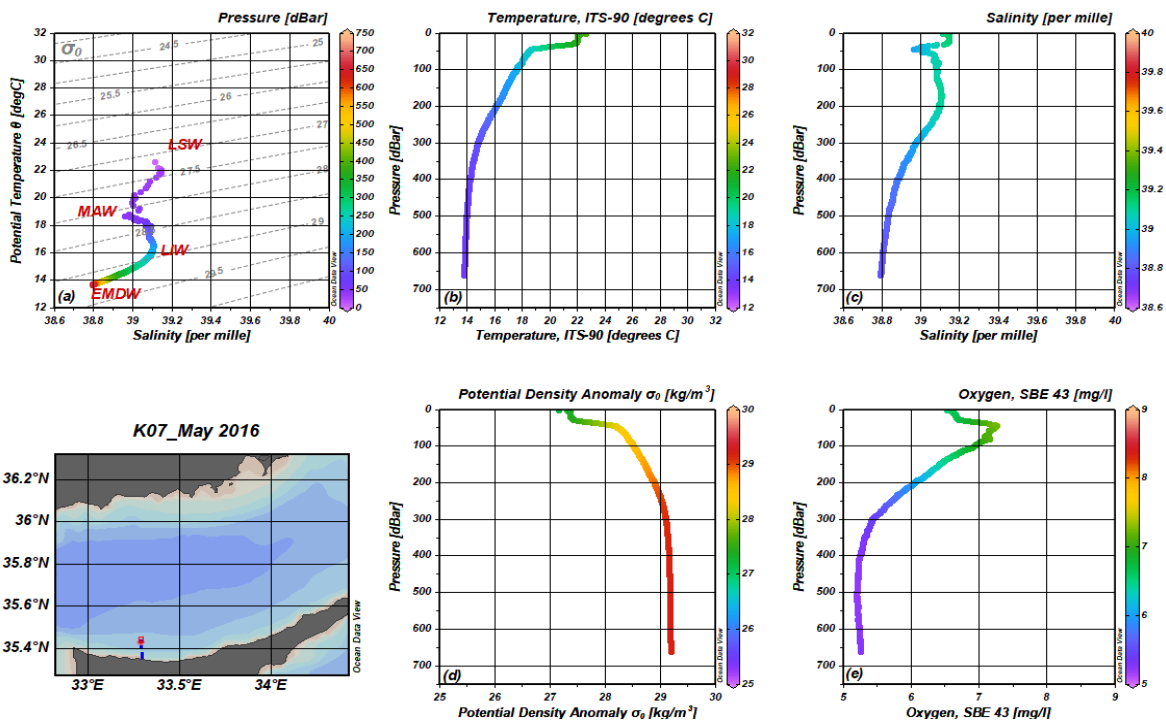


Figure 3.7: May 2016 cruise results of the station K07. (a): T-S diagram. (b): Temperature vs depth profile. (c) Salinity vs depth profile. (d): Potential density vs depth profile. (e): Oxygen vs depth profile.

During the June 2016 cruise, SST was marked at ~ 25.00 °C, the water column was well mixed and uniform from the sea surface to the depths of ~ 30 meters, where thermocline, halocline, pycnocline and oxycline were located, as shown in Figure 3.8 (a) and (b). Above thermocline, warm and saline LSW with ~ 24.00 °C of temperature, ~ 39.20 per mille of salinity and ~ 26.85 kg/m³ of potential density was present in the area as shown in Figure 3.8. Below halocline, MAW was marked at 38.94 per mille of salinity and 20.24 °C of

temperature, at a depth of 36 meters, as shown in Figure 3.8 (a) and (c). It is also observed that MAW was well oxygenated, as shown in Figure 3.8 (e). Further below, as shown in Figure 3.8 (c), deep salinity maximum LIW was located at depths of 150 and 190 meters. LIW was clearly observed at 39.10 per mille of salinity, ~ 16.55 °C of temperature and ~ 28.78 kg/m³ of potential density in the T-S diagram, Figure 3.8 (a). At the bottom of the sea, dense and cold East Mediterranean Deep Water (EMDW) was present in the area with ~ 13.76 °C of temperature, ~ 38.78 per mille of salinity and ~ 29.19 kg/m³ potential density, as shown with orange colour in the T-S diagram, Figure 3.8 (a).

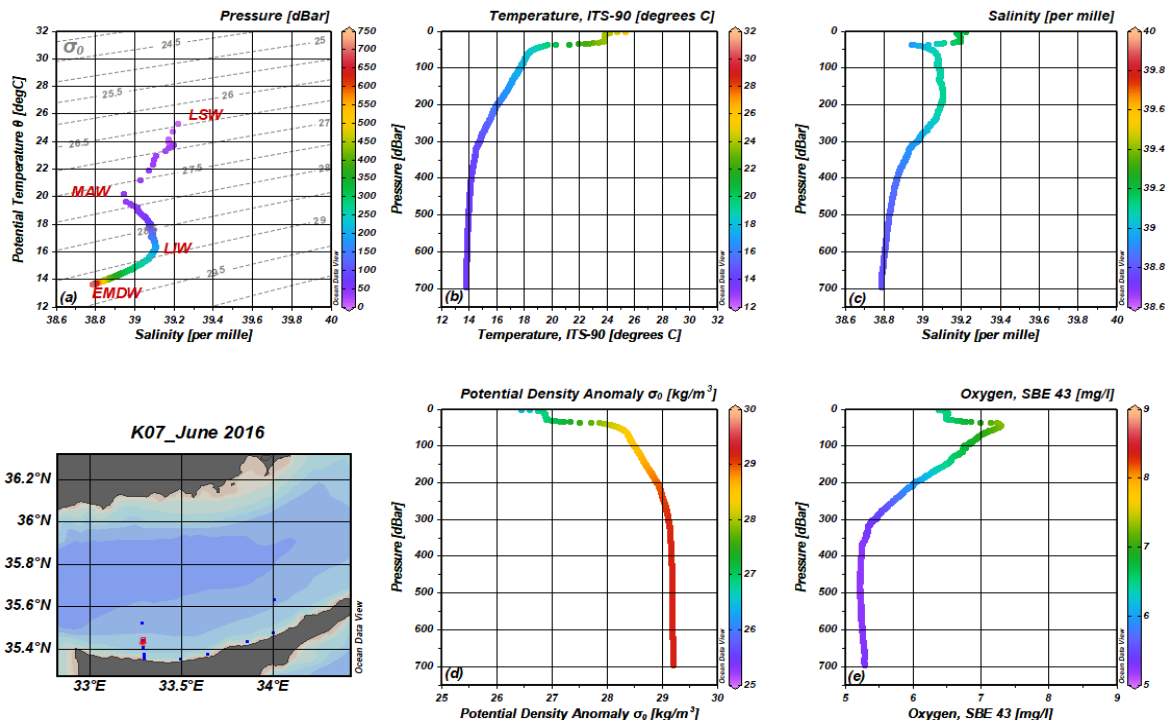


Figure 3.8: June 2016 cruise results of the station K07. (a): T-S diagram. (b): Temperature vs depth profile. (c) Salinity vs depth profile. (d): Potential density vs depth profile. (e): Oxygen vs depth profile.

At the August 2016 cruise, with the increasing temperatures over the course of summer, SST was marked at ~ 29.35 °C, and the study area was observed to be dominated by strong seasonal stratification, as shown in Figure 3.9 (a) and (b). The water column was well mixed and uniform from the sea surface to the depths of ~ 20 meters, where thermocline, halocline, pycnocline and oxycline were located, as shown in Figure 3.9. Above thermocline, warm and saline LSW with ~ 29.00 °C of temperature, ~ 39.42 per mille of salinity and ~ 25.40

kg/m³ of potential density was present in the area, as shown in Figure 3.9. Below halocline, MAW was marked by 38.83 per mille of salinity and 21.65 °C of temperature, located at a depth of 26 meters, as shown in Figure 3.9 (a) and (c). It is also observed that MAW was well oxygenated, as shown in Figure 3.9 (e). Further below, as shown in Figure 3.9 (c), deep salinity maximum LIW was located at depths of between 145 and 185 meters. LIW was clearly observed at 39.10 per mille of salinity, ~16.40 °C of temperature and 28.80 kg/m³ of potential density in the T-S diagram, Figure 3.9 (a). At the bottom of the sea, dense and cold EMDW was present in the area with ~13.76 °C of temperature, ~38.78 per mille of salinity and ~29.19 kg/m³ potential density, as shown with orange colour in the T-S diagram, Figure 3.9 (a).

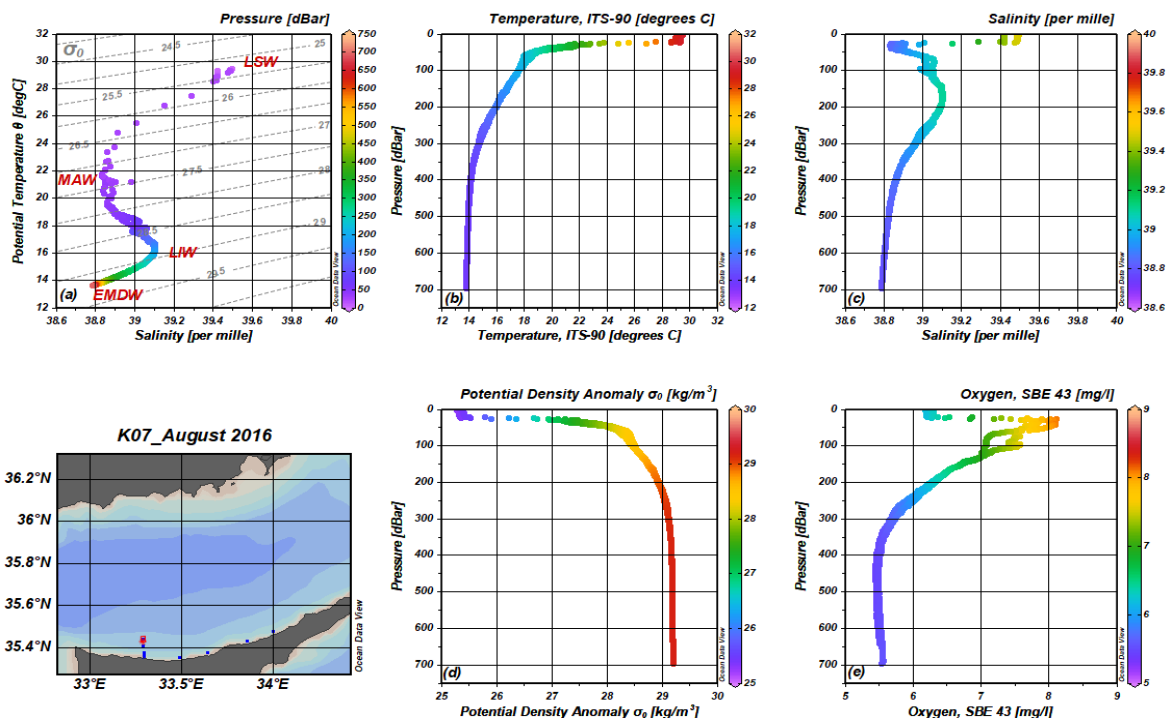


Figure 3.9: August 2016 cruise results of the station K07. (a): T-S diagram. (b): Temperature vs depth profile. (c) Salinity vs depth profile. (d): Potential density vs depth profile. (e): Oxygen vs depth profile.

During the September 2016 cruise, as shown in Figure 3.10 (b), SST was marked at about 29.60 °C. The water column was well mixed and uniform from the sea surface to the depths of ~28 meters, where thermocline, halocline, pycnocline and oxycline were located, as shown in Figure 3.10. Above thermocline, warm and saline LSW with ~29.00 °C of

temperature, ~ 39.65 per mille of salinity and $\sim 25.65 \text{ kg/m}^3$ of potential density was present in the area, as shown in Figure 3.10. Below halocline, MAW was marked at 38.83 per mille of salinity and $21.69 \text{ }^\circ\text{C}$ of temperature, at a depth of 33 meters, as shown in Figure 3.10 (a) and (c). It is also observed that MAW was well oxygenated, as shown in Figure 3.10 (e). Further below, as shown in Figure 3.10 (c), deep salinity maximum LIW located at depths of between 145 and 165 meters. LIW was clearly observed at 39.10 per mille of salinity, $\sim 16.25 \text{ }^\circ\text{C}$ of temperature and 28.85 kg/m^3 of potential density in the T-S diagram, Figure 3.10 (a). At the bottom of the sea, dense and cold EMDW was present in the area with $\sim 13.78 \text{ }^\circ\text{C}$ of temperature, ~ 38.79 per mille of salinity and $\sim 29.19 \text{ kg/m}^3$ potential density, as shown with orange colour in the T-S diagram, Figure 3.10 (a).

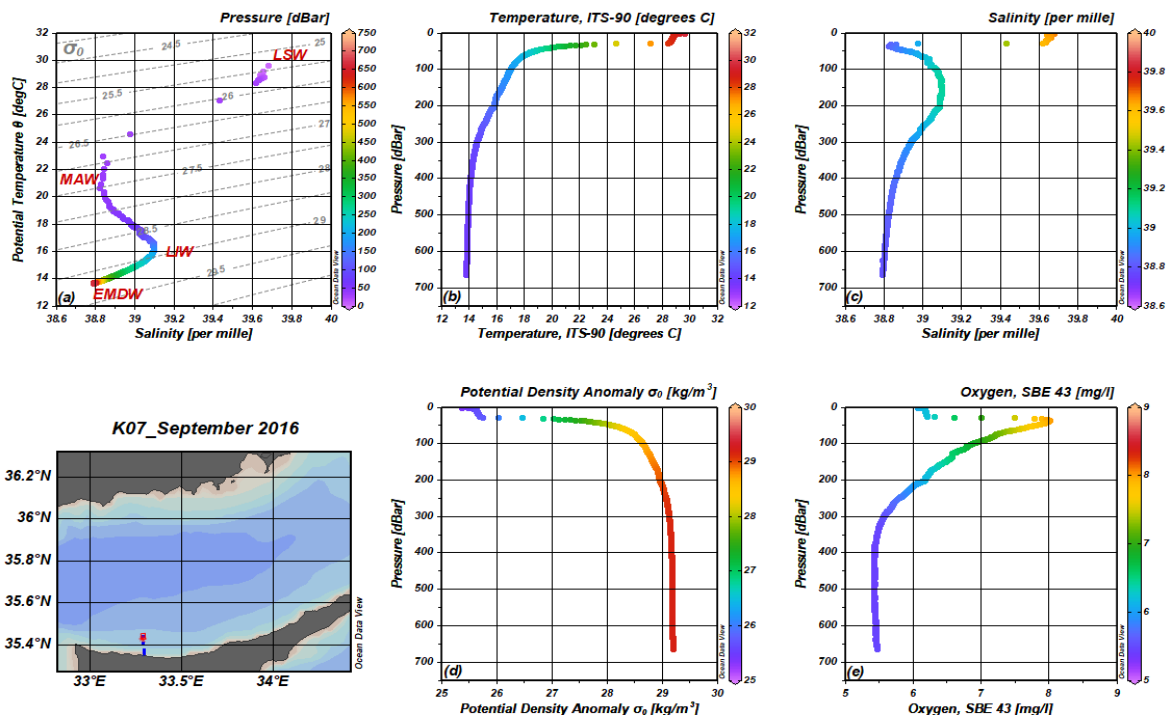


Figure 3.10: September 2016 cruise results of the station K07. (a): T-S diagram. (b): Temperature vs depth profile. (c) Salinity vs depth profile. (d): Potential density vs depth profile. (e): Oxygen vs depth profile.

During the October 2016 cruise, with the beginning of the Autumn, SST was observed to be cooling down and marked at about $25.85 \text{ }^\circ\text{C}$, as shown in Figure 3.11 (b). The water column was well mixed and uniform from the sea surface to a depth of 40 meters, where thermocline, halocline, pycnocline and oxycline were located, as shown in Figure 3.11. Above

thermocline, warm and saline LSW with ~ 25.75 °C of temperature, ~ 39.60 per mille of salinity and ~ 26.57 kg/m³ of potential density was present in the area, as shown in Figure 3.11. Below halocline, MAW was marked at 38.82 per mille of salinity and 20.74 °C of temperature, at a depth of 50 meters, as shown in Figure 3.11 (a) and (c). It is also observed that MAW was well oxygenated, as shown in Figure 3.11 (e). Further below, as shown in Figure 3.11 (c), deep salinity maximum LIW was located at depths of between 160 and 180 meters. LIW was clearly observed at 39.10 per mille of salinity, ~ 16.25 °C of temperature and 28.85 kg/m³ of potential density in the T-S diagram, Figure 3.11 (a). At the bottom of the sea, dense and cold EMDW was present in the area with ~ 13.82 °C of temperature, ~ 38.80 per mille of salinity and ~ 29.19 kg/m³ potential density, as shown with orange colour in the T-S diagram, Figure 3.11 (a).

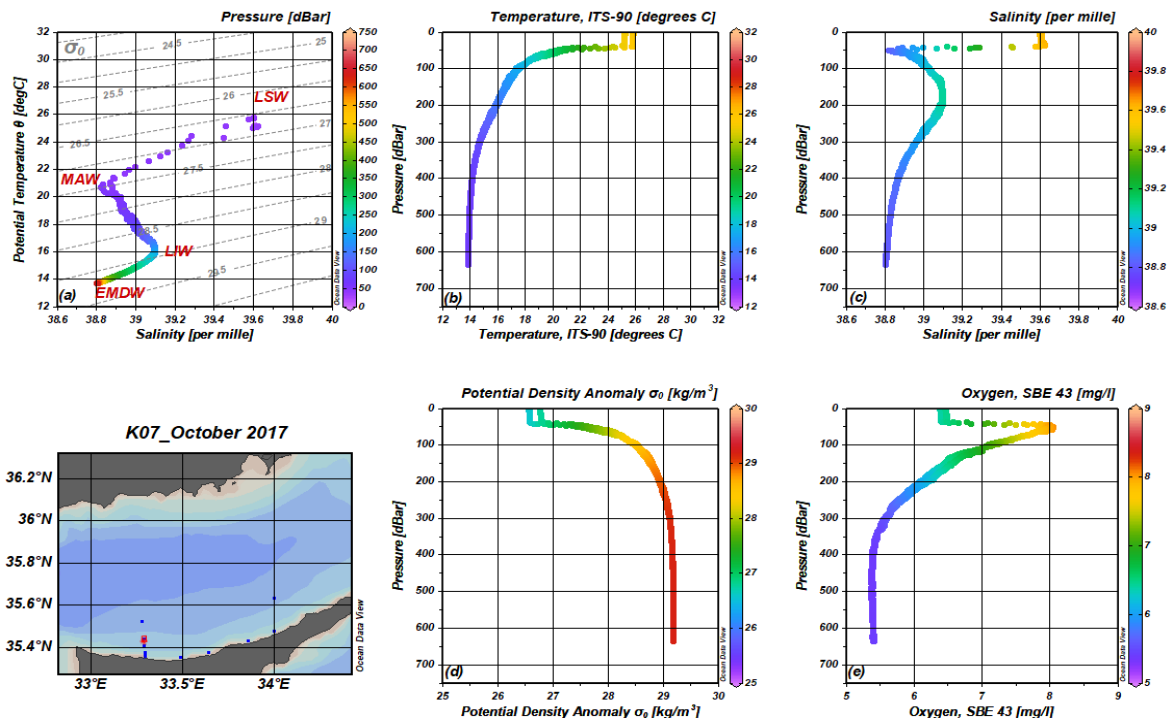


Figure 3.11: October 2016 cruise results of the station K07. (a): T-S diagram. (b): Temperature vs depth profile. (c) Salinity vs depth profile. (d): Potential density vs depth profile. (e): Oxygen vs depth profile.

At the November 2016 cruise, SST was observed to be cool further down to marked at about 21.27 °C, as shown in Figure 3.12 (b). The water column was well mixed and uniform from the sea surface to a depth of 70 meters, where thermocline, halocline, pycnocline and oxycline were located, as shown in Figure 3.12. Above thermocline, warm and saline LSW with ~21.27 °C of temperature, ~39.45 per mille of salinity and ~27.81 kg/m³ of potential density was present in the area as shown in Figure 3.12. Below halocline, MAW was marked at 38.92 per mille of salinity and 19.00 °C of temperature, at a depth of 75 meters, as shown in Figure 3.12 (a) and (c). It is also observed that MAW was well oxygenated, as shown in Figure 3.12 (e). Further below, as shown in Figure 3.12 (c), deep salinity maximum LIW was located at depths of between 190 and 210 meters. LIW was clearly observed at 39.10 per mille of salinity, ~16.25 °C of temperature and 28.85 kg/m³ of potential density in the T-S diagram, Figure 3.12 (a). At the bottom of the sea, dense and cold EMDW was present in the area with ~13.86 °C of temperature, ~38.81 per mille of salinity and ~29.19 kg/m³ potential density, as shown with orange colour in the T-S diagram, Figure 3.12 (a).

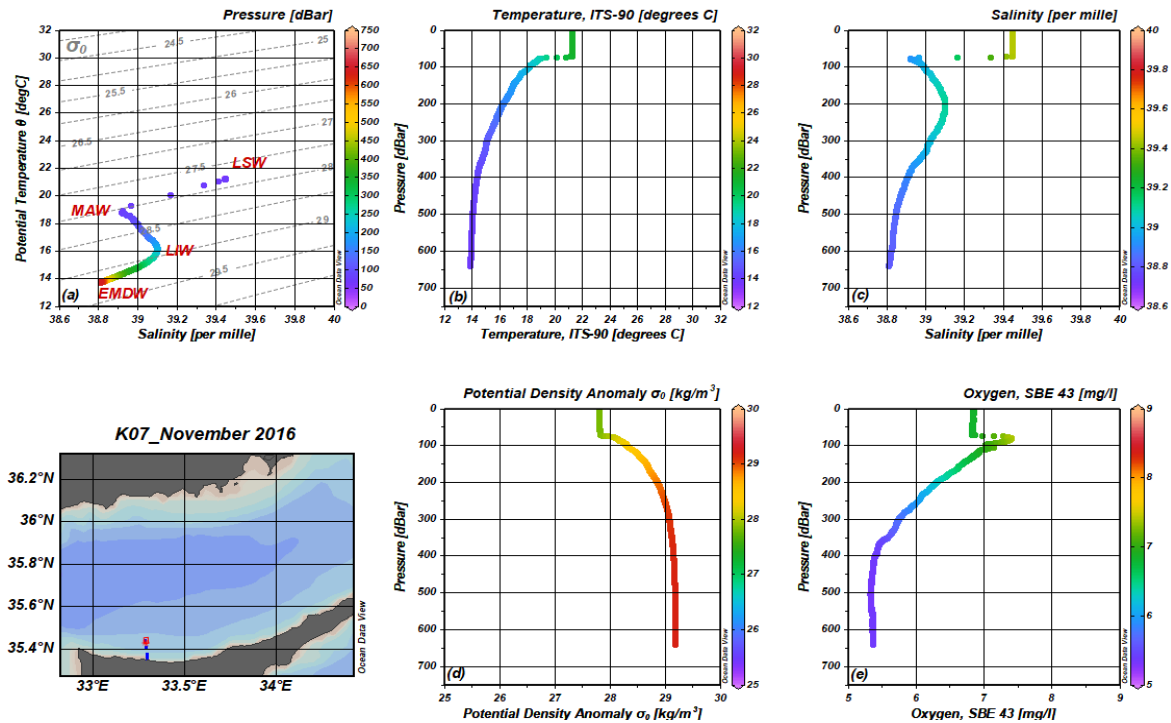


Figure 3.12: November 2016 cruise results of the station K07. (a): T-S diagram. (b): Temperature vs depth profile. (c) Salinity vs depth profile. (d): Potential density vs depth profile. (e): Oxygen vs depth profile.

During the February 2017 cruise, LIW, MAW and LSW were observed to disappear in the study area, as shown in Figure 3.13 (a). Intensive vertical mixing processes dominated the study area, and the water column was well mixed and uniform from the sea surface to depths of ~200 meters, as shown in Figure 3.13. SST was marked at ~17.60 °C and mix layer temperature marked at ~16.70 °C, salinity at ~39.22 per mille and potential density at ~28.85 kg/m³, as shown in Figure 3.13. Mix layer was oxygenated to the depths of about 200 meters, as shown in oxygen profile, Figure 3.13 (e). At the bottom of the sea, dense and cold EMDW was present in the area with ~13.81 °C of temperature, ~38.80 per mille of salinity and ~29.19 kg/m³ potential density, as shown with orange colour in the T-S diagram, Figure 3.13 (a).

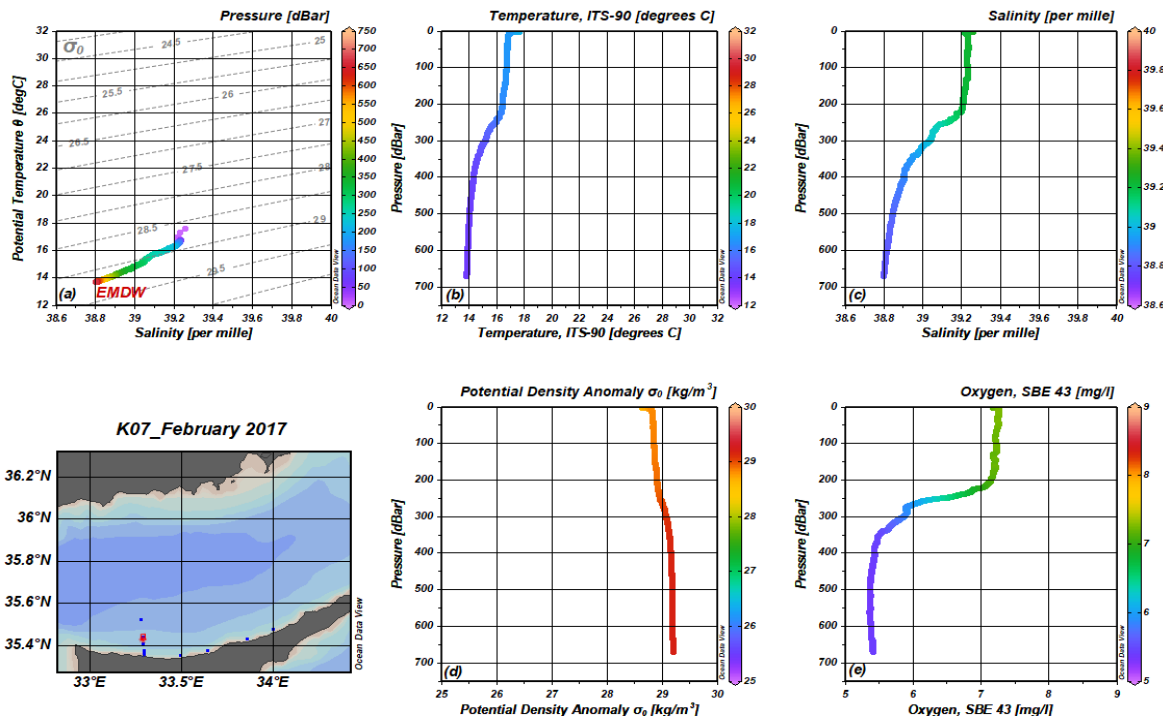


Figure 3.13: February 2017 cruise results of the station K07. (a): T-S diagram. (b): Temperature vs depth profile. (c) Salinity vs depth profile. (d): Potential density vs depth profile. (e): Oxygen vs depth profile.

During the March 2017 cruise, LIW, MAW and LSW were not present in the study area, as shown in Figure 3.14 (a). Although water column was well mixed and uniform to the depths of about 150 meters, upper 20 meters of the water column was slightly warmer and saltier with ~17.50 °C of temperature and 39.24 per mille of salinity, as shown in Figure 3.14 (b)

and (c). SST was marked at ~ 17.60 °C and mix layer temperature marked at ~ 16.70 °C, salinity at ~ 39.22 per mille and potential density at ~ 28.85 kg/m³, as shown in Figure 3.14. Mix layer was oxygenated to the depths of about 100 meters, as shown in oxygen profile, Figure 3.14 (e). At the bottom of the sea, dense and cold EMDW was present in the area with ~ 13.77 °C of temperature, ~ 38.79 per mille of salinity and ~ 29.19 kg/m³ potential density, as shown with orange colour in the T-S diagram, Figure 3.14 (a).

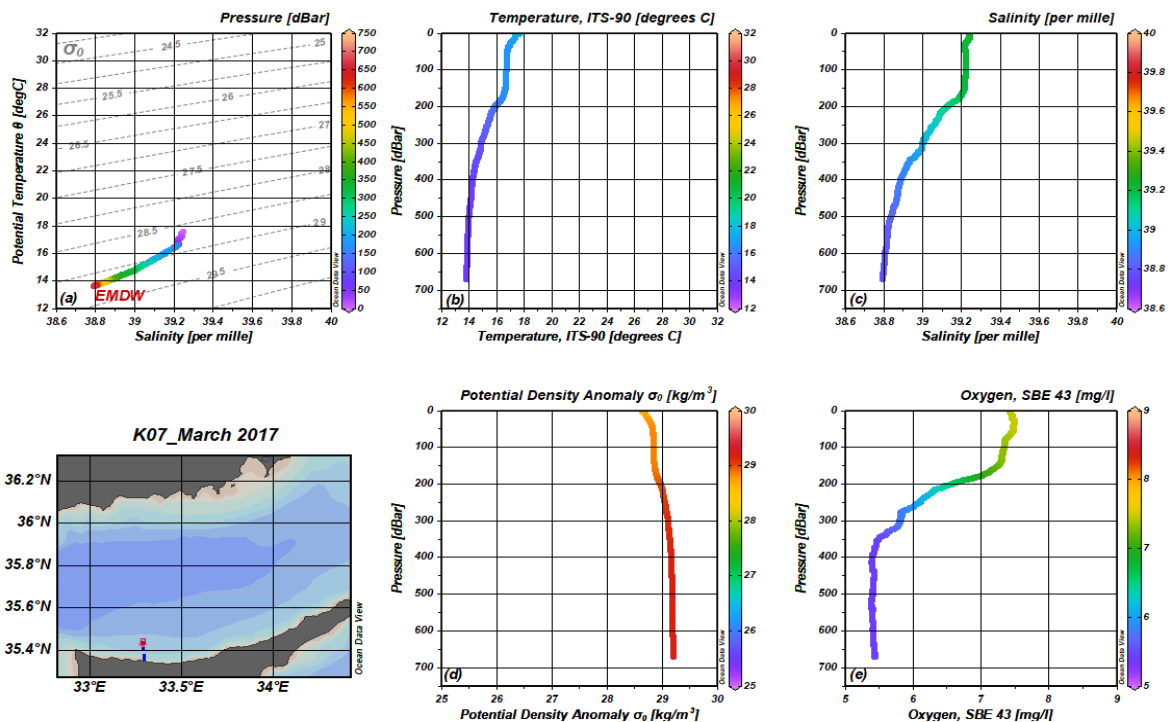


Figure 3.14: March 2017 cruise results of the station K07. (a): T-S diagram. (b): Temperature vs depth profile. (c) Salinity vs depth profile. (d): Potential density vs depth profile. (e): Oxygen vs depth profile.

At the April 2017 cruise, seasonal stratification of the water column was observed to be reformed at the depths of ~ 20 meters, as shown in Figure 3.15. Upper 20 meters of the water column was warmer and less dense with ~ 18.80 °C and ~ 28.30 kg/m³, as shown in Figure 3.15 (b) and (d). Deep salinity maximum LIW was observed to reappear at depths of between 20 and 60 meters, marked at 39.26 per mille of salinity, ~ 18.00 °C of temperature and ~ 28.52 kg/m³ of potential density in the T-S diagram, Figure 3.15 (a). The water column was oxygenated to the depths of ~ 100 meters, as shown in oxygen profile, Figure 3.15 (e). At the bottom of the sea, dense and cold EMDW was present in the area with ~ 13.79 °C of

temperature, ~ 38.89 per mille of salinity and $\sim 29.18 \text{ kg/m}^3$ potential density, as shown with orange colour in the T-S diagram, Figure 3.15 (a).

During the July 2017 cruise, with the increasing temperatures over the course of summer, SST was marked at about $30.00 \text{ }^\circ\text{C}$, and the study area was observed to be dominated by strong seasonal stratification, as shown in Figure 3.16 (a) and (b). The water column was well mixed and uniform from the sea surface to the depths of ~ 15 meters, where thermocline, halocline, pycnocline and oxycline were located, as shown in Figure 3.16. Above thermocline, LSW with $\sim 29.00 \text{ }^\circ\text{C}$ of temperature, ~ 39.53 per mille of salinity and $\sim 25.40 \text{ kg/m}^3$ of potential density was present in the area, as shown in Figure 3.16. Below halocline, MAW was marked at 39.06 per mille of salinity and $21.93 \text{ }^\circ\text{C}$ of temperature, at a depth of 22 meters, as shown in Figure 3.16 (a) and (c). It is also observed that MAW was well oxygenated, as shown in Figure 3.16 (e). Further below, as shown in Figure 3.16 (c), LIW was located at depths of between 50 and 100 meters. LIW was clearly observed at 39.21 per mille of salinity, $\sim 18.00 \text{ }^\circ\text{C}$ of temperature and $\sim 28.55 \text{ kg/m}^3$ of potential density in the T-S diagram, Figure 3.16 (a). At the bottom of the sea, dense and cold EMDW was present in the area with $\sim 13.83 \text{ }^\circ\text{C}$ of temperature, ~ 38.80 per mille of salinity and $\sim 29.19 \text{ kg/m}^3$ potential density, as shown with orange colour in the T-S diagram, Figure 3.16 (a).

At the September 2017 cruise, as shown in Figure 3.17 (b), SST was marked at about $29.00 \text{ }^\circ\text{C}$. The water column was well mixed and uniform from the sea surface to a depth of 23 meters, where thermocline, halocline, pycnocline and oxycline were located, as shown in Figure 3.17. Above thermocline, LSW with $\sim 29.50 \text{ }^\circ\text{C}$ of temperature, ~ 39.75 per mille of salinity and $\sim 25.78 \text{ kg/m}^3$ of potential density was present in the area, as shown in Figure 3.17. Below halocline, MAW was marked at 38.95 per mille of salinity and $21.50 \text{ }^\circ\text{C}$ of temperature, at a depth of 34 meters, as shown in Figure 3.17 (a) and (c). It is also observed that MAW was well oxygenated, as shown in Figure 3.17 (e). Further below, as shown in Figure 3.17 (c), LIW was located at depths of between 90 and 125 meters. LIW was clearly observed at 39.21 per mille of salinity, $\sim 17.50 \text{ }^\circ\text{C}$ of temperature and 28.63 kg/m^3 of potential density in the T-S diagram, Figure 3.17 (a). At the bottom of the sea, dense and cold EMDW was present in the area with $\sim 13.81 \text{ }^\circ\text{C}$ of temperature, ~ 38.80 per mille of salinity and $\sim 29.19 \text{ kg/m}^3$ potential density, as shown with orange colour in the T-S diagram, Figure 3.17 (a).

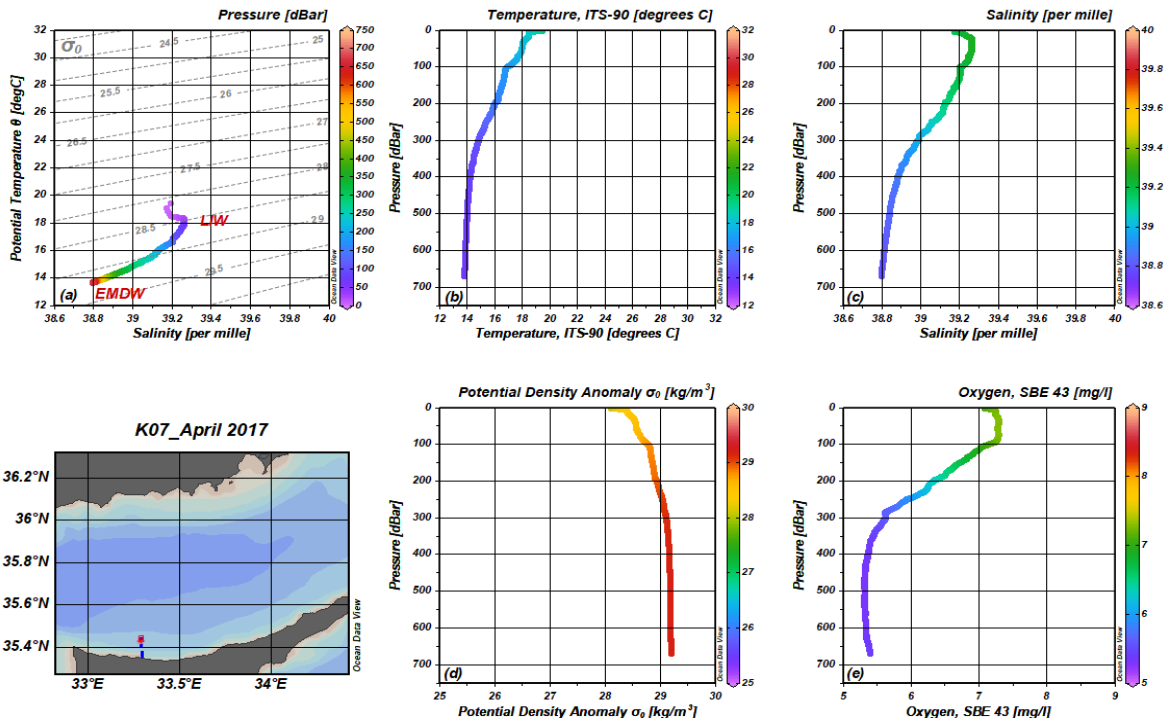


Figure 3.15: April 2017 cruise results of the station K07. (a): T-S diagram. (b): Temperature vs depth profile. (c) Salinity vs depth profile. (d): Potential density vs depth profile. (e): Oxygen vs depth profile.

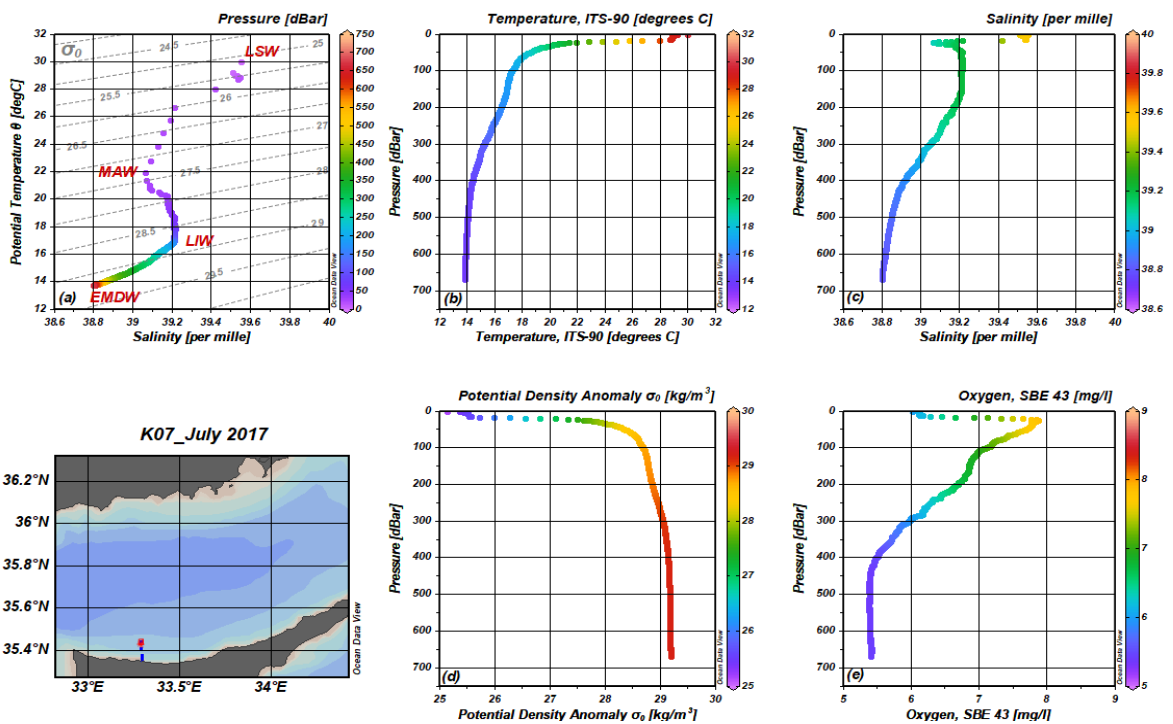


Figure 3.16: July 2017 cruise results of the station K07. (a): T-S diagram. (b): Temperature vs depth profile. (c) Salinity vs depth profile. (d): Potential density vs depth profile. (e): Oxygen vs depth profile.

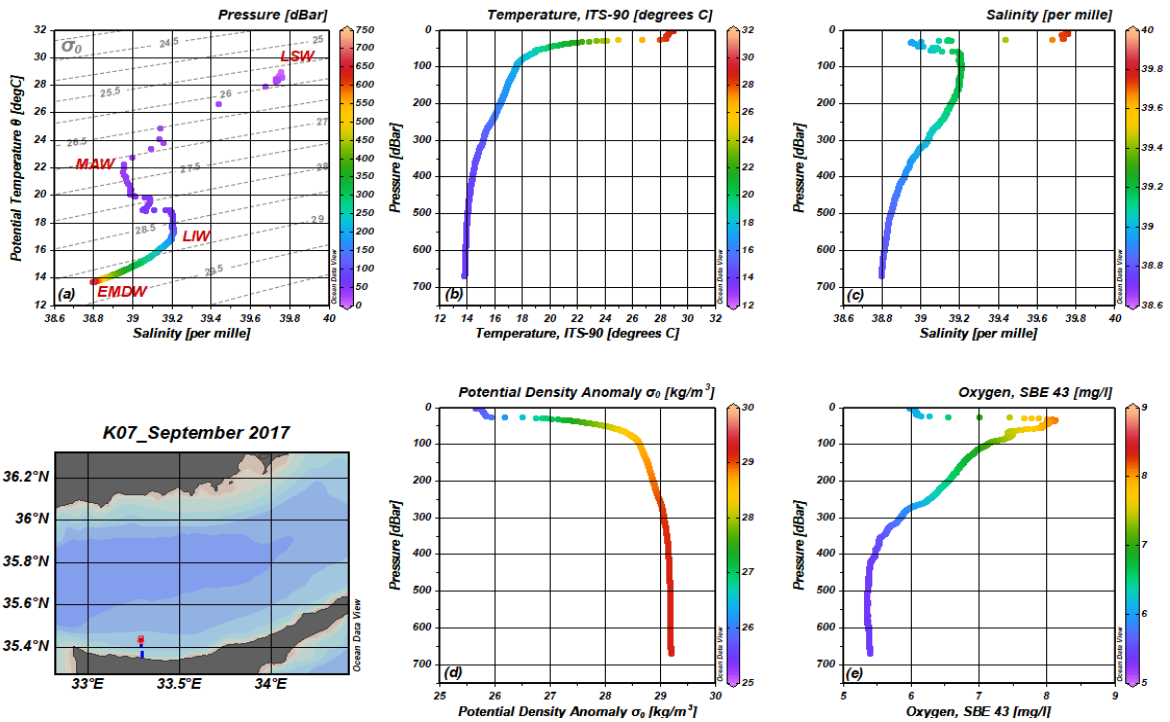


Figure 3.17: September 2017 cruise results of the station K07. (a): T-S diagram. (b): Temperature vs depth profile. (c) Salinity vs depth profile. (d): Potential density vs depth profile. (e): Oxygen vs depth profile.

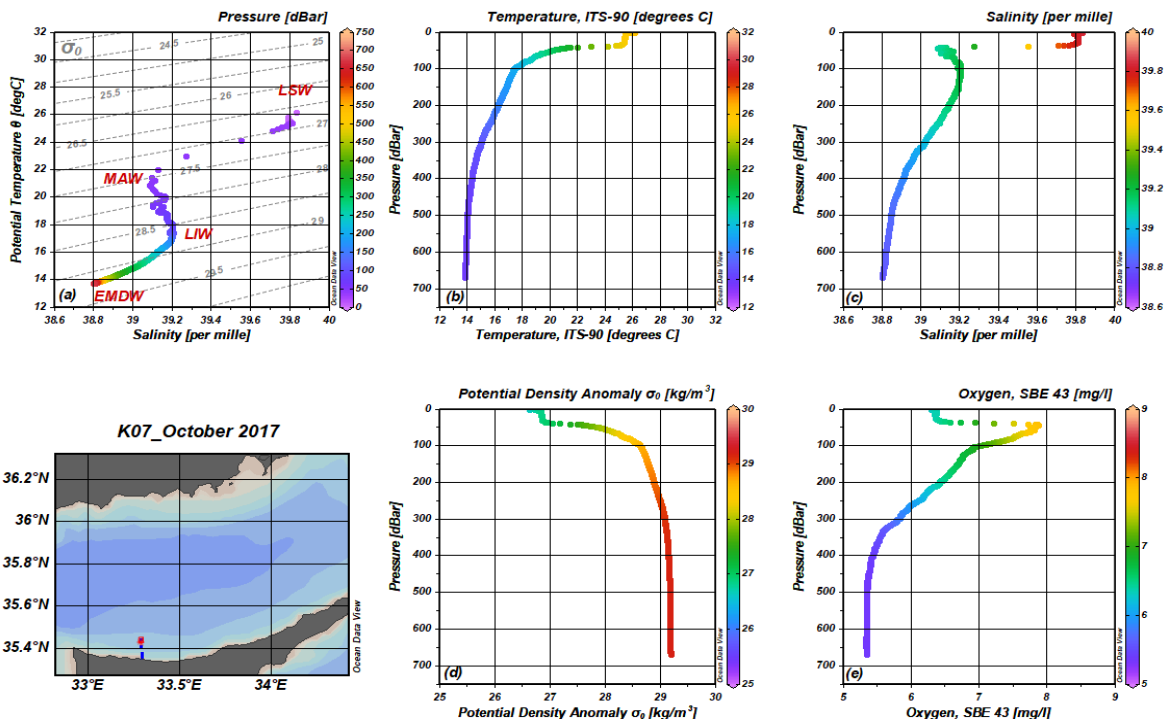


Figure 3.18: October 2017 cruise results of the station K07. (a): T-S diagram. (b): Temperature vs depth profile. (c) Salinity vs depth profile. (d): Potential density vs depth profile. (e): Oxygen vs depth profile.

During the October 2017 cruise, SST was observed to be cool down and marked at ~ 26.15 °C, as shown in Figure 3.18 (b). The water column was well mixed and uniform from the sea surface to a depth of 35 meters, where thermocline, halocline, pycnocline and oxycline were located, as shown in Figure 3.18. Above thermocline, warm and saline LSW with ~ 25.40 °C of temperature, ~ 39.80 per mille of salinity and ~ 26.70 kg/m³ of potential density was present in the area, as shown in Figure 3.18. Below halocline, MAW was marked at 39.08 per mille of salinity and 20.90 °C of temperature, at a depth of 44 meters, as shown in Figure 3.18 (a) and (c). It is also observed that MAW was well oxygenated, as shown in Figure 3.18 (e). Further below, as shown in Figure 3.18 (c), deep salinity maximum LIW was located at depths of between 100 and 130 meters. LIW was clearly observed at 39.21 per mille of salinity, ~ 17.25 °C of temperature and 28.69 kg/m³ of potential density in the T-S diagram, Figure 3.18 (a). At the bottom of the sea, dense and cold EMDW was present in the area with ~ 13.83 °C of temperature, ~ 38.80 per mille of salinity and ~ 29.19 kg/m³ potential density, as shown with orange colour in the T-S diagram, Figure 3.18 (a).

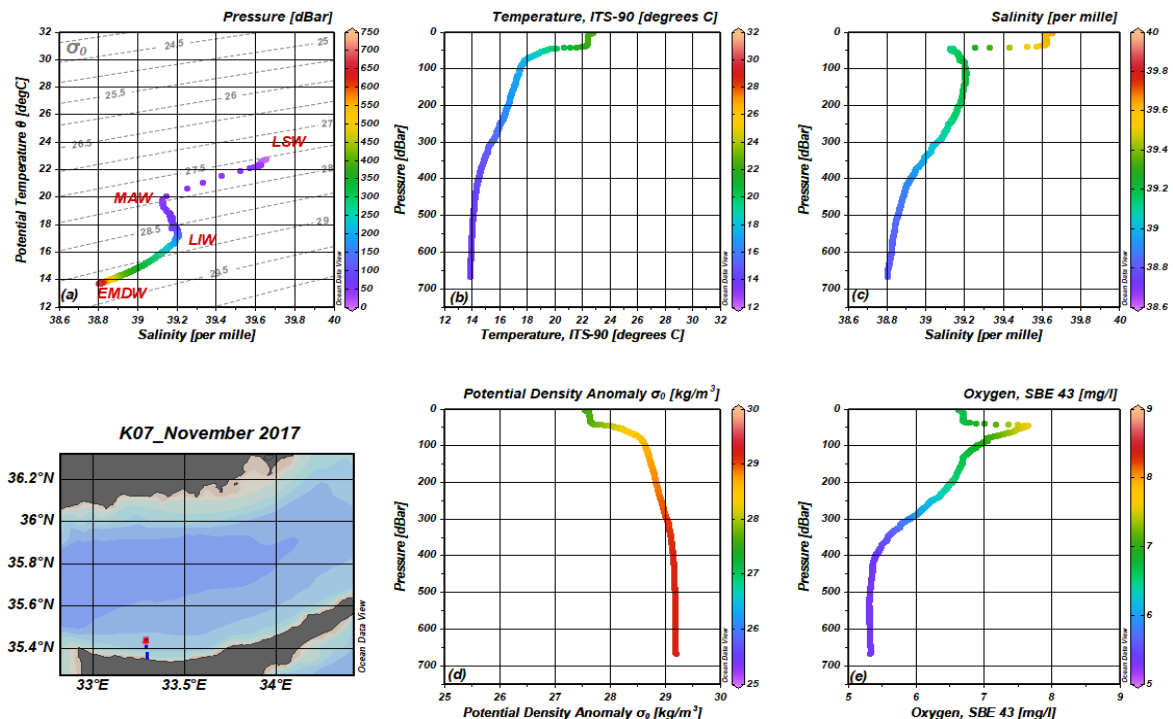


Figure 3.19: November 2017 cruise results of the station K07. (a): T-S diagram. (b): Temperature vs depth profile. (c) Salinity vs depth profile. (d): Potential density vs depth profile. (e): Oxygen vs depth profile.

During the November 2017 cruise, SST observed to be cool further down, and marked at about 21.78 °C, as shown in Figure 3.19 (b). The water column was well mixed and uniform from the sea surface to a depth of 35 meters, where thermocline, halocline, pycnocline and oxycline were located, as shown in Figure 3.19. Above thermocline, warm and saline LSW with ~22.60 °C of temperature, ~39.62 per mille of salinity and ~27.63 kg/m³ of potential density was present in the area, as shown in Figure 3.19. Below halocline, MAW was marked at 39.12 per mille of salinity and 19.80 °C of temperature, at a depth of 45 meters, as shown in Figure 3.19 (a) and (c). It is also observed that MAW was oxygenated, as shown in Figure 3.19(e). Further below, as shown in Figure 3.19 (c), deep salinity maximum LIW was located at depths of between 110 and 135 meters. LIW was clearly observed at 39.21 per mille of salinity, ~17.29 °C of temperature and 28.868 kg/m³ of potential density in the T-S diagram, Figure 3.19 (a). At the bottom of the sea, dense and cold EMDW was present in the area with ~13.83 °C of temperature, ~38.80 per mille of salinity and ~29.19 kg/m³ potential density, as shown with orange colour in the T-S diagram, Figure 3.19 (a).

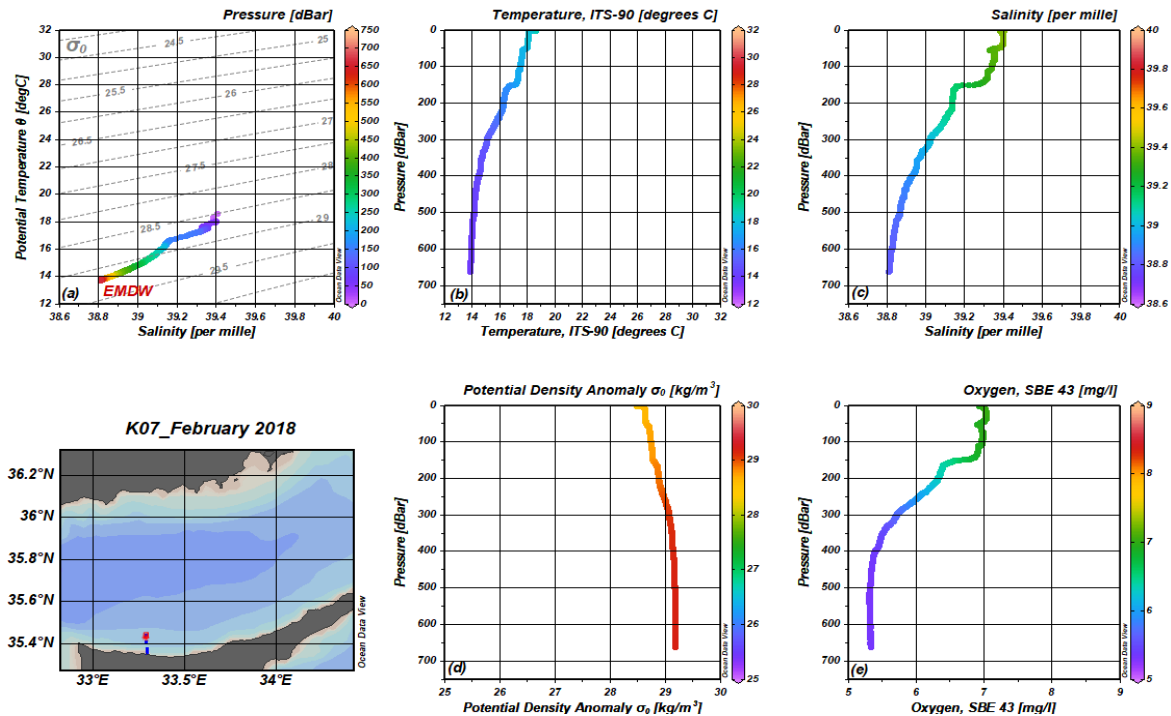


Figure 3.20: February 2018 cruise results of the station K07. (a): T-S diagram. (b): Temperature vs depth profile. (c) Salinity vs depth profile. (d): Potential density vs depth profile. (e): Oxygen vs depth profile.

At the February 2018 cruise, LIW, MAW and LSW were observed to be disappeared from the study area, as shown in Figure 3.20 (a). Although water column was mixed to the depths of about 150 meters, upper 40 meters of the water column was slightly warmer and saltier with ~ 18.05 °C of temperature and 39.38 per mille of salinity, as shown in Figure 3.20 (b) and (c). SST was marked at ~ 18.64 °C and mix layer temperature marked at ~ 17.50 °C, salinity at ~ 39.34 per mille and potential density at ~ 28.72 kg/m³, as shown in Figure 3.20. Mix layer was oxygenated to depths of about 130 meters, as shown in the oxygen profile, Figure 3.20 (e). At the bottom of the sea, dense and cold EMDW was present in the area with ~ 13.86 °C of temperature, ~ 38.81 per mille of salinity and ~ 29.19 kg/m³ potential density, as shown with orange colour in the T-S diagram, Figure 3.20 (a).

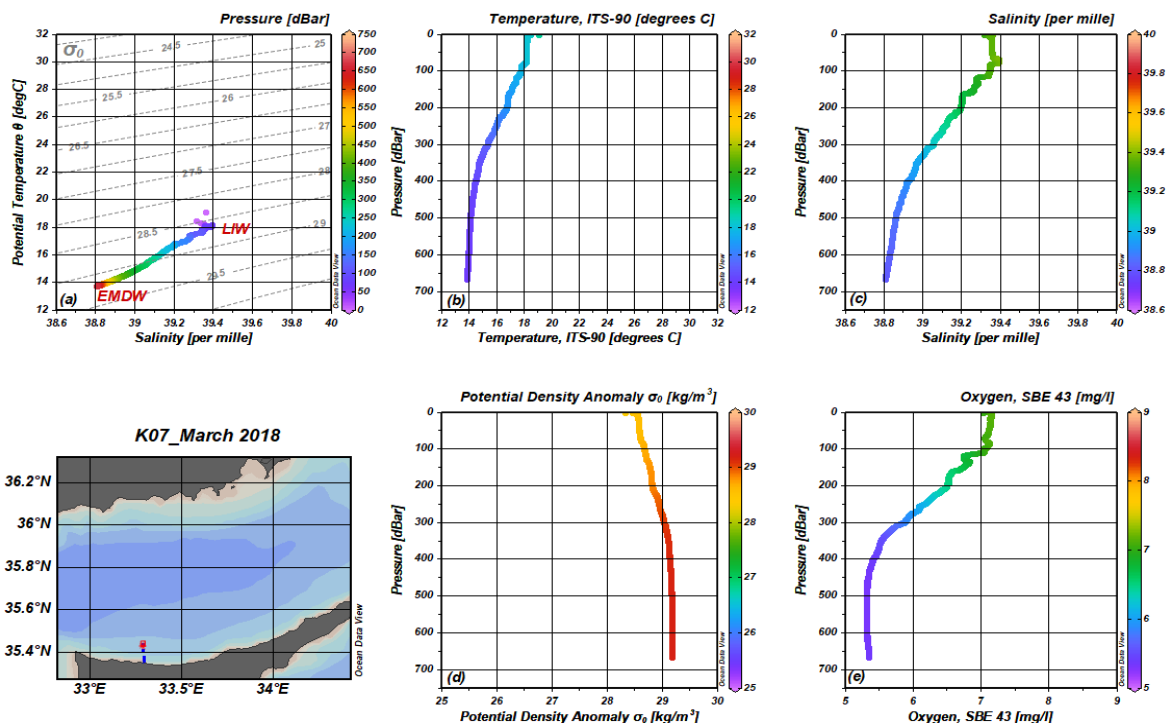


Figure 3.21: March 2018 cruise results of the station K07. (a): T-S diagram. (b): Temperature vs depth profile. (c) Salinity vs depth profile. (d): Potential density vs depth profile. (e): Oxygen vs depth profile.

During the March 2018 cruise, LSW and MAW were not present in the study area, as shown in Figure 3.21 (a). Although water column was well mixed and uniform to the depths of ~ 80 meters, a saltier and warmer water mass was observed at depths of between 67 and 77 meters

with 39.38 per mille of salinity and 18.14 °C of temperature, as shown in Figure 3.21. SST was marked at ~19.08 °C, and mix layer temperature was marked at ~18.15 °C, salinity at ~39.35 per mille and potential density at ~28.57 kg/m³, as shown in Figure 3.21. Mix layer was oxygenated to the depths of about 100 meters, as shown in oxygen profile, Figure 3.21 (e). At the bottom of the sea, dense and cold EMDW was present in the area with ~13.84 °C of temperature, ~38.80 per mille of salinity and ~29.19 kg/m³ potential density, as shown with orange colour in the T-S diagram, Figure 3.21 (a).

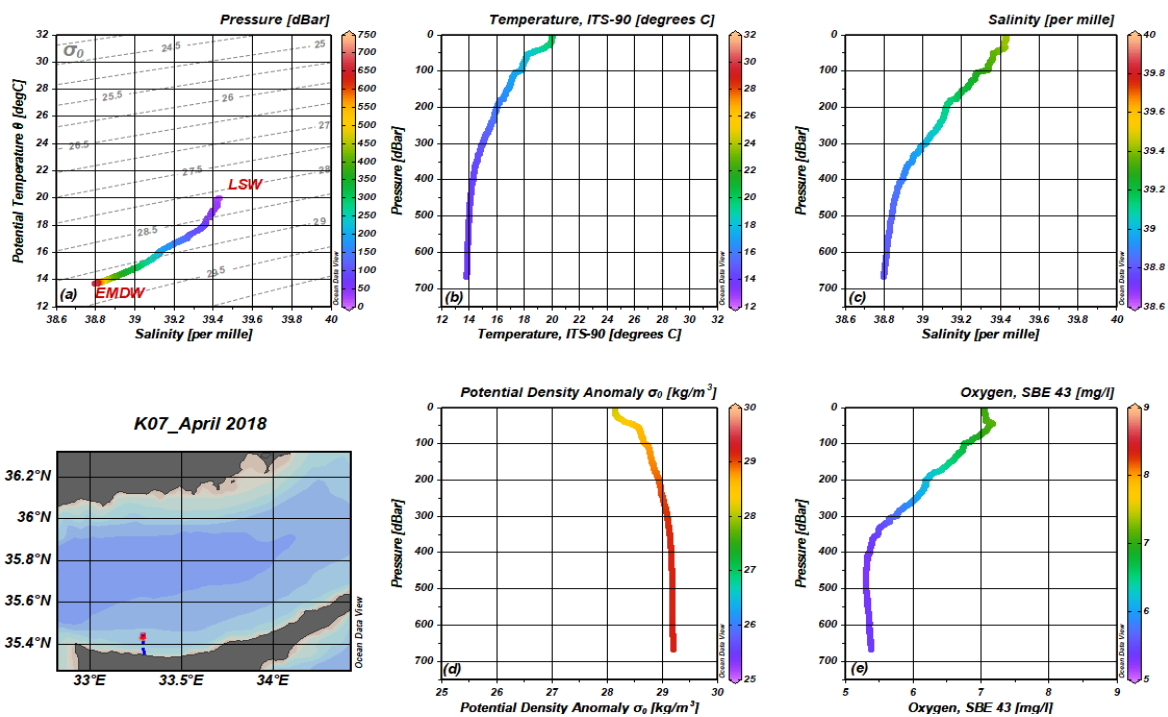


Figure 3.22: April 2018 cruise results of the station K07. (a): T-S diagram. (b): Temperature vs depth profile. (c) Salinity vs depth profile. (d): Potential density vs depth profile. (e): Oxygen vs depth profile.

At the April 2018 cruise, seasonal stratification of the water column was observed to be reformed at depths of ~35 meters, where thermocline, halocline, pycnocline and oxycline were located, as shown in Figure 3.22. SST was marked at 20.02 °C, as shown in Figure 3.22. Above thermocline, warm and saline LSW with ~20.00 °C of temperature, ~39.43 per mille of salinity and ~28.15 kg/m³ of potential density was present in the area, as shown in Figure 3.22. LIW and MAW were not present in the study, area as shown in Figure 3.22 (a). The water column was oxygenated to the depths of about 70 meters, as shown in the oxygen

profile, Figure 3.22 (e). At the bottom of the sea, dense and cold EMDW was present in the area with ~ 13.80 °C of temperature, ~ 38.79 per mille of salinity and ~ 29.18 kg/m³ potential density, as shown with orange colour in the T-S diagram, Figure 3.22 (a).

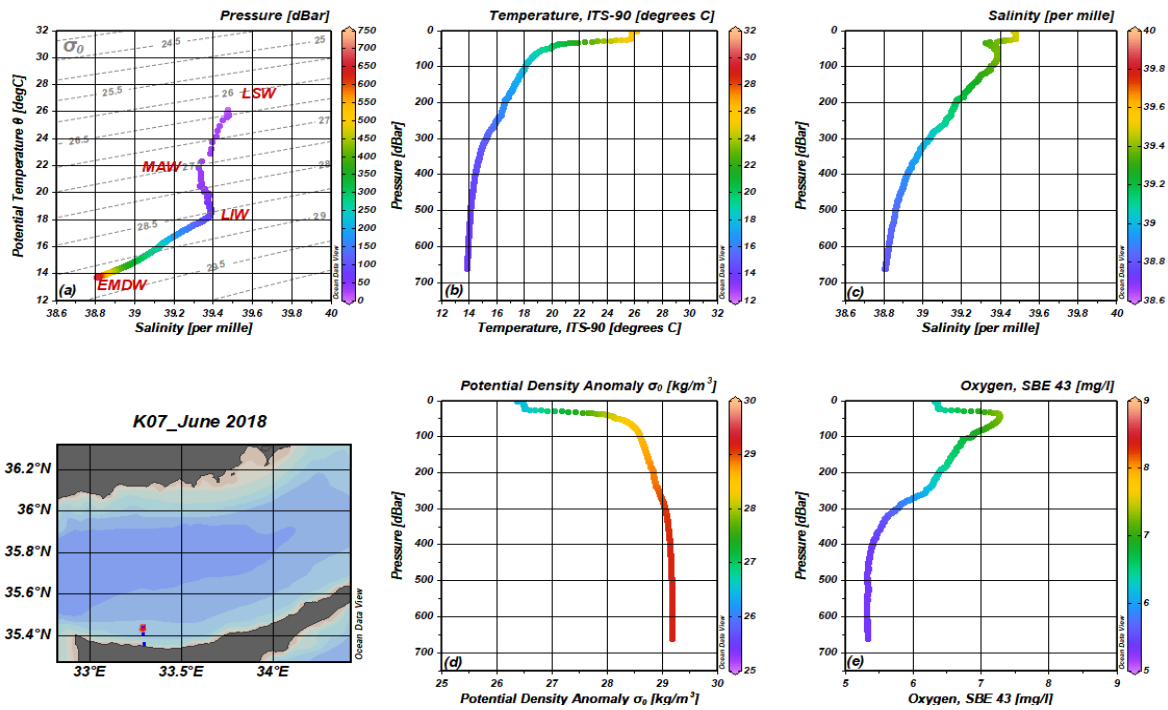


Figure 3.23: June 2018 cruise results of the station K07. (a): T-S diagram. (b): Temperature vs depth profile. (c) Salinity vs depth profile. (d): Potential density vs depth profile. (e): Oxygen vs depth profile.

During the June 2018 cruise, SST was observed to be warmed up to ~ 26.15 °C, with the increasing temperatures over the course of the spring season, and the study area was observed to be dominated by strong seasonal stratification, as shown in Figure 3.23 (a) and (b). The water column was well mixed and uniform from the sea surface to a depth of 22 meters, where thermocline, halocline, pycnocline and oxycline were located, as shown in Figure 3.23. Above thermocline, warm and saline LSW with ~ 25.80 °C of temperature, ~ 39.48 per mille of salinity and ~ 26.48 kg/m³ of potential density was present in the area, as shown in Figure 3.23. Below halocline, MAW was marked at 39.32 per mille of salinity and 21.85 °C of temperature, at a depth of 32 meters, as shown in Figure 3.23 (a) and (c). It is also observed that MAW was well oxygenated, as shown in Figure 3.23 (e). Further below, as shown in Figure 3.23 (c), deep salinity maximum LIW was located at depths of between

60 and 85 meters. LIW was clearly observed at 39.38 per mille of salinity, ~ 18.80 °C of temperature and ~ 28.45 kg/m³ of potential density in the T-S diagram, Figure 3.23 (a). At the bottom of the sea, dense and cold EMDW was present in the area with ~ 13.85 °C of temperature, ~ 38.80 per mille of salinity and ~ 29.19 kg/m³ potential density, as shown with orange colour in the T-S diagram, Figure 3.23 (a).

3.2 Time Series Plots of KTS Studies

Monthly time series plots of temperature [°C], salinity [per mille] and potential density [kg/m³] versus depth [m] (pressure [dBar]) for each KTS station are presented separately in this section to describe seasonal and annual mixing processes, seasonal and permanent stratification layers, vertical structure of the water column and water masses of Levantine Surface Water (LSW), Modified Atlantic Water (MAW), Levantine Intermediate Water (LIW) and East Mediterranean Deep Water (EMDW) or so-called Transition Layer Water (TLW), throughout the study.

3.2.1 Station K07

Station K07 is the deepest and offshore station of the KTS studies. With bottom depths of about 670 meters and a distance of 5 nautical miles from the coastline, it is expected to reveal all physical oceanographic characteristics of the Cilician Basin. K07 considered being the least affected station by direct man impact, shortly as a reference.

Upper 25 meters of the water column was well mixed and uniform, almost throughout the study, as shown in Figure 3.24. During winter seasons, especially between January and March, intense mixing processes were observed in the study area. Thus upper 150 – 200 meters of the water column was dense, well mixed and uniform, as shown with yellow colour in Figure 3.24 (c). With the increasing temperatures over the course of spring and summer seasons, SST was observed to be warm up. Seasonal stratification of the water column, thus seasonal thermocline, halocline and pycnocline (vertical gradients in colours shown in Figure 3.24) were observed at depths of between 25 and 80 meters, especially between May and November. Strong seasonal stratification was observed in summer seasons throughout the study, as shown in Figure 3.24.

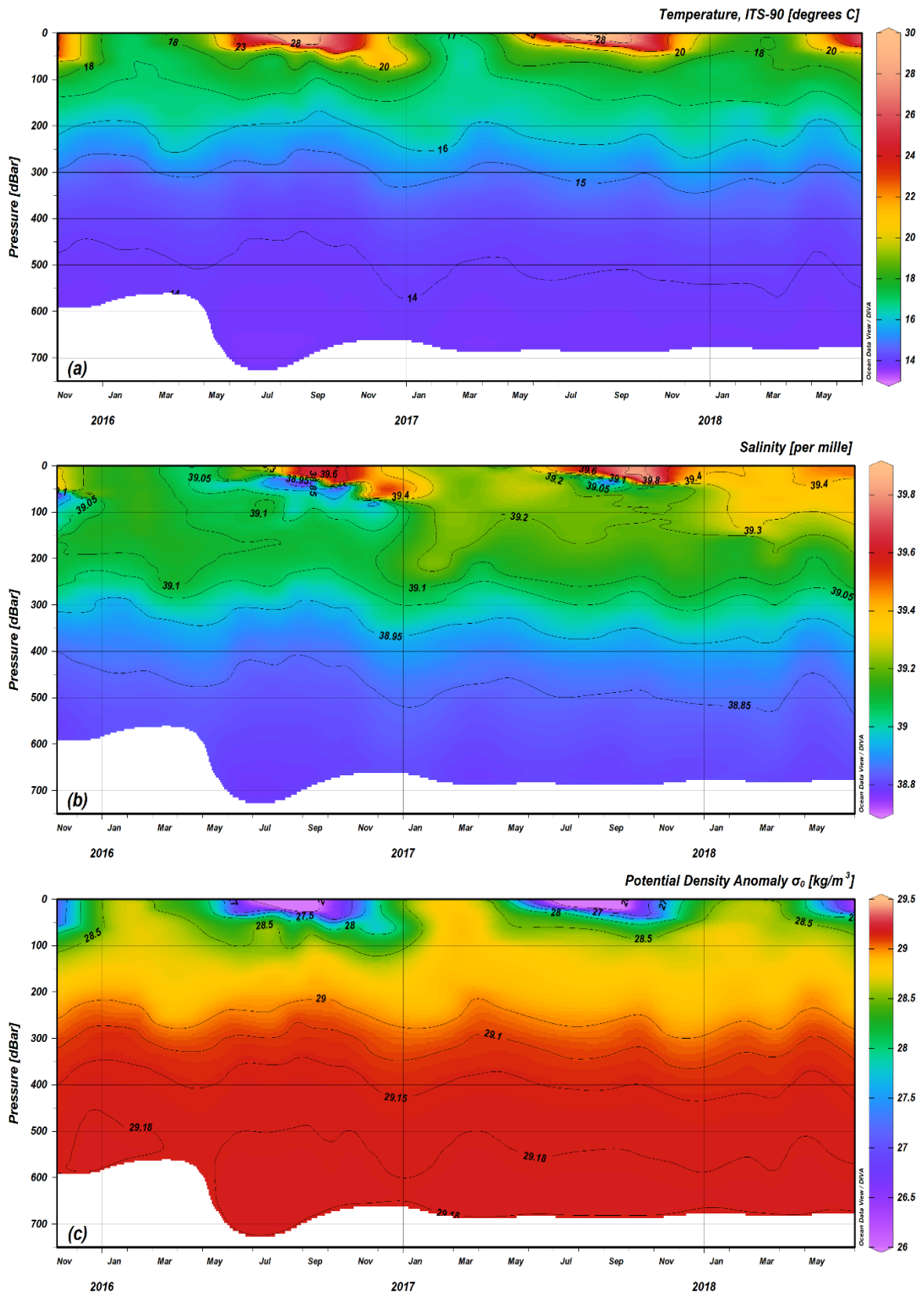


Figure 3.24: Time series plots of station K07. (a): temperature versus depth, (b): salinity versus depth, (c): potential density versus depth at K07.

Permanent stratification layer, thus permanent thermocline, shown as blue to violet colour in Figure 3.24 (a), permanent halocline, shown as blue colour in Figure 3.24 (b) and permanent pycnocline, shown as orange to red colour in Figure 3.24 (c) was marked at depths of between 300 and 400 meters throughout the study.

All water masses identical to the Levantine Basin (i.e. LSW, MAW, LIW and EMDW) were observed at station K07 throughout the study. Warm and saline water mass (yellow and red colours in Figure 3.24 (a) and (b)) above the seasonal stratification layer represents the Levantine Surface Water (LSW) and was observed annually during stratified seasons, especially between May and November. Relatively less saline water mass which was trapped by two saltier water masses from above and below, and located just below seasonal stratification layer (blue and violet coloured in Figure 3.24 (b)) represents Modified Atlantic Water (MAW), and its origin is Atlantic water. MAW was observed at station K07 during stratified seasons throughout the study, but most pronounced in 2016. Deep salinity maximum water mass (green and yellow coloured in Figure 3.24 (b)) which was located at intermediate depths below MAW, represents the Levantine Intermediate Water (LIW). As shown in Figure 3.24 (b), LIW was observed at station K07 during stratified seasons throughout the study, but with different characteristics between years (green colour in 2016, yellowish in 2017 and yellow in 2018) as shown in Figure 3.24 (b). Below permanent thermocline, uniform and relatively cold (violet colour in Figure 3.24 (a)), fresher (violet colour in Figure 3.24 (b)) and dense (red colour in Figure 3.24 (c)) water mass with $<14\text{ }^{\circ}\text{C}$ temperatures, <38.85 per mille salinities and $>29.180\text{ kg/m}^3$ potential density was observed continuously at the bottom of the sea. This water mass represented EMDW and located at depths of 500 meters and more throughout the study.

During the study, as shown in Figure 3.24, annual and seasonal cycles of mixing and stratification processes, and presence of water mass (i.e. LSW, MAW, LIW, EMDW) identical to the Cilician Basin were observed at station K07. Furthermore, significant salinity increases and changes of physical oceanographic characteristics on the upper thermocline were observed at the surface and intermediate depths consecutively every year, as shown in Figure 3.24 (b).

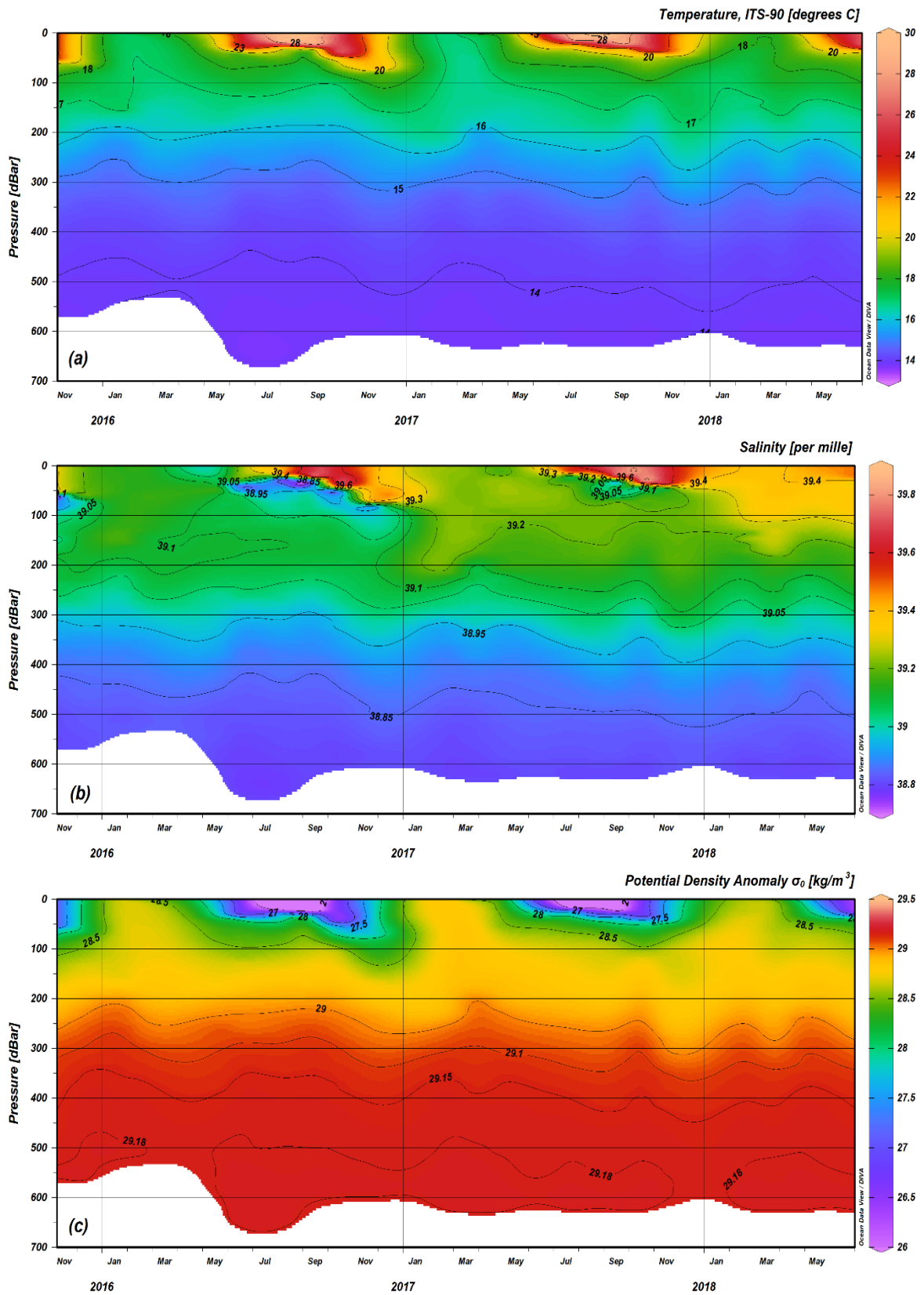


Figure 3.25: Time series plots of station K06. (a): temperature versus depth, (b): salinity versus depth, (c): potential density versus depth at K06.

3.2.2 Station K06

Along with station K07, station K06 with bottom depths of about 610 meters and distance of 3.5 nm from the coastline, considered as one of the two open sea stations in KTS, and expected to reveal similar physical oceanographic characteristics with station K07.

As shown in Figure 3.25, upper 25 meters of the water column was well mixed and uniform, almost all along the study. During winter seasons, especially between January and March intense mixing processes were observed in the study area; thus upper 150 – 200 meters of the water column was dense, well mixed and uniform, as shown with yellow colour in Figure 3.25 (c). With increasing temperatures over the course of spring and summer seasons (Figure 3.25 (a)), SST was observed to be warmed up, and especially between May and November, seasonal stratification of the water column; thus seasonal thermocline, halocline and pycnocline (vertical gradients in colours shown in Figure 3.25) was observed at depths of between 25 and 80 meters. Strong seasonal stratification was observed in summer seasons throughout the study, as shown in Figure 3.25.

Permanent stratification layer, thus permanent thermocline, shown as blue to violet colour in Figure 3.25 (a), permanent halocline, shown as blue colour in Figure 3.25 (b) and permanent pycnocline, shown as orange to red colour in Figure 3.25 (c) was marked at depths of between 300 and 400 meters throughout the study.

All water masses identical to the Levantine Basin (i.e. LSW, MAW, LIW and EMDW) were observed at station K06 throughout the study. Warm and saline LSW (yellow and red colours in Figure 3.25 (a) and (b)) was observed annually during stratified seasons, especially between May and November. Relatively less saline MAW was located just below seasonal stratification layer (blue and violet coloured in Figure 3.25 (b)) and trapped by two saltier water masses from above and below, was observed at station K06 during stratified seasons throughout the study, but most pronounced in 2016. Deep salinity maximum LIW (green and yellow coloured in Figure 3.25 (b)) was located at intermediate depths below MAW. As shown in Figure 3.25(b), LIW was observed at station K06 during stratified seasons throughout the study, but with different characteristics between years (green colour in 2016, yellowish in 2017 and yellow in 2018), as shown in Figure 3.25 (b). Below permanent thermocline, at depths of 500 meters and more, uniform and relatively cold (violet colour in

Figure 3.25 (a)), fresher (violet colour in Figure 3.25(b)) and dense (red colour in Figure 3.25 (c)) EMDW with <14 °C temperatures, <38.85 per mille salinities and >29.180 kg/m³ potential density was observed continuously at the bottom of the sea throughout the study.

During the study, annual and seasonal cycles of mixing and stratification processes, and presence of water mass (i.e. LSW, MAW, LIW, EMDW) identical to the Cilician Basin were clearly observed at station K06, as shown in Figure 3.25. Furthermore, as shown in Figure 3.25 (b), significant salinity increases and changes of physical oceanographic characteristics on the upper thermocline were observed at the surface and intermediate depths consecutively every year.

3.2.3 Station K05

Station K05 is a relatively shallow and coastal station with bottom depths of about 425 meters and distance of 1.5 nm from coastline. Due to its location, deepwater formations identical to the Cilician Basin is not expected to be observed in this station.

As shown in Figure 3.26, upper 25 meters of the water column was well mixed and uniform, almost all along the study. During winter seasons, especially between January and March intense mixing processes were observed in the study area; thus upper 150 – 200 meters of the water column was dense, well mixed and uniform, as shown with yellow colour in Figure 3.26 (c). Over the course of spring and summer seasons, SST observed to be warmed up (Figure 3.26 (a)), and especially between May and November seasonal stratification of the water column, thus seasonal thermocline, halocline and pycnocline (vertical gradients in colours shown in Figure 3.26) was observed at depths of between 25 and 80 meters. Strong seasonal stratification was observed in summer seasons throughout the study, as shown in Figure 3.26.

Permanent stratification layer, thus permanent thermocline, shown as blue to violet colour in Figure 3.26 (a), permanent halocline, shown as blue colour in Figure 3.26 (b) and permanent pycnocline, shown as orange to red colour in Figure 3.26 (c) was marked at depths of about 300 meters throughout the study.

Due to the bottom depth of this station, only the surface and intermediate water masses identical to the Levantine Basin (i.e. LSW, MAW and LIW) was observed at station K05

throughout the study. LSW (yellow and red colours in Figure 3.26 (a) and (b)) was observed annually above seasonal stratification layer during stratified seasons, especially between May and November. MAW was located just below seasonal stratification layer (blue and violet coloured in Figure 3.26 (b)), and trapped by two saltier water masses from above and below, observed at station K05 during stratified seasons, but most pronounced in 2016. LIW (green and yellow coloured in Figure 3.26 (b)) was located at intermediate depths below MAW. As shown in Figure 3.26 (b), LIW was observed at station K05 during stratified seasons throughout the study, but with different characteristics between years (green colour in 2016, yellowish in 2017 and yellow in 2018), as shown in Figure 3.26 (b).

As shown in Figure 3.26, annual and seasonal cycles of mixing and stratification processes and presence of water mass (i.e. LSW, MAW and LIW) identical to the Cilician Basin were observed at station K05 throughout the study. Furthermore, significant salinity increases and changes of physical oceanographic characteristics on the upper thermocline were observed at the surface and intermediate depths consecutively every year, as shown in Figure 3.26 (b).

3.2.4 Station K04

Station K04 is one of four coastal stations distributed within 0.5 nm in KTS to cover the neritic zone. With bottom depths of about 150 meters, K04 is the deepest coastal station in KTS and expected to reveal physical oceanographic characteristics of subsurface and intermediate waters of the Cilician Basin.

As shown in Figure 3.27, upper 25 meters of the water column was well mixed and uniform, almost all along the study. Due to intense mixing processes during winter seasons, especially between January and March, water column observed to be dense, well mixed and uniform from sea surface to the bottom of the sea, as shown with yellow colour in Figure 3.27(c). With increasing temperatures over the course of spring and summer seasons (Figure 3.27 (a)), surface waters warmed up and especially between May and November, seasonal stratification of the water column, thus seasonal thermocline, halocline and pycnocline (vertical gradients in colours shown in Figure 3.27) observed at depths of between 25 and 80 meters. Strong seasonal stratification observed in summer seasons throughout the study, as shown in Figure 3.27.

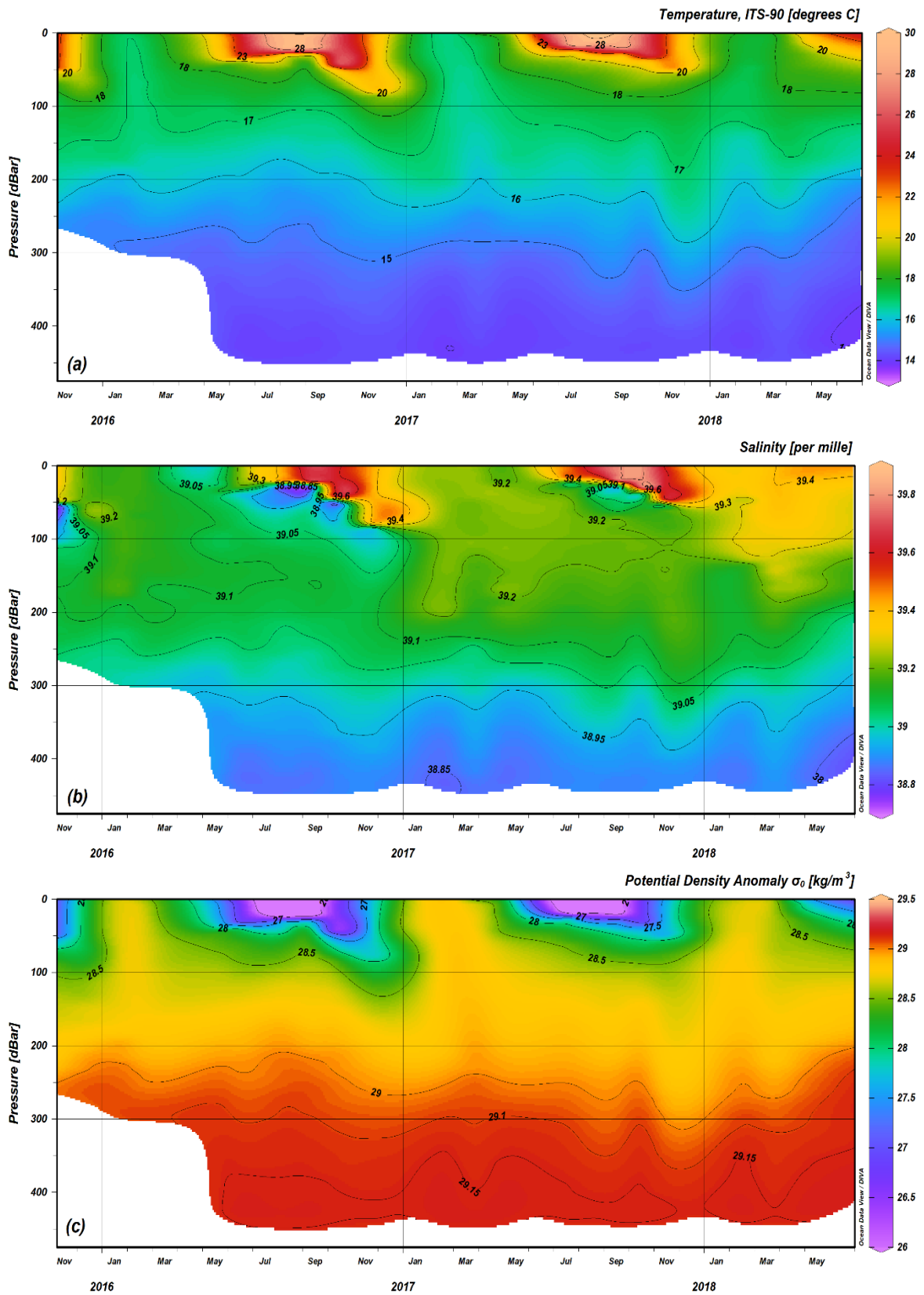


Figure 3.26: Time series plots of station K05. (a): temperature versus depth, (b): salinity versus depth, (c): potential density versus depth at K05.

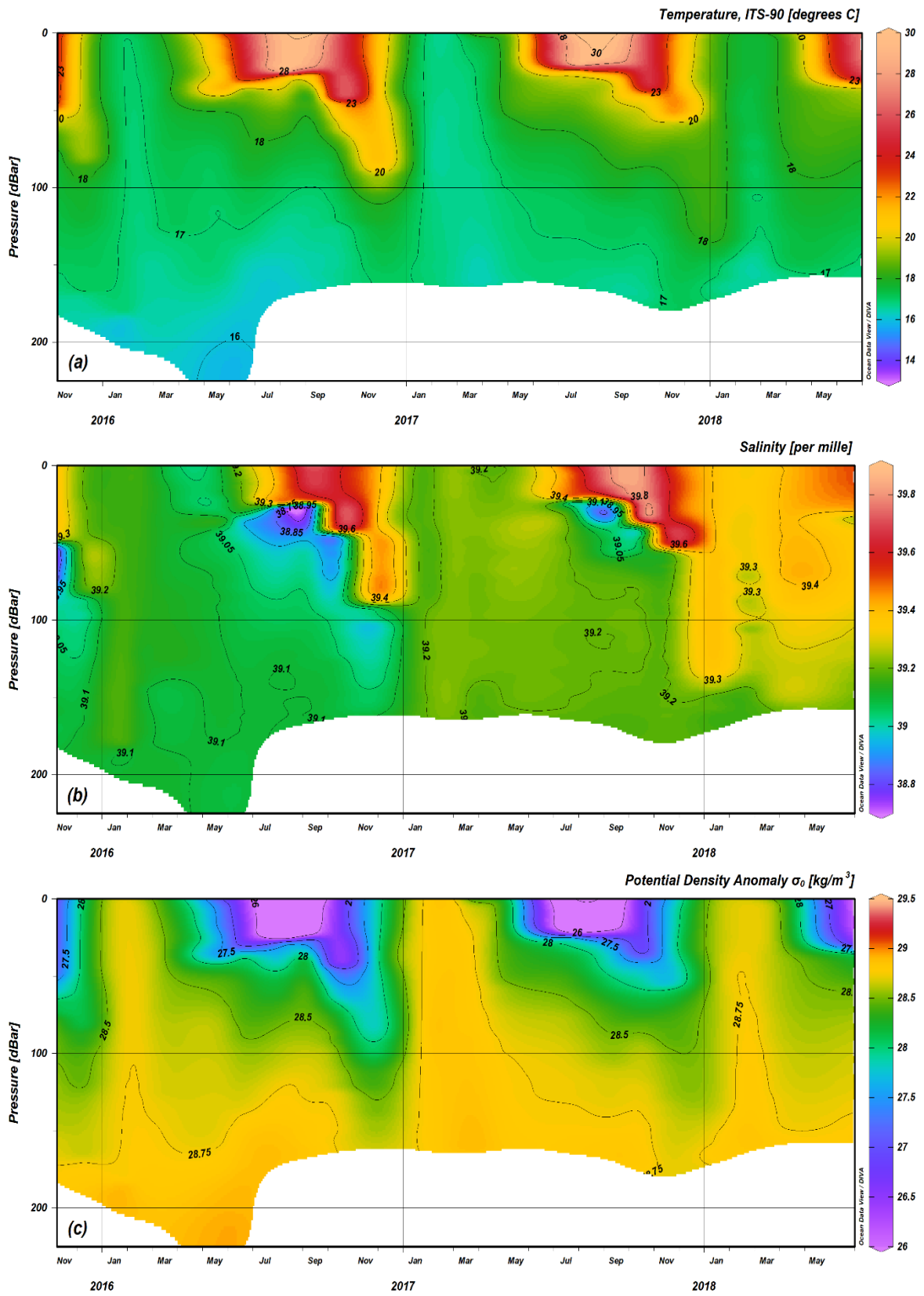


Figure 3.27: Time series plots of station K04. (a): temperature versus depth, (b): salinity versus depth, (c): potential density versus depth at K04.

Due to the bottom depth of this station, only the surface and intermediate water masses identical to the Levantine Basin (i.e. LSW, MAW and LIW) was observed at station K04 throughout the study. Warm and saline LSW (yellow and red colours in Figure 3.27 (a) and (b)) above seasonal stratification observed annually during stratified seasons, especially between May and November. Relatively less saline MAW, trapped by two saltier water masses from above and below was observed just below seasonal stratification layer (blue and violet coloured in Figure 3.27 (b)) during stratified seasons throughout the study, but most pronounced in 2016. Deep salinity maximum LIW (green and yellow coloured in Figure 3.27 (b)) was located at intermediate depths, between MAW and bottom of the sea. As shown in Figure 3.27 (b), LIW was observed at station K04 during stratified seasons throughout the study, but with different characteristics between years (green colour in 2016, yellowish in 2017 and yellow in 2018) as shown in Figure 3.27 (b).

During the study, as shown in Figure 3.27, annual and seasonal cycles of mixing and stratification processes, and presence of water mass (i.e. LSW, MAW and LIW) identical to the basin itself were observed at station K04. Furthermore, as shown in Figure 3.27 (b), significant salinity increases and changes of physical oceanographic characteristics on the upper thermocline were observed at the surface and intermediate depths consecutively every year.

3.2.5 Station K03

Station K03 is one of four coastal stations distributed within 0.5 nm in KTS to cover the neritic zone. With bottom depths of about 100 meters, it is expected to reveal physical oceanographic characteristics of subsurface and intermediate waters of the Cilician Basin. Along with stations K01 and K02, station K03 considered to be most affected by anthropogenic processes in KTS.

As shown in Figure 3.28, upper 25 meters of the water column was well mixed and uniform, almost all along the study. During winter seasons, especially between January and March, intense mixing processes observed in the study area, thus water column was dense, well mixed and uniform from the sea surface to the bottom of the sea as shown with yellow colour in Figure 3.28 (c). With increasing temperatures over the course of spring and summer seasons (Figure 3.28 (a)), SST was observed to be warmed up and especially between May

and November, seasonal stratification of the water column, thus seasonal thermocline, halocline and pycnocline (vertical gradients in colours shown in Figure 3.28) was observed at depths of between 25 and 75 meters. Strong seasonal stratification observed in summer seasons throughout the study, as shown in Figure 3.28.

Due to the relatively shallow bottom depth of this station, only the surface and subsurface water masses identical to the Levantine Basin (i.e. LSW, MAW and LIW) were observed at station K03 throughout the study. Warm and saline LSW (yellow and red colours in Figure 3.28 (a) and (b)) was observed annually above seasonal stratification layer, during the stratified seasons, especially between May and November. Relatively less saline MAW was located just below seasonal stratification (blue and violet coloured in Figure 3.28 (b)), trapped by two saltier water masses from above and below, observed at station K03 during stratified seasons throughout the study, but most pronounced in 2016. Due to relatively shallow bottom depth of the station, the only upper portion of the LIW (green and yellow coloured in Figure 3.28 (b)) was observed at intermediate depths, between MAW and the bottom of the sea. As shown in Figure 3.28 (b), LIW was observed at station K03 during stratified seasons throughout the study, but with different characteristics between years (green colour in 2016, yellowish in 2017 and yellow in 2018) as shown in Figure 3.28 (b).

As shown in Figure 3.28, annual and seasonal cycles of mixing and stratification processes, and presence of water mass (i.e. LSW, MAW and LIW) identical to the Cilician Basin were clearly observed at station K03, throughout the study. Furthermore, significant salinity increases and changes of physical oceanographic characteristics on the upper thermocline were observed at the surface and intermediate depths consecutively every year, as shown in Figure 3.28 (b).

3.2.6 Station K02

Station K02 is one of four coastal stations distributed within 0.5 nm in KTS to cover the neritic zone. With bottom depths of about 50 meters, it is expected to reveal physical oceanographic characteristics of surface and subsurface waters of the Cilician Basin. Along with stations K01 and K03, station K02 considered being most affected by anthropogenic processes in KTS.

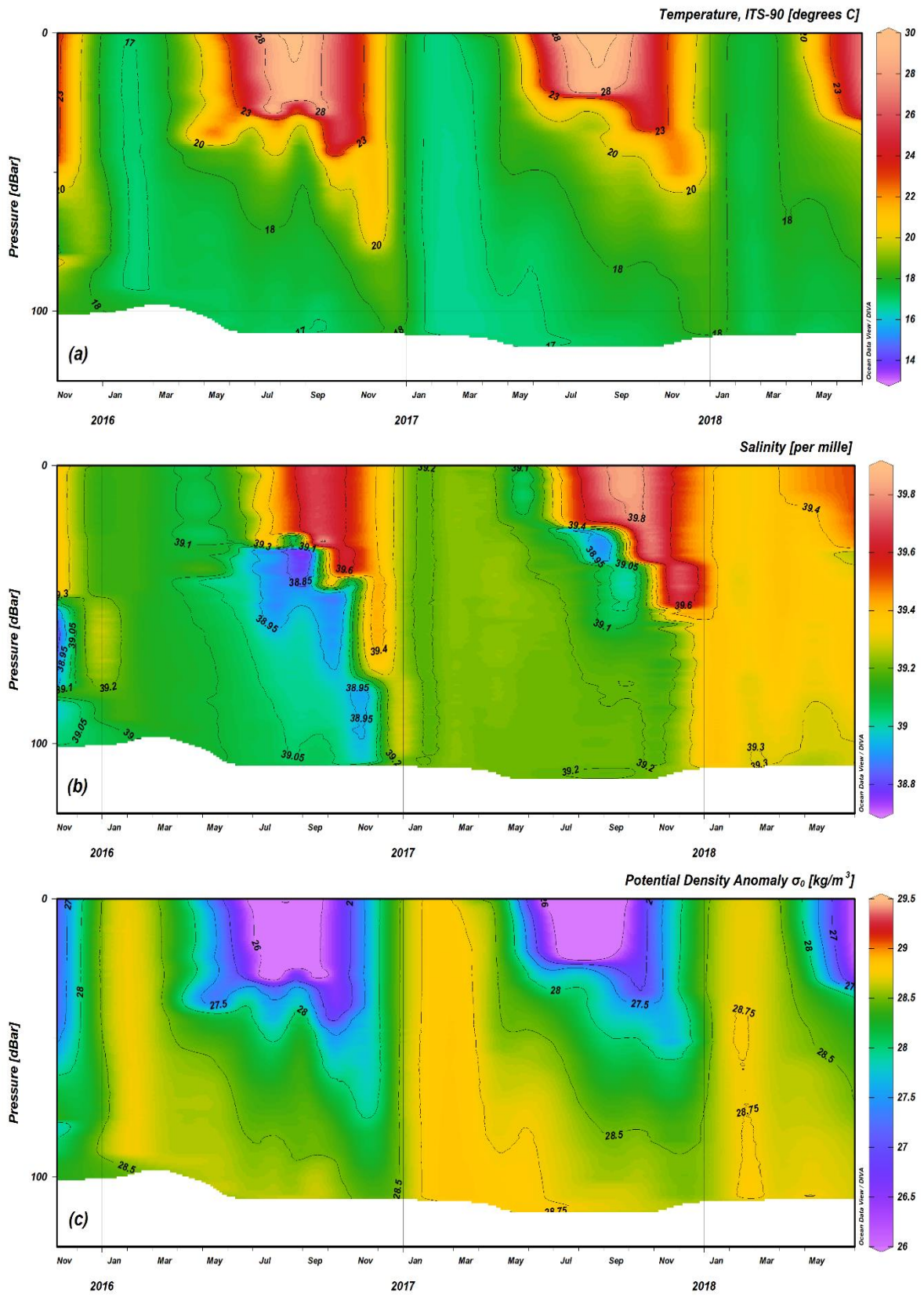


Figure 3.28: Time series plots of station K03. (a): temperature versus depth, (b): salinity versus depth, (c): potential density versus depth at K03.

As shown in Figure 3.29, upper 25 meters of the water column was well mixed and uniform, almost all along the study. During winter seasons, especially between January and March intense mixing processes were observed in the study area; thus water column was dense, well mixed and uniform from the sea surface to the bottom of the sea as shown with yellow colour in Figure 3.29 (c). With increasing temperatures over the course of spring and summer seasons (Figure 3.29 (a)), SST was observed to be warmed up and especially between May and November, seasonal stratification of the water column, thus seasonal thermocline, halocline and pycnocline (vertical gradients in colours shown in Figure 3.29) was observed at depths of between 25 meters and bottom of the sea. Strong seasonal stratification was observed in summer seasons throughout the study, as shown in Figure 3.29.

Due to the relatively shallow bottom depth of this station, only the surface and subsurface water masses identical to the Levantine Basin (i.e. LSW and MAW) were observed at station K02 throughout the study. Warm and saline LSW (yellow and red colours in Figure 3.29 (a) and (b)) was observed annually above seasonal stratification layer during stratified seasons, especially between May and November. Relatively less saline MAW was located just below the seasonal stratification layer (blue and violet coloured in Figure 3.29 (b)). MAW was observed at station K02 during stratified seasons throughout the study, but most pronounced in 2016, where located between seasonal halocline and bottom of the sea. In 2017, MAW was less pronounced but present in the area, trapped by two saltier water masses from above and below, as shown in Figure 3.29(b).

As shown in Figure 3.29, annual and seasonal cycles of mixing and stratification processes and presence of water mass (i.e. LSW and MAW) identical to the Cilician Basin were observed at station K02. Furthermore, as shown in Figure 3.29 (b), significant salinity increases and changes of physical oceanographic characteristics on the upper thermocline were observed at the surface and intermediate depths consecutively every year in this station.

3.2.7 Station K01

Station K01 is one of four coastal stations distributed within 0.5 nm to cover the neritic zone. With bottom depths of about 25 meters, it is expected to reveal physical oceanographic characteristics of surface waters of the Cilician Basin.

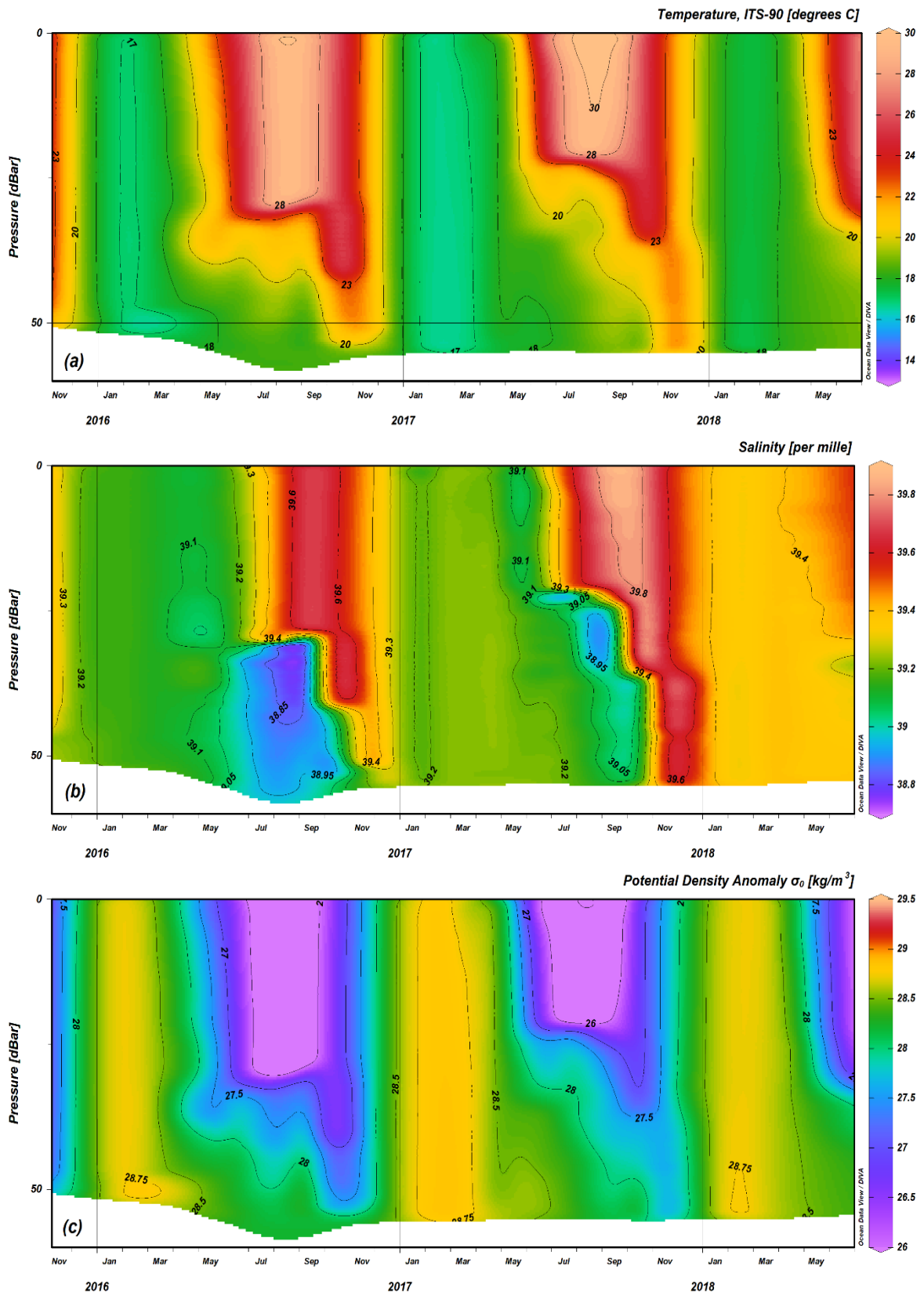


Figure 3.29: Time series plots of station K02. (a): temperature versus depth, (b): salinity versus depth, (c): potential density versus depth at K02.

As it is the shallowest and nearest station to the coastline in KTS studies, it is expected to be the most affected station by anthropogenic processes in KTS region.

As shown in Figure 3.30, due to relatively shallow bottom depths, the water column was well mixed and uniform from sea surface to the bottom of the sea in all seasons throughout the study, except summer of 2017. In summer of 2017, seasonal stratification layer, thus seasonal thermocline, halocline and pycnocline (vertical gradients in colours shown in Figure 3.30), was observed at depths of about 20 meters, between June and September. Intense mixing processes were dominant in the area during the winter seasons. The water column was dense, well mixed and uniform from the sea surface to the bottom of the sea as shown with yellow colour in Figure 3.30 (c), especially between January and March.

Due to the shallow bottom depth of this station, only the surface and subsurface water masses identical to the Levantine Basin (i.e. LSW and MAW) were observed at station K01 throughout the study. With increasing temperatures throughout spring and summer, SST was observed to be warmed up as shown with yellow, red and beige colours in Figure 3.30 (a). Warm and saline LSW was observed annually from June to November, as shown in yellow, red and beige colours in Figure 3.30 (a) and (b). MAW (violet and blue coloured in Figure 3.30 (b)) was observed only in summer of 2017, just below halocline from June to September in station K01.

During the study, seasonal mixing cycles, seasonal stratification, and presence of water masses (i.e. LSW, MAW) identical to Cilician Basin were observed in station K01, as shown in Figure 3.30. Furthermore, significant salinity increases and changes of physical oceanographic characteristics on the upper thermocline were observed at the surface and intermediate depths consecutively every year in this station, as shown in Figure 3.30 (b).

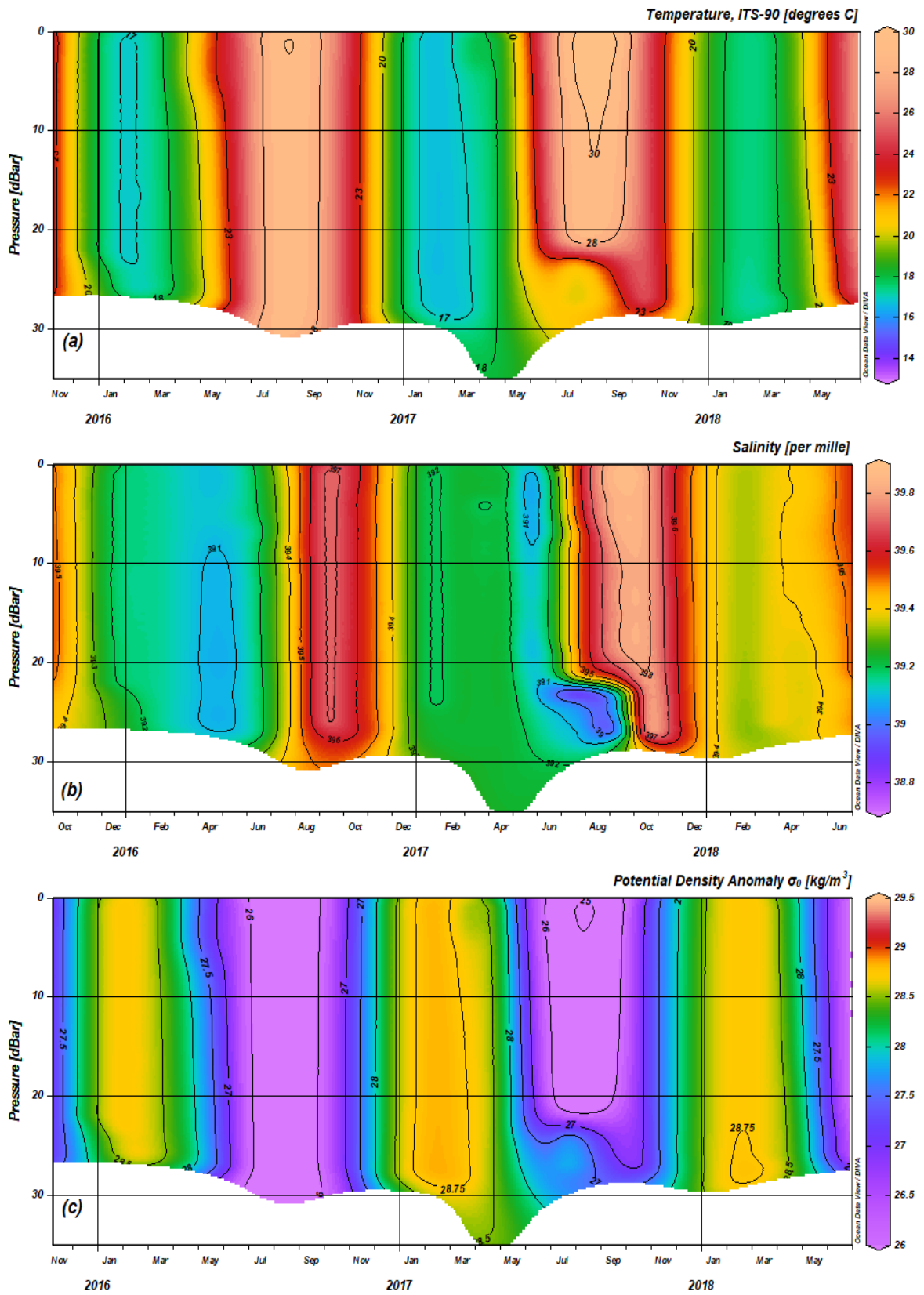


Figure 3.30: Time series plots of station K01. (a): temperature versus depth, (b): salinity versus depth, (c): potential density versus depth at K01.

CHAPTER 4

DISCUSSIONS

The results of the KTS data sets presented in this study were collected within the framework of the 114Y139 Code numbered TUBITAK project. The project mentioned above (Salihoglu et al., 2019) is the most recent, comprehensive and systematic study conducted in the Cilician Basin after the POEM studies of which the fieldwork was completed in 1995 by the study of the Levantine Intermediate Water Experiment (The LIWEX Group, 2003).

In this study, analysis of high-frequency data sets which were collected in a total of twenty-seven monthly cruises during the Kıbrıs Time Series (KTS) studies is presented to investigate sub-mesoscale physical oceanographic characteristics of the south-western Cilician Basin (offshore of Kyrenia, Northern Cyprus). The two major subjects discussed in this study are;

- i. The water masses and the physical oceanographic characteristics which are identical to the Levantine Basin, thus to the Cilician Basin were extensively investigated in the study area. The possibility of regional LIW formation has been investigated.
- ii. Consecutive salinity shifts thus temperature and potential density changes in water mass characteristics at the surface and intermediate layers (i.e. LSW, MAW and LIW) on upper thermocline has been observed and recorded.

4.1 Physical Oceanographic Characteristics of the Study Area

The general circulation of the Cilician Basin is a highly complex and dynamic system with meandering and reversing currents and reappearing cyclonic/anti-cyclonic energetic mesoscale eddies with temporal and spatial variabilities. The dominant driving mechanism of the general circulation temporarily and spatially change between the current systems (i.e. Cilician Current and Asia Minor Current) and the eddies (Salihoglu et al., 2019).

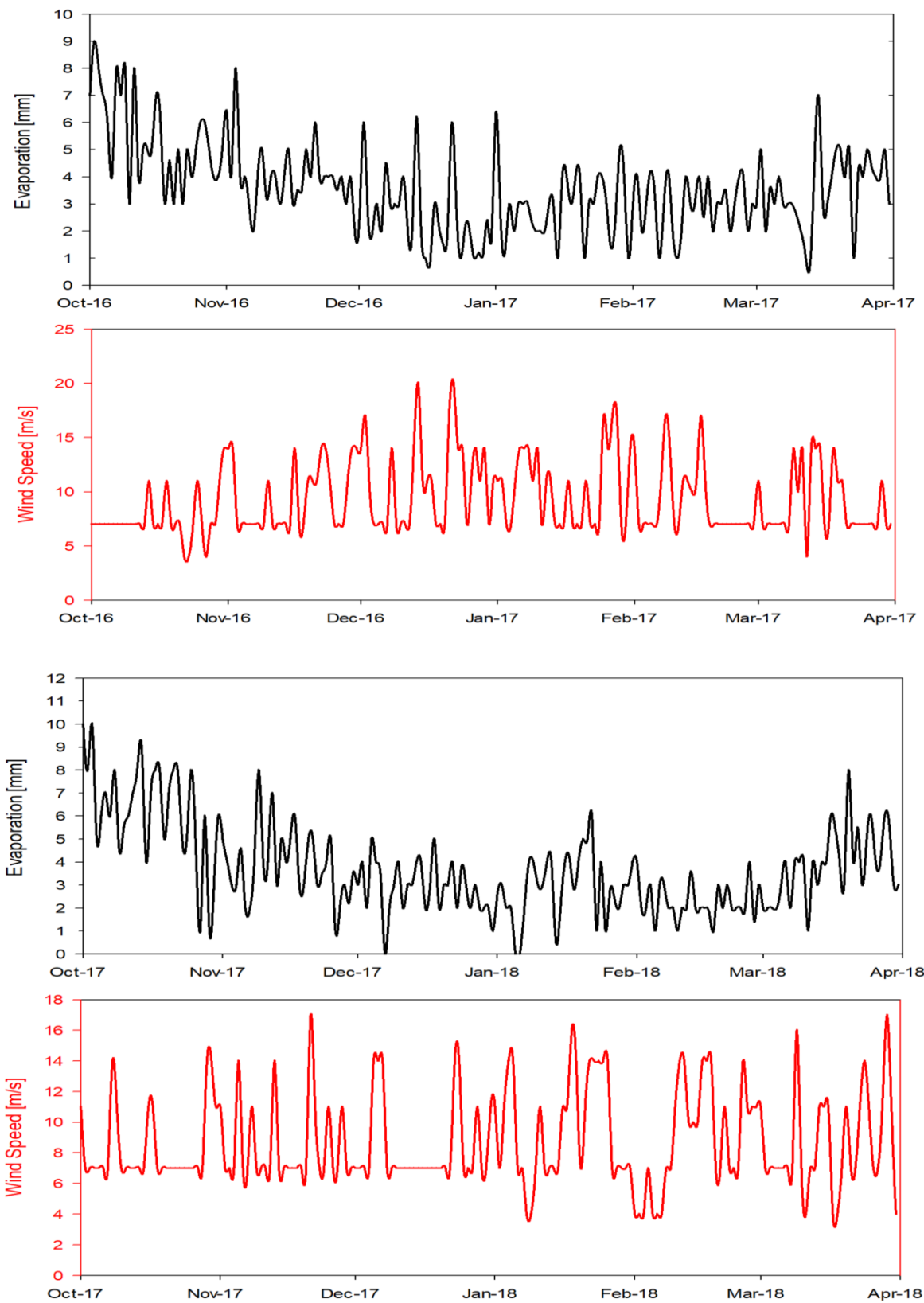


Figure 4.1: Evaporation and wind speed data from October 2016 to April 2017 (upper figure) and October 2017 to April 2018 (lower figure).

All physical oceanographic characteristics identical to the Levantine Basin revealed to be present in the study area. Due to the excessive heat, evaporation and atmospheric interactions, upper 25 meters of the water column was well mixed and uniform, almost all along the study. In winter seasons, especially between January and March, the study region was dominated by intense vertical mixing processes due to wind and sinking of relatively high-density water masses to the depths of about 150 to 200 meters. This sinking of relatively high-density water masses occurred due to evaporative cooling coinciding with strong winds, as shown in Figure 4.1. Between April and December, vertical structure of the water column indicated strong seasonal stratification, especially intensifying during summer seasons. All these processes and vertical structure of the water column observed in the study area were consistent with the previous studies (Bergamasco & Malanotte-Rizzoli, 2010; Hecht et al., 1988; Kucuksezgin & Pazi, 2006; Malanotte-Rizzoli & Hecht, 1988; Malanotte-Rizzoli & Robinson, 1988; Onken & Yuce, 2000; Özsoy et al., 1989, 1993; Robinson et al., 1991; The LIWEX Group, 2003; The POEM Group, 1992), except salinity shifts and changes observed in characteristics of water mass on upper thermocline, especially in the latter part of the study.

Various water masses identical to the physical oceanographic characteristic of the Levantine Basin (i.e. LSW, MAW, LIW and EMDW) were present in the study area. As shown in Figure 4.2, typical "Scorpion Tail" form of the multi-layered vertical structure of the water column observed throughout the study during stratified seasons, especially between May and November. Warm and saline LSW located within the surface mix layer, above the seasonal thermocline. Regionally formed deep salinity maximum LIW located at intermediate depths and Atlantic originated subsurface salinity minimum MAW trapped between LSW and LIW. Permanent halocline located at depths of about 300 - 400 meters, throughout the study. The EMDW were consistently present in the study area with ~ 13.85 °C of temperature, 38.80 per mille of salinity and 29.18 kg/m^3 of potential density below the permanent halocline, at depths of about 500 meters and below.

As it is well known in the literature, salty and warm LSW forms in entire Levantine Basin due to excessive heat, evaporation and relatively weak winds during summer seasons (Malanotte-Rizzoli & Hecht, 1988; Özsoy et al., 1989). As presented in Chapter 3 of this study, the surface layer of the study area was dominated by the warm and saline LSW during

the stratified seasons throughout the study, especially between May and November. In winter seasons, high salinity content LSW became denser due to excessive heat loss and evaporative cooling caused by dry and cold “Poyraz” winds. These processes reduced the stability of the water column, and eventually caused convective mixing of the water column to intermediate depths and sinking of relatively saline and high-density water to the depths of about 200 meters, as can be seen in temperature, salinity and potential density anomaly plots, in Chapter 3 of this study.

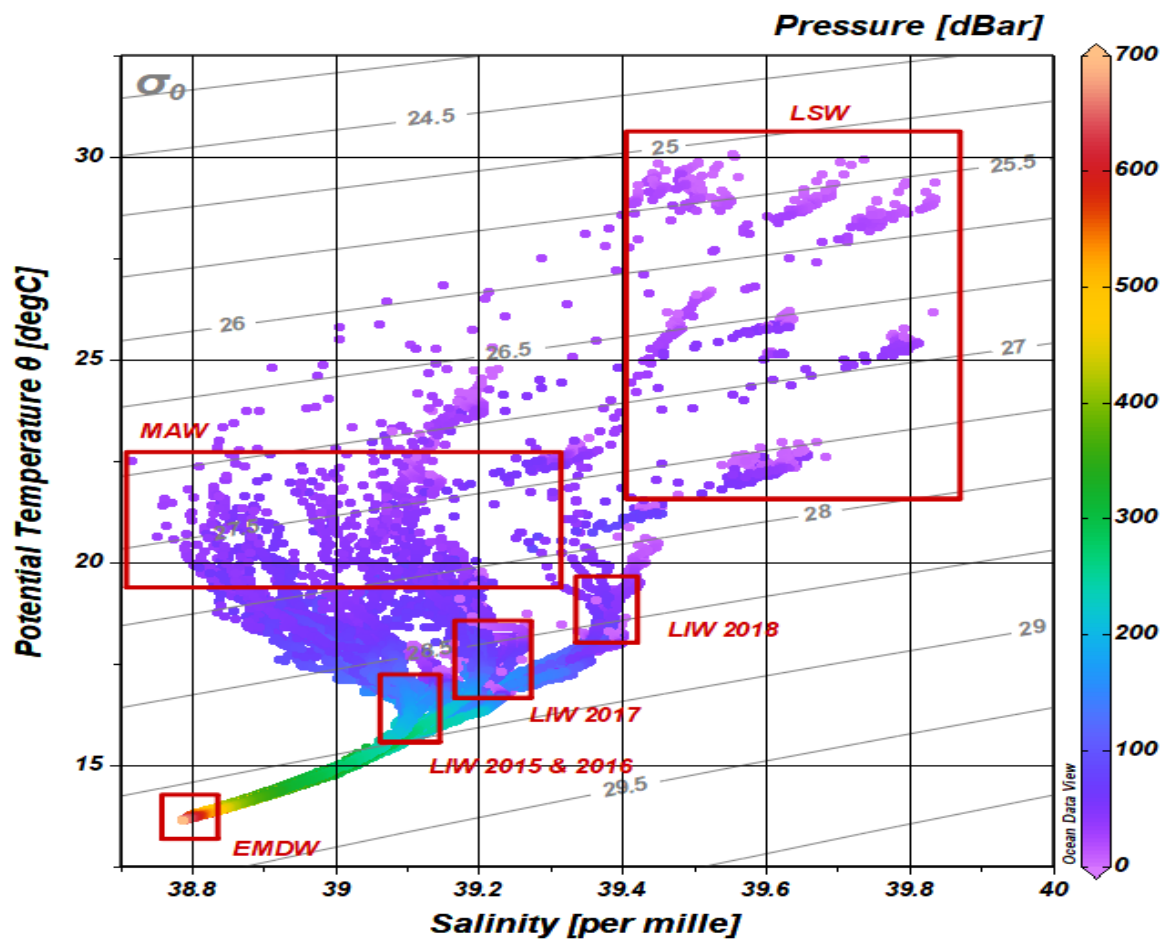


Figure 4.2: Water masses defined in the T-S diagram of the KTS studies.

Analysed results of the high-frequency KTS studies revealed that, physical oceanographic characteristics of the winter mixed layer, which forms every year in winter seasons due to convective mixing processes, and the physical oceanographic characteristics of the LIW (Table 4.1), which was located at intermediate depths during the stratified seasons in each

year, were similar throughout the study . It is observed and recorded that, each year, the physical oceanographic characteristics of the LIW (Table 4.1) were defined by the physical oceanographic characteristics of the winter mixed layer. Physical oceanographic characteristics of the LIW, which was located at intermediate depths during stratified seasons, and the dense water mass which was formed each year within the winter mix layer, were similar in each year, as shown in T-S diagrams and Time Series Plots in sections 3.1 and 3.2. Furthermore, consecutive salinity shifts and changes of physical oceanographic characteristics observed on upper thermocline is possibly an indicator of local formation of the LIW. It is also observed that, depth range or centre of the LIW located in the study area was within the depth range or above the depth of the winter mixed layer in each year. These results suggest that LIW located in the study area during the study is locally formed within the winter mix layer in the study area.

Table 4.1: LIW characteristics at KTS station K07.

Date	Temperature [°C]	Salinity [per mille]	Potential Density [kg/m ³]	Depth Range [m]
November 2015	16.97 – 16.17	39.10	28.68 – 28.87	150 - 200
December 2015	16.92 – 16.42	39.12	28.70 – 28.83	140 - 170
May 2016	16.91 – 16.26	39.10	28.69 – 28.86	140 - 190
June 2016	16.88 – 16.17	39.10	28.70 – 28.87	150 - 190
August 2016	16.75 – 16.10	39.10	28.74 – 28.89	145 - 185
September 2016	16.46 – 16.00	39.10	28.80 – 28.91	140 - 170
October 2016	16.27 – 16.02	39.10	28.85 – 28.90	165 - 185
November 2016	16.41 – 16.01	39.10	28.82 – 28.91	190 - 215
April 2017	18.36 – 17.86	39.26	28.45 – 28.58	20 - 60
July 2017	18.57 – 17.26	39.21	28.36 – 28.69	50 - 100
September 2017	17.65 – 17.23	39.21	28.59 – 28.69	90 - 125
October 2017	17.43 – 17.03	39.21	28.64 – 28.74	100 - 130
November 2017	17.37 – 17.15	39.21	28.76 – 28.71	110 - 135
March 2018	18.15 – 18.09	39.39	28.60 – 28.62	67 - 77
April 2018	NA	NA	NA	NA
June 2018	18.95 – 18.29	39.39	28.39 – 28.56	60 - 85

NA: Not Applicable. Possibly due to mixing processes in the water column.

In literature, Rhodes Gyre and Antalya Basin described as the main LIW formation sites in several studies. Additionally, in the same studies, the north-eastern part of the Levantine Basin, the Cilician Basin was discussed as a potential LIW formation region (The LIWEX

Group, 2003; The POEM Group, 1992). The preconditioning and formation phases of LIW formation in Rhodes Gyre evidently described by the LIWEX Group (2003). Very salty surface waters produced due to excessive evaporation in summer seasons. By the end of autumn and beginning of winter, dry and cold "Poyraz" winds cause excessive heat loss on surface layers of the water column. These processes induce evaporative cooling of the sea surface which increases the salinity, hence the density of the surface waters that reduce the stability of the water column, though even weak winds can induce vertical mixing of the water column through the intermediate depths in winter seasons. By the end of winter mixing processes, these newly formed water masses spreads along from the convection site by isopycnal surfaces, driven by cyclonic / anti-cyclonic eddies on upper thermocline (The LIWEX Group, 2003).

The similar conditions of above mentioned LIW formation processes in the Rhodes Gyre (The LIWEX Group, 2003) were present in the study area during the entire study period. Furthermore, the results of the model study by Lascaratos and colleagues (1993) revealed that the LIW should be centred within or above the winter mixed layer depth in the formation region. If not and centred below the winter mixed layer depth, it suggests that LIW is not locally formed and advected by other source region (A Lascaratos et al., 1993). In the northern Levantine Basin, the formation of LIW was observed and recorded only in the Rhodes Gyre and Antalya Basin (Onken & Yuce, 2000; Özsoy et al., 1993; The LIWEX Group, 2003; The POEM Group, 1992). Yet in literature, there is no evidence that the cyclonic circulation of the Rhodes Gyre penetrates to the Cilician Basin, therefore the LIW observed in the study is not an advection from the Rhodes Gyre.

The study of Küçüksezgin and Pazı (2006) revealed that the LIW was present in the Cilician Basin during their three separate cruises, respectively in May 1997, July 1998 and October 2003. Multi-layered vertical structure, the "Scorpion Tail" form of the water column and the presence of the LIW was observed in the study area during July 1998 and October 2003 cruises. However, the "Scorpion Tail" form of the water column was not formed in the study area during their May 1997 cruise.

114Y139 code numbered TUBITAK Project (Salihoglu et al., 2019) which also comprised the subject of this study, the KTS studies, is the most recent oceanographic study conducted in the Cilician Basin between 2015 and 2018.

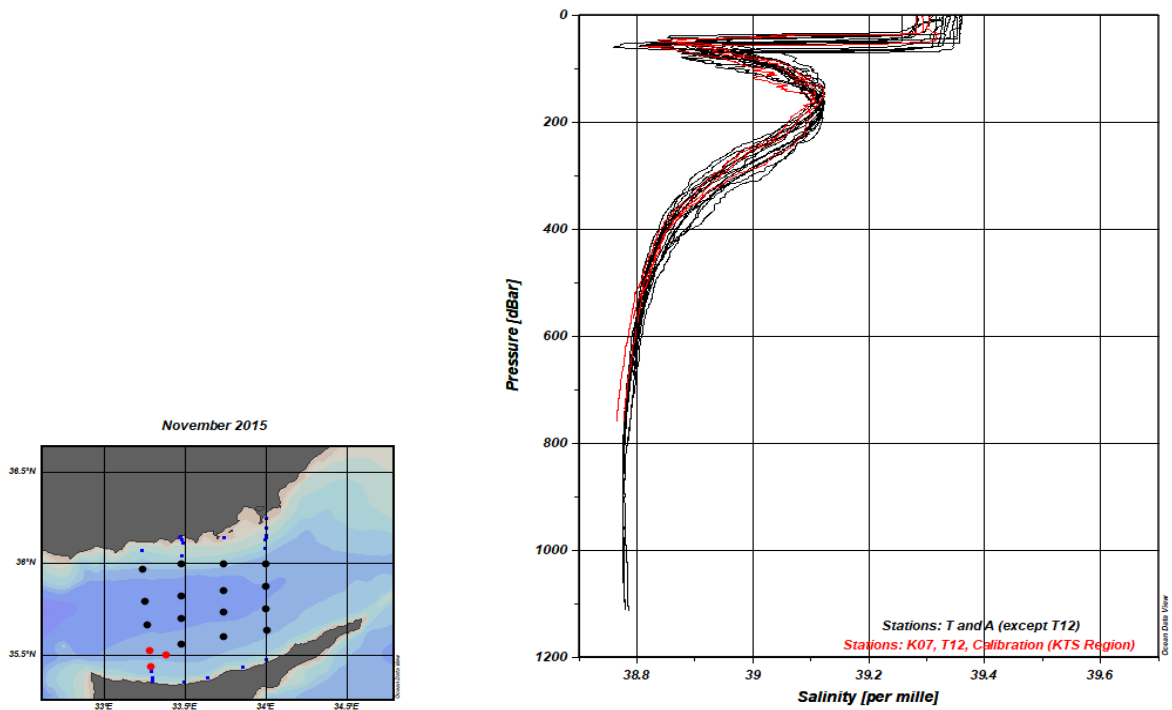


Figure 4.3: Salinity profiles of 114Y139 Code numbered TUBITAK Project stations in November 2015.

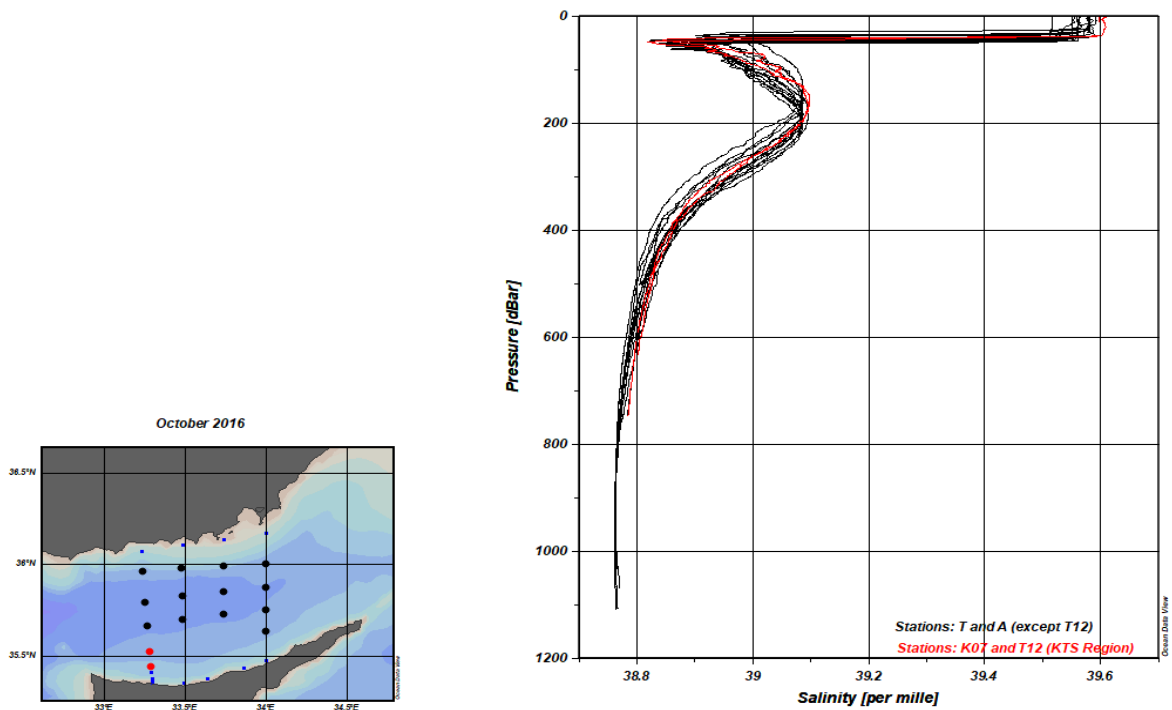


Figure 4.4: Salinity profiles of 114Y139 Code numbered TUBITAK Project stations in October 2016.

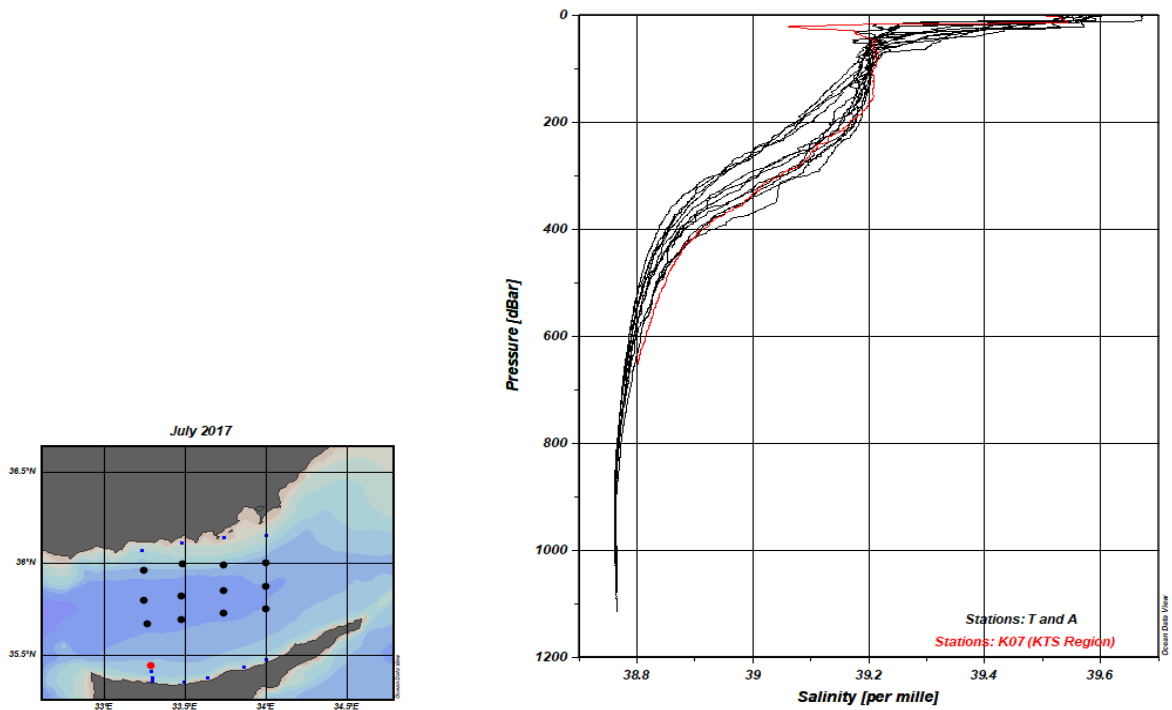


Figure 4.5: Salinity profiles of 114Y139 Code numbered TUBITAK Project stations in July 2017.

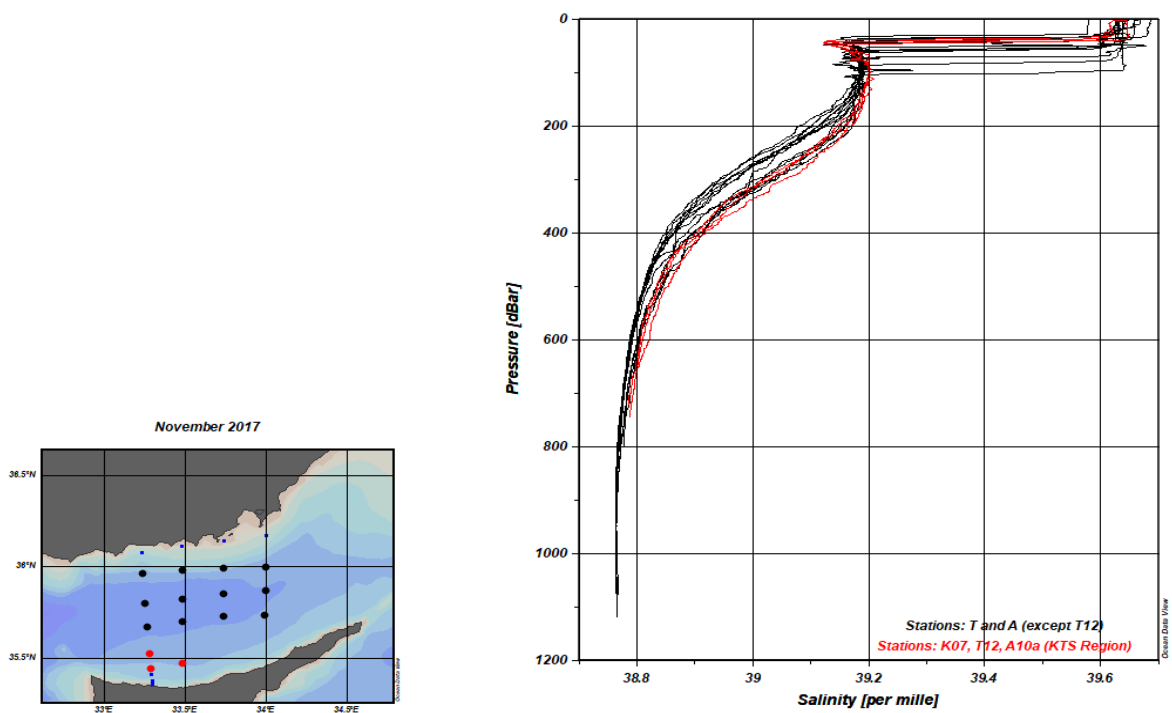


Figure 4.6: Salinity profiles of 114Y139 Code numbered TUBITAK Project stations in November 2017.

In order to analyse and understand physical oceanographic characteristics of the Cilician Basin, the results of KTS stations were compared with all the other stations (“T” and “A” stations in Figure 2.1) of the project mentioned above. At the first part of the study, in 2015 and 2016, the results are observed to be similar and consistent, as shown in Figure 4.3 and Figure 4.4. With ~39.10 per mille of salinity, characteristics of the LIW and the "Scorpion Tail" form of the water column were identical in 2015 and 2016, within the project and with the previous studies. However, in 2017, significant changes and differences were observed on the physical oceanographic characteristics in the upper thermocline, hence in the LIW. In July 2017, the LIW and the "Scorpion Tail" form of the water column was observed only in KTS station K07, as shown in Figure 4.5. As already described in Chapter 3, the LIW and the “Scorpion Tail” form of the water column was observed at station K07 all along the stratified seasons in 2017. On the other hand, at the other stations (“T” and “A” stations) of the project, presence of the LIW and multi-layered structure of the water column was observed only in November 2017, as shown in Figure 4.6.

Results of this study revealed that in each year, the deep salinity maximum LIW was present in the study area during stratified seasons, and disappeared in winter seasons due to mixing processes. By the end of mixing processes, LIW was reappeared at intermediate depths in similar characteristics with winter mixed layer, repeatedly every year.

Based on the results of this study and facts from literature, this study concluded that the study area is possibly a formation site of LIW and yet, it is the first study to reveal that the LIW forms locally in the Cilician Basin.

4.2 Salinity Shift and Change of Upper Thermocline Characteristics in KTS Area

Although results of 2015 and 2016 of this study seems to be similar and consistent with the results of the POEM Group (1993) and also with the results of Onken and Yuce (2000), and Kucuksezgin and Pazi (2006), the analyses of the whole data set revealed consecutive salinity increases, thus changes in temperature and potential density on upper thermocline, (i.e. LSW, MAW and LIW), throughout the study, especially in 2017 and 2018. Compared to the results of 2015 and 2016 of this study and the previous studies, significant and consecutive changes in salinity with increasing trend and shifts in temperature and potential

density on upper thermocline characteristics were observed in 2017 and 2018. In total of about 0.30 per mille of salinity increase in LIW was observed throughout the study, between November 2015 and June 2018. Compared to the previous year, about 0.10 per mille of salinity increases were recorded in 2017 and 0.20 per mille in 2018. Below the permanent halocline, physical oceanographic characteristics were observed to be unaffected and unchanged.

Upper thermocline circulation and water masses of the northern Levantine Basin, their features, characteristics, driving dynamics, structure and patterns were revealed by the studies of the POEM Group (Bergamasco & Malanotte-Rizzoli, 2010; Hecht et al., 1988; Malanotte-Rizzoli & Hecht, 1988; Malanotte-Rizzoli & Robinson, 1988; Özsoy et al., 1989, 1993; Robinson et al., 1991; The LIWEX Group, 2003; The POEM Group, 1992). Additionally, the studies of Onken and Yuce (2000) and Kucuksezgin and Pazi (2006) in north-eastern Levantine Basin were revealed similar and consistent results with the POEM studies (Kucuksezgin & Pazi, 2006; Onken & Yuce, 2000). In literature, characteristics of LIW defined as shown in Table 1.1. The POEM Group consistently detected the LIW with 39.10 – 39.20 per mille of salinity, ~16.00 °C of temperature and 28.90 kg/m³ of potential density in their study between 1985 and 1991 with the exception of ≥ 39.30 per mille of salinity in March 1991 which high surface salinity caused by increased surface fluxes in summer of 1990, concluded as the possible reason (Özsoy et al., 1993).

Figure 4.2, Figure 4.7, Figure 4.8, Figure 4.9 and Table 4.1 presented to discuss and describe salinity increases and changes in physical oceanographic characteristics of water masses observed in the upper thermocline at the study area.

Figure 4.2 and Figure 4.7, the T-S diagrams of the KTS studies revealed that identical "Scorpion Tail" form of the multi-layered vertical structure of the water column was present in the area throughout the study. However, in 2017 and 2018, significant shifts and changes were observed in physical oceanographic characteristics of LSW, LIW and MAW. In 2015 and 2016, LIW was marked at ~39.10 per mille salinity, 16.00 – 16.75 °C temperature and 28.75 – 28.87 kg/m³ potential density anomaly, as described in literature (A Lascaratos et al., 1993; Onken & Yuce, 2000; Özsoy et al., 1989, 1993; Robinson et al., 1991; The LIWEX Group, 2003). In 2017 and 2018, although the "Scorpion Tail" form was present in the area, LIW was marked at ~39.20 per mille salinity, 17.00 – 17.75 °C temperature, 28.65 – 28.75

kg/m³ potential density anomaly and ~39.39 per mille salinity, 18.20 – 19.00 °C temperature, 28.45 – 28.55 kg/m³ potential density anomaly, respectively. In the same period, MAW was marked with salinities at 38.80 – 38.99 per mille in 2015 and 2016, at 38.95 – 39.12 per mille in 2017 and at 39.32 per mille in 2018, respectively. Significant salinity increases were also observed in LSW, especially between summer seasons of 2016 and 2017. LSW was recorded at ~39.65 per mille in September 2016 and ~39.80 per mille at the beginning of October 2017, respectively.

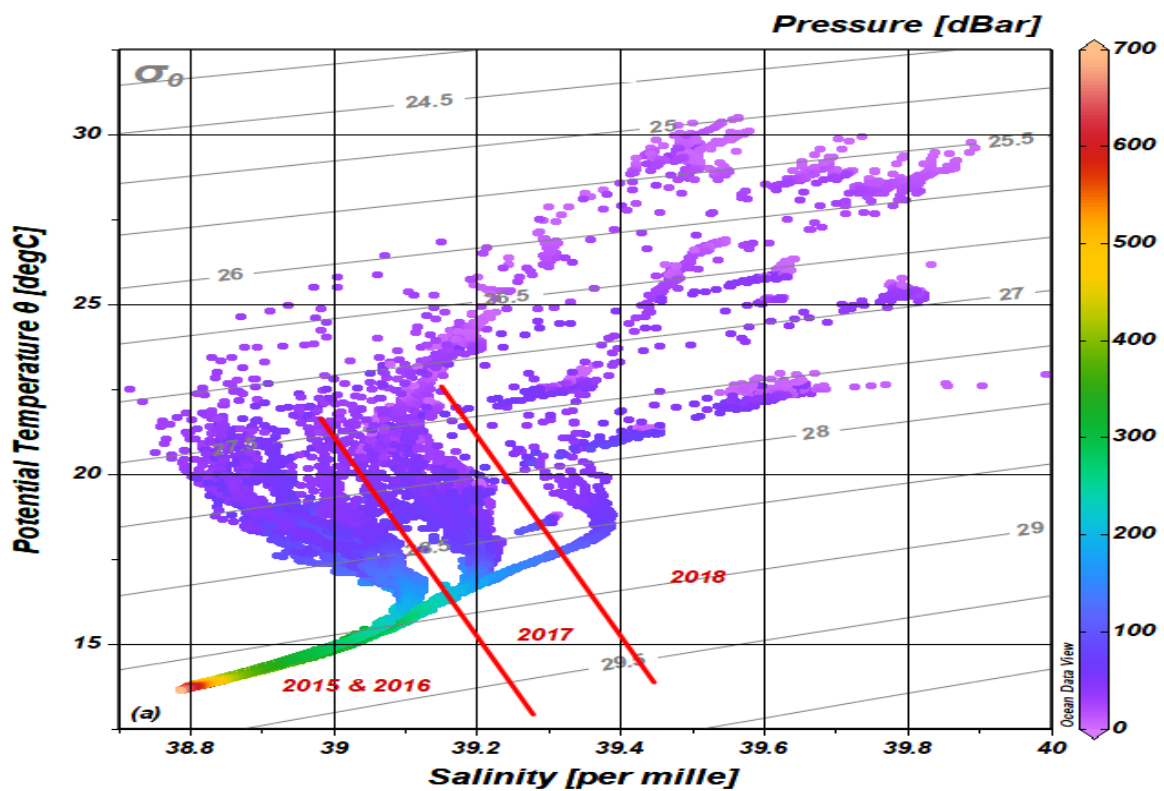


Figure 4.7: Shifts of water mass characteristics between years observed on the T-S diagram of KTS studies.

As shown in Figure 4.8, salinity shifts and changes in physical oceanographic characteristics of the water masses on upper thermocline were clearly observed consecutively every year in the study area. About 0.20 per mille of salinity increase was recorded in the surface mixed layer, which is dominated by the salty LSW during stratified seasons, between 2016 and 2017. Highest increase was recorded in MAW with 0.50 per mille of salinity. Possibly the most critical and significant salinity increase and changes of physical oceanographic

characteristics were recorded in LIW. As shown in Table 4.1 and Figure 4.8, along with ~ 0.30 per mille of salinity increase, increases in temperature and eventually decreases in potential density were caused significant shoaling in LIW.

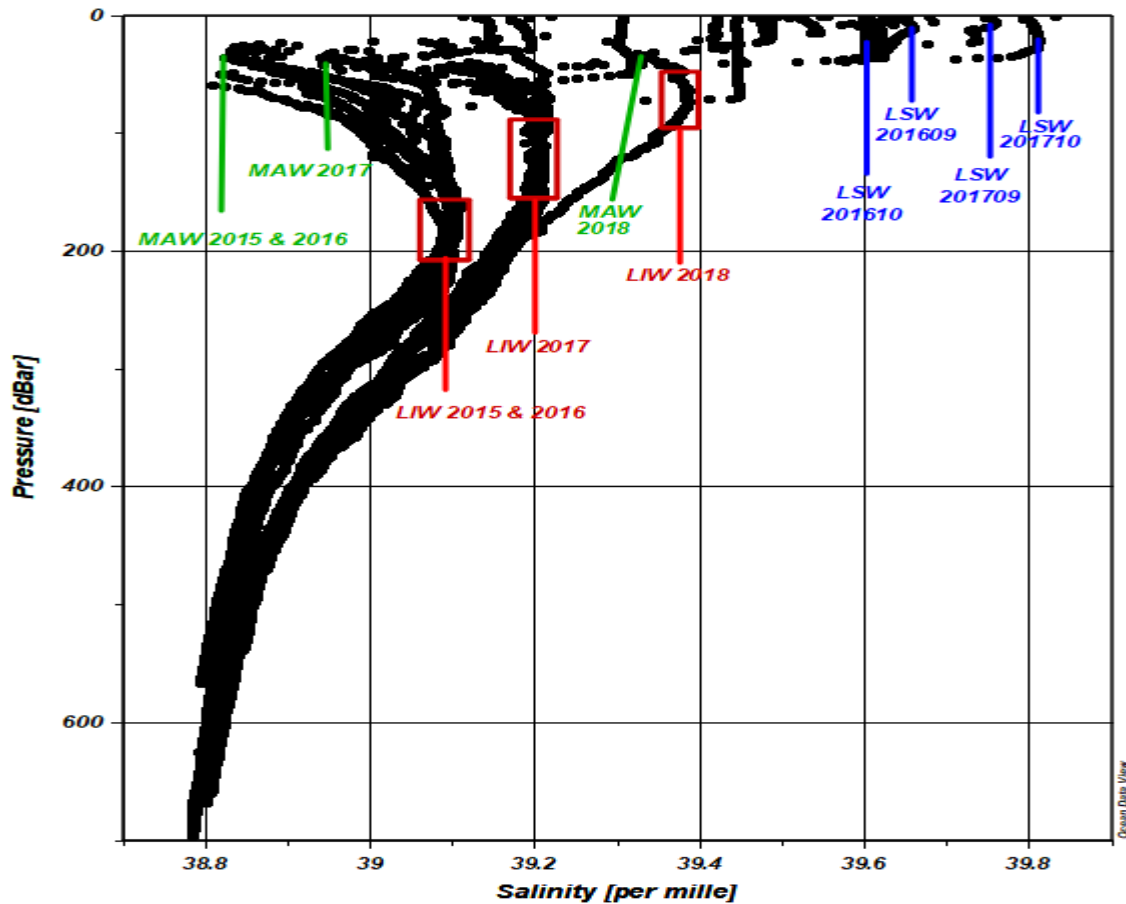


Figure 4.8: Salinity profiles of KTS station K07 during stratified seasons between 2015 and 2018.

Colour scaling of time series plots of salinity measurements at stations K01, K03 and K07 which is presented in Figure 4.9 are self-explanatory on seasonal and annual salinity shift which was observed throughout the study in the area. As shown in Figure 4.9, coloured scaling of salinities in winter mixed layer were blue (~ 39.10 per mille) in 2016, green (~ 39.20 per mille) in 2017 and dark green to yellow (~ 39.40 per mille) in 2018. In summer seasons of 2016 and 2017, the coloured scale of the surface mixed layer was orange and red, respectively.

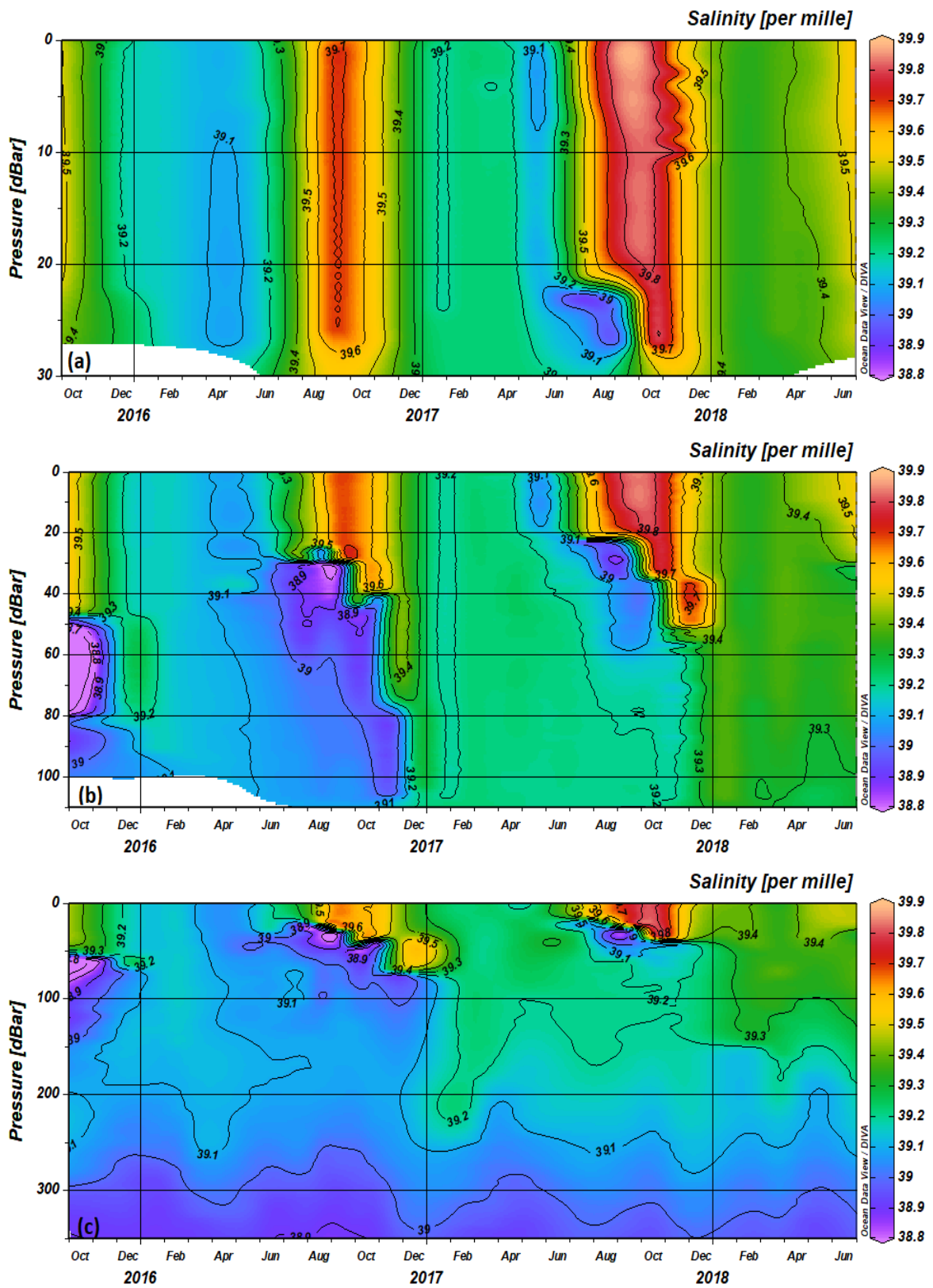


Figure 4.9: Time series plots of salinity measurements vs depth. (a): Station K01. (b): Station K03. (c): Station K07.

The study of Salihoglu and colleagues in 2019 revealed that similar salinity increases were observed in the Cilician Basin during the seasonal cruises between 2015 and 2017. Possibly due to the frequency (seasonal cruises) of the study, salinity shift at “T” and “A” stations were not as pronounced as KTS stations.

By the contribution of METU – IMS, the data sets of “Erdemli Time Series” (ETS) study analysed in order to understand if the observed phenomena are local to the KTS study region, or it is basin-wide. The ETS results revealed that, salinity shift and changes in physical oceanographic characteristics on upper thermocline is observed not only in the KTS study region, but in the entire Cilician Basin, especially in 2018. Salinity was recorded with 39.93 per mille in surface mixed layer in September 2018, and with 39,56 per mille in winter mixed layer in December 2018. However, in 2019, a significant decrease in salinity was observed in the ETS studies.

Evaporation data of the study region and possibility of instrumental error (CTD, SBE 19Plus V2 SeaCAT Profiler) analysed to investigate if there were any correlation or explanation to the salinity increases observed during the study.

Evaporation data between January 2015 and June 2018 (Figure 4.10, Table 4.2, and Table 4.3) analysed to investigate if there were any correlation or explanation to the salinity increases observed during the study. Approximately 30 to 35 mm of total annual evaporation increases were recorded consecutively every year. Cumulatively, about 70 mm of total evaporation increases were recorded during the study period. Seasonal distribution of total evaporation was observed to be almost same in oceanographic spring and summer seasons. The differences occurred in oceanographic autumn and winter seasons, as shown in Table 4.2 and Table 4.3.

70 mm of total evaporation increases shall not be sufficient to change salinity characteristics on the upper thermocline, as presented in this study. Therefore, this study conclude that the salinity increases observed during the study shall not be due to evaporation. This subject requires further investigation and available data of this study is not sufficient to show if these salinity shifts are because of regional processes or global changes.

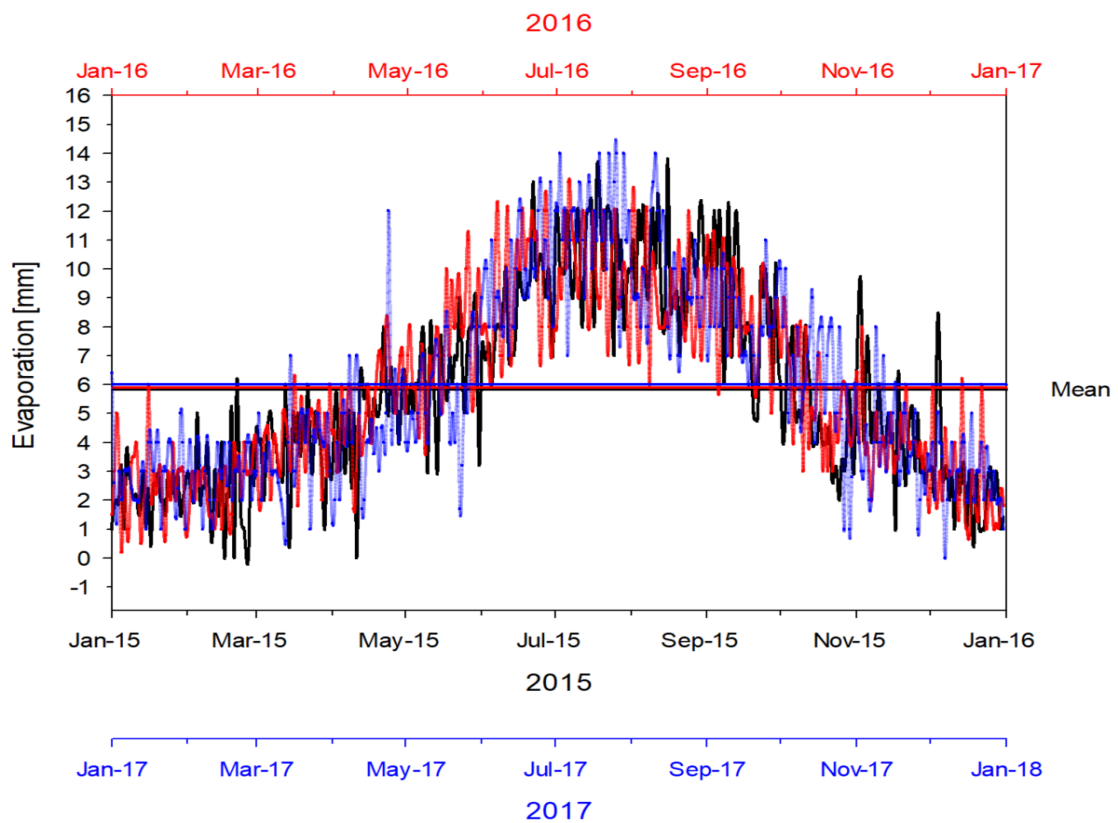


Figure 4.10: Total annual evaporation data between January 2015 and January 2018.

Table 4.2: Monthly comparison of total annual evaporation between January 2015 to June 2018.

EVAPORATION [mm]	2015	2016	2017	2018
January	67.10	78.10	90.50	90.30
February	67.80	73.20	82.60	63.80
March	116.80	123.90	110.60	120.60
April	146.50	158.90	137.90	167.70
May	197.30	227.40	175.50	250.20
June	258.90	282.10	295.00	277.50
July	328.50	308.40	358.00	
August	316.60	281.50	298.00	
September	264.20	257.00	248.00	
October	145.80	169.60	194.60	
November	139.00	121.10	116.90	
December	79.40	79.60	89.30	
TOTAL EVAPORATION [mm]	2127.90	2160.80	2196.90	970.10

Table 4.3: Total evaporation in oceanographic spring and summer seasons between 2015 and 2018.

EVAPORATION [mm]	2015	2016	2017	2018
April	146.50	158.90	137.90	167.70
May	197.30	227.40	175.50	250.20
June	258.90	282.10	295.00	277.50
July	328.50	308.40	358.00	
August	316.60	281.50	298.00	
September	264.20	257.00	248.00	
TOTAL EVAPORATION [mm]	1512.00	1515.30	1512.40	695.40

Finally, we shall conclude that the most significant outcomes of this study are;

- i. The study area is possibly a formation site of LIW.
- ii. Salinity shifts and changes of physical oceanographic characteristics observed on upper thermocline shall be explained neither by evaporation nor instrumental error (CTD). Therefore, it requires further investigation in order to explain the observed phenomena.
- iii. Oceanographic time-series studies and high-frequency sub-mesoscale oceanographic researches are crucial to determine physical oceanographic features of the region. Also, to investigate temporal and spatial effects of these physical oceanographic features and changes of unstable, stable and quasi-stable physical oceanographic characteristics observed in the area.

REFERENCES

- Akpınar, A., Yılmaz, E., Fach, B. A., & Salihoglu, B. (2016). Physical oceanography of the Eastern Mediterranean Sea. In *The Turkish Part of the Mediterranean Sea* (Vol. 43, p. 250).
- Alhammoud, B., Béranger, K., Mortier, L., Crépon, M., & Dekeyser, I. (2005). Surface circulation of the Levantine Basin: Comparison of model results with observations. *Progress in Oceanography*, 66(2–4), 299–320. <https://doi.org/10.1016/j.pocean.2004.07.015>
- Bergamasco, A., & Malanotte-Rizzoli, P. (2010). The circulation of the Mediterranean Sea: a historical review of experimental investigations. *Advances in Oceanography and Limnology*, 1(1), 11–28. <https://doi.org/10.1080/19475721.2010.491656>
- Cardin, V., Civitarese, G., Hainbucher, D., Bensi, M., & Rubino, A. (2015). Thermohaline properties in the Eastern Mediterranean in the last three decades: Is the basin returning to the pre-EMT situation? *Ocean Science*, 11(1), 53–66. <https://doi.org/10.5194/os-11-53-2015>
- El-Geziry, T. M., & Bryden, I. G. (2010). The circulation pattern in the Mediterranean Sea: issues for modeller consideration. *Journal of Operational Oceanography*, 3(2), 39–46. <https://doi.org/10.1080/1755876X.2010.11020116>
- Fofonoff, N. P. (1985). Physical properties of seawater: A new salinity scale and equation of state for seawater. *Journal of Geophysical Research*, 90(C2), 3332. <https://doi.org/10.1029/jc090ic02p03332>
- Hainbucher, D., Cardin, V., Siena, G., Hübner, U., Moritz, M., Drübbisch, U., & Basan, F. (2015). Hydrography in the Mediterranean Sea during a cruise with RV Poseidon in April 2014. *Earth System Science Data*, 7(2), 231–237. <https://doi.org/10.5194/essd-7-231-2015>
- Hecht, A., Pinnardi, N., & Robinson, A. R. (1988). Currents, Water Masses, Eddies and Jets in the Mediterranean Levantine Basin. *Journal of Physical Oceanography*.
- Kucuksezgin, F., & Pazi, I. (2006). Circulation, hydrographic and nutrient characteristics of the Cilician Basin, Northeastern Mediterranean Sea. *Journal of Marine Systems*, 59(3–

- 4), 189–200. <https://doi.org/10.1016/j.jmarsys.2005.10.003>
- Lascaratos, A, Williams, R. G., & Tragou, E. (1993). A mixed-layer study of the formation of Levantine Intermediate Water. *Journal of Geophysical Research*, 98(C8), 14739–14749. <https://doi.org/10.1029/93JC00912>
- Lascaratos, Alex, Roether, W., Nittis, K., & Klein, B. (1999). Recent changes in deep water formation and spreading in the Eastern Mediterranean Sea: A review. *Progress in Oceanography*, 44(1–3), 5–36. [https://doi.org/10.1016/S0079-6611\(99\)00019-1](https://doi.org/10.1016/S0079-6611(99)00019-1)
- Malanotte-Rizzoli, P., & Hecht, A. (1988). Large-scale properties of the eastern Mediterranean: a review. *Oceanologica Acta*, 11(4), 323–335. [https://doi.org/10.1016/S0967-0645\(99\)00020-X](https://doi.org/10.1016/S0967-0645(99)00020-X)
- Malanotte-Rizzoli, P., & Robinson, A. R. (1988). POEM: Physical Oceanography Eastern Mediterranean. *Eos*, 69(14), 194–196, 203.
- Marullo, S., Santoleri, R., Malanotte-Rizzoli, P., & Bergamasco, A. (1999). The sea surface temperature field in the Eastern Mediterranean from advanced very high resolution radiometer (AVHRR) data: Part I. Seasonal variability. *Journal of Marine Systems*, 20(1–4), 63–81. [https://doi.org/10.1016/S0924-7963\(98\)00071-2](https://doi.org/10.1016/S0924-7963(98)00071-2)
- Millero, F. (2011). History of the Equation of State of Seawater. *Oceanography*, 23(3), 18–33. <https://doi.org/10.5670/oceanog.2010.21>
- Onken, R., & Yuce, H. (2000). Winter circulation and convection in the Antalya Basin (Eastern Mediterranean). *Journal of Physical Oceanography*, 30(5), 1099–1110. [https://doi.org/10.1175/1520-0485\(2000\)030<1099:WCACIT>2.0.CO;2](https://doi.org/10.1175/1520-0485(2000)030<1099:WCACIT>2.0.CO;2)
- Özsoy, E., Hecht, A., & Ünlüata, Ü. (1989). Circulation and hydrography of the Levantine Basin. Results of POEM coordinated experiments 1985-1986. *Progress in Oceanography*, 22(2), 125–170. [https://doi.org/10.1016/0079-6611\(89\)90004-9](https://doi.org/10.1016/0079-6611(89)90004-9)
- Özsoy, E., Hecht, A., Ünlüata, Ü., Brenner, S., Oğuz, T., Bishop, J., ... Rozenraub, Z. (1991). A review of the Levantine Basin circulation and its variability during 1985-1988. *Dynamics of Atmospheres and Oceans*, 15(3–5), 421–456. [https://doi.org/10.1016/0377-0265\(91\)90027-D](https://doi.org/10.1016/0377-0265(91)90027-D)
- Özsoy, E., Hecht, A., Ünlüata, Ü., Brenner, S., Sur, H. I., Bishop, J., ... Oğuz, T. (1993). A

- synthesis of the Levantine Basin circulation and hydrography, 1985-1990. *Deep-Sea Research Part II*, 40(6), 1075–1119. [https://doi.org/10.1016/0967-0645\(93\)90063-S](https://doi.org/10.1016/0967-0645(93)90063-S)
- Pinardi, N., Zavatarelli, M., Adani, M., Coppini, G., Fratianni, C., Oddo, P., ... Bonaduce, A. (2015). Mediterranean Sea large-scale low-frequency ocean variability and water mass formation rates from 1987 to 2007: A retrospective analysis. *Progress in Oceanography*, 132, 318–332. <https://doi.org/10.1016/j.pocean.2013.11.003>
- Robinson, A. R., & Golnaraghi, M. (1993). The physical and dynamical oceanography of the Mediterranean Sea. In *Proceedings of the 4th National Symposium on Oceanography and Fisheries, Rhodes Island* (pp. 9–13).
- Robinson, A. R., Golnaraghi, M., Leslie, W. G., Artegiani, A., Hecht, A., Lazzoni, E., ... Ünlüata, Ü. (1991). The Eastern Mediterranean general circulation: features, structure and variability. *Dynamics of Atmospheres and Oceans*, 15(3–5), 215–240. [https://doi.org/10.1016/0377-0265\(91\)90021-7](https://doi.org/10.1016/0377-0265(91)90021-7)
- Robinson, A. R., Leslie, W. G., Theocharis, A., & Lascaratos, A. (2001). Mediterranean Sea Circulation. *RWOS*, 1–19. <https://doi.org/10.1016/rwos.2001.0376>
- Salihoğlu, I., Saydam, C., Baştürk, Ö., Yılmaz, K., Göçmen, D., Hatipoğlu, E., & Yılmaz, A. (1990). Transport and distribution of nutrients and chlorophyll-a by mesoscale eddies in the northeastern Mediterranean. *Marine Chemistry*, 29(C), 375–390. [https://doi.org/10.1016/0304-4203\(90\)90024-7](https://doi.org/10.1016/0304-4203(90)90024-7)
- Salihoglu, I., Tugrul, S., Gucu, A. C., Salihoglu, B., Kocak, M., Tezcan, D., ... Temel, O. (2019). *Determination of influence of anthropogenic and natural processes on the Cilician Basin (Between Turkish Republic of Northern Cyprus and Turkey) marine ecosystem*. Girne, Mersin.
- Tanhua, T., Hainbucher, D., Schroeder, K., Cardin, V., Álvarez, M., & Civitarese, G. (2013). The Mediterranean Sea system: A review and an introduction to the special issue. *Ocean Science*, 9(5), 789–803. <https://doi.org/10.5194/os-9-789-2013>
- The LIWEX Group (2003). The Levantine Intermediate Water Experiment (LIWEX) Group: Levantine basin—A laboratory for multiple water mass formation processes. *Journal of Geophysical Research*, 108(C9), 8101. <https://doi.org/10.1029/2002JC001643>

- The POEM Group (1992). General circulation of the Eastern Mediterranean. *Earth-Science Reviews*, 32(4), 285–309. [https://doi.org/http://dx.doi.org/10.1016/0012-8252\(92\)90002-B](https://doi.org/http://dx.doi.org/10.1016/0012-8252(92)90002-B)
- Velaoras, D., Krokos, G., Nittis, K., & Theocharis, A. (2014). Dense intermediate water outflow from the Cretan Sea: A salinity driven, recurrent phenomenon, connected to thermohaline circulation changes. *Journal of Geophysical Research, Oceans*, 119, 4797–4820. <https://doi.org/10.1002/2014JC009937>
- Wüst, G. (1961). On the vertical circulation of the Mediterranean Sea. *Journal of Geophysical Research*, 66(10), 3261–3271. <https://doi.org/10.1029/JZ066i010p03261>